# Numerical - Based Thermal Analysis of Proton Exchange Membrane Fuel Cells

by

**Navpreet Kaur**

A thesis
presented to the University Of Waterloo
in fulfillment of the
thesis requirement for the degree of
Master of Applied Science
in
Mechanical and Mechatronics Engineering

Waterloo, Ontario, Canada, 2025

© Navpreet Kaur 2025

# Author's Declaration

I hereby declare that I am the sole author of this thesis. This is a true copy of the thesis, including any required final revisions, as accepted by my examiners.

I understand that my thesis may be made electronically available to the public.

# Abstract

With the urgent global concerns of climate change, governments, industry and researchers all now place a top priority on the shift to more sustainable energy technology. Fuel cells have emerged as an alternative to conventional sources of power, due to their ability to generate electricity with high efficiency and low emissions. Fuel cells are electrochemical devices that directly convert the chemical energy from fuels like hydrogen into electrical energy with high conversion efficiencies. Among various fuel cells, proton exchange membrane fuel cells (PEMFCs) have gained popularity and one of the important aspects of PEMFC is to maintain ideal operating conditions, particularly temperature for its effective operation. A numerical simulation has been conducted to analyze the temperature distribution within rectangular cooling plates with active area of 4437mm$^2$. The performance of channels with varying width of channels, rib and header is evaluated in terms of temperature uniformity index, temperature difference and pressure drop for 15 different cases. The results show that the geometrical variations of the cooling plate play a crucial role in maintaining a uniform temperature. It was observed that the temperature uniformity index and the temperature difference decreased by approximately 30% for a higher channel-to-rib (CR) ratio compared to the base case with a smaller CR ratio. Additionally, the pressure drop for a higher CR ratio was lower than that of the other cases. To further improve the temperature distribution, design modifications were made by introducing pins at various locations in the header's inlet and outlet for 9 different cases. Although the impact of the pins was minimal due to the relatively small header size, the maximum temperature recorded was still lower than that of the baseline cases. Consequently, improved cooling performance can be effectively achieved by varying the channel geometry across the plate in parallel straight channels and through further design adjustments, such as strategically incorporating pins.

# Acknowledgements

I would like to express my deepest gratitude to my advisor, Dr. Xianguo Li, for his unwavering support, valuable insights and guidance throughout this journey. His knowledge and patience have played a key role in shaping this research and helping me work through any challenges.

I am grateful to my colleagues in Fuel Cell and Green Energy Lab for their collaboration, support and the discussions we shared. Their input has been invaluable in the completion of this work. I would like to thank Pramoth Varsan Madhvan for his assistance and support throughout my research; and Amirhossein Amirsoleymani in setting up the simulation environment used in this research.

My sincere thanks to my parents and siblings for their unconditional love and understanding throughout my life. I extend my gratitude to my husband for his never-ending moral support and encouragement.

# Table of Contents

**Author's Declaration……... ii**

**Abstract……... iii**

**Acknowledgements…….. iv**

**List of Figures…….. vii**

**List of Tables…… x**

**1. Introduction……... 1**

**1.1 Background…… 1**

**1.2 Principle of Proton Exchange Membrane Fuel Cells (PEMFCs)……... 3**

**1.3 Heat Generation and Heat Removal…… 7**

**1.4 Cooling Techniques in PEMFC…… 12**

1.4.1 Air Cooling……... 13

1.4.2 Heat Spreaders…….. 13

1.4.3 Phase Change Cooling…….. 16

1.4.4 Liquid Cooling…….. 17

**1.5 Cooling Channel Geometry…… 18**

**1.6 Objective and Scope of Thesis Research……... 20**

**2. Literature Review…….. 22**

**3. Methodology……... 41**

**3.1 Geometric Model……... 41**

**3.2 Assumptions……...… 50**

**3.3 Model Formulation……... 51**

**3.4 Calculations and Numerical Procedure……... 55**

3.4.1 Temperature Difference between Minimum and Maximum Temperature 55

3.4.2 Temperature Uniformity Index, $U_T$…… 55

3.4.3 Pressure Drop……. 56

3.4.4 Numerical Procedure…….. 56

**3.5 Grid Independency…….. 57**

**3.6 Model Validation……. 58**

**4. Results and Discussion……. 60**

**4.1 Temperature Distribution and Pressure Drop…….. 60**

**4.2 Design Modification…… 75**

**5. Conclusions and Recommendations for Future Work…….. 78**

**5.1 Conclusions……...… 78**

**5.2 Recommendations for Future Work…….. 79**

**REFERENCES……... 80**

# List of Figures


**Figure 1:** (a) Schematic of Proton Exchange Membrane Fuel Cell Stack, (b) Components [4, 5]……. 2

**Figure 2:** Operating principle of PEMFC [18, 19]……... 4

**Figure 3:** Variations of heat generation and power generation with current densities for a PEMFC [24]……. 6

**Figure 4 :** The output of PEMFC [9]……. 8

**Figure 5:** Polarization characteristics of a typical PEMFC [31]……... 10

**Figure 6:** A representative temperature profile of different components of PEMFC with typical heat generation values along the channel region [33]……... 11

**Figure 7:** Main cooling strategies of PEMFC [37]……... 12

**Figure 8:** Schematic representation of working concept of conventional heat pipe [49]….. 15

**Figure 9:** The liquid cooling circuit schematic of a PEMFC [54]……. 17

**Figure 10:** Cooling channel geometry of a PEMFC [57]……... 19

**Figure 11:** Schematic view of cross-flow PEMFC design (a) without and (b) with cooling channels and main components [68]…… 23

**Figure 12:** (a) Cross section representation of geometry with no cooling, (b) Geometry with cooling, (c) Variation of temperature and $H_2O$ mass fraction with $H_2$ flow rates [69]……..... 24

**Figure 13:** (a) Schematic of a developed geometric model of parallel serpentine design, (b) Coolant temperature increment and maximum temperature difference within the bipolar plate versus coolant flow rate per cell [70]…….. 25

**Figure 14:** Two flow field designs for a cooling plate (a) straight channel, (b) zigzag channels, (c) close view of a zigzag configuration [61]…… 26

**Figure 15:** (a) Maximum surface temperature of models A and B at the center-plane of the cooling plate (Re = 330, volume flow rate = $6 \times 10^{-6}$ $m^3/s$), (b) Maximum surface temperature of models A and B at the center-plane of the cooling plate with heat flux = 4255 $W/m^2$ [61]…….. 26

**Figure 16:** Six cooling channel flow fields: (a) conventional serpentine, (b) typical of MPSFF, (c) typical of serpentine, (d) parallel serpentine, (e) conventional spiral, (f) conventional parallel [72]……. 27

**Figure 17:** (a) Temperature uniformity indices and catalyst-membrane interface temperature ranges for different cooling plates at V = 0.6 V and Re = 400, (b) Pressure drop through the cooling plate versus Reynolds number [72]…… 28

**Figure 18:** Configurations of flow channels in the cooling plate [74]…… 29

**Figure 19:** (a) Variation of maximum surface temperature according to Reynolds number, (b) Temperature difference between the inlet and outlet of the cooling plate according to Reynolds number, (c) Pressure drop through the cooing plate as a function of Reynolds number [74]…… 29

**Figure 20:** (a) Six serpentine flow-fields used as coolant channels, effect of flow velocity on performance of cooling plates: (b) surface temperature difference, (c) temperature uniformity index, $U_T$ [75]…….. 31

**Figure 21:** Six different cooling channel fields: (a) parallel, (b) serpentine in the beginning, (c) serpentine in the middle, (d) serpentine at the end, (e) horizontal serpentine, (f) four section serpentine [76]……. 32

**Figure 22:** (a) Average temperature of the membrane mid-plane, (b) Average temperature of the anode and cathode terminals, (c) Outlet temperature of the cooling fluid, (d) Maximum temperature of the membrane mid plane. (i) parallel, (ii) serpentine in the beginning, (iii) serpentine in the middle, (iv) serpentine at the end, (v) horizontal serpentine, (vi) four section serpentine [76]……... 33

**Figure 23:** Effect of heat flux on (a) maximum temperature, (b) pressure drop [77]……. 34

**Figure 24:** Variations in cooling channel geometry [78]……... 35

**Figure 25:** (a) Maximum cell temperature difference variation with different ridge width and heat flux densities, (b) Maximum cell temperature difference variation with different channel depth and heat flux densities, (c) Maximum cell temperature difference variation with different aspect ratios and heat flux densities [78]…..... 36

**Figure 26:** Coolant channel designs: (a) conventional parallel, (b) conventional serpentine, (c) oblique-fins, (d) coiled, (e) parallel-serpentine, (f) novel hybrid parallel-serpentine-oblique-fins channel designs [79]……... 37

**Figure 27:** Temperature distribution at the middle of the cathode catalyst layer (a) conventional parallel, (b) conventional serpentine, (c) oblique-fins, (d) coiled, (e) parallel-serpentine, (f) novel hybrid parallel-serpentine-oblique-fins channel designs at coolant inlet Reynolds ~600 and cell voltage = 0.7 V [79]…. 37

**Figure 28:** Three coolant flow field designs for a large-scale cooling plate. (a) parallel flow field, (b) parallel serpentine flow field along Y-axis, (c) parallel serpentine flow field along X-axis [80]……. 38

**Figure 29:** Different configurations of flow fields (a) Novel A, (b) Novel B, (c) serpentine channel [81]……. 39

**Figure 30:** (a) Variation of temperature difference, (b) Variation of average temperature, (c) Variation of temperature uniformity index, (d) Variation of pressure drop of different cooling channels with varying flow rate [81]……. 39

**Figure 31:** Typical unit cell of PEMFC and computational domain [61]……... 41

**Figure 32:** Geometry of cooling plate used in the numerical simulation…… 42

**Figure 33:** Schematic representation of cooling plate and heat slab..……. 42

**Figure 34:** Heat slab for the heat flux boundary ……... 44

**Figure 35:** **(a):** Coolant flow field design with CR = 1, **(b):** Coolant flow field design with CR = 3.125, **(c):** Coolant flow field design with CR = 0.329, (**d):** Coolant flow field design with CR = 1.69, **(e):** Coolant flow field design with CR = 0.14……..... 46

**Figure 36:** (a) Location of pins with CR ratio of 3.125, (b) pin location 1, (c) pin location 2, (d) pin location 3……... 49

**Figure 37:** Grid independency for channel width 1.5mm against maximum temperature and pressure drop……. 57

**Figure 38:** Evolution of pressure along the channel length…… 58

**Figure 39:** Temperature distribution for case 1 to case 15……. 60

**Figure 40:** Normalized mass flow distribution for different cases…….…… 66

**Figure 41:** Temperature difference against channel width and header width……. 67

**Figure 42:** $U_T$ against channel width and header width…….. 67

**Figure 43:** (a) $U_T$ Vs channel width for header 1 mm, (b) $U_T$ Vs channel width for header 2 mm, (c) $U_T$ Vs channel width for header 3 mm……. 68

**Figure 44:** Pressure drop along the channel for case 1 to case 15…….. 69

**Figure 45:** Pressure drop against channel width and header width……. 74

**Figure 46:** Temperature difference against pin location and header width…… 75

**Figure 47:** $U_T$ against pin location and header width……. 76

**Figure 48:** Pressure drop against pin location and header width……... 76

# List of Tables

**Table 1:** Different cases with variation in CR ratio and header width……. 45

**Table 2:** Different pin locations with CR ratio pf 3.125 and varying header width……... 48

**Table 3:** Parameters used for cooling plate simulation……. 53

**Table 4:** Operating conditions of the computational domain……... 54

**Table 5:** Boundary conditions of 3D model……. 54

# 1. Introduction

## 1.1 Background

The need for clean and efficient sources of energy has never been greater, as the world faces increasing environmental and economic challenges related to climate change, air pollution and energy security. Amidst these urgent global concerns, governments, industries and researchers have made the transition to sustainable technology a top priority. Fuel cells have emerged as a promising alternative to conventional sources of energy such as fossil fuels, nuclear power, and traditional batteries, due to their ability to generate electricity with high efficiency, low emissions, and versatile fuel options [1]. Fuel cells are electrochemical devices that directly convert chemical energy from fuels like hydrogen into electrical energy with an overall efficiency of about 80%. Furthermore, they have the potential to significantly diminish the emissions of major pollutants such as carbon dioxide ($CO_2$), nitrogen oxides (NOx), and sulphur oxides (SOx), achieving reductions of over 90%.[2]. Extensive research has been conducted on various types of fuel cells. Proton Exchange Membrane Fuel cells (PEMFC) are one type that uses polymer electrolyte membranes, such as Nafion, as a proton conductor and platinum-based material as catalyst [3]. PEMFCs consist of a central component known as the Membrane Electrode Assembly (MEA). The essential constituents of the MEA include proton exchange membranes (PEMs), catalyst layers (CL), gas diffusion layers (GDL), and bipolar plates, which extend from the central region to the outer sides, as illustrated in Figure 1 (a) and (b) [4,5]. These fuel cells are notable for their low operating temperature and high-power density. As a result, they are considered a promising option for various applications, including transportation, stationary and portable uses [6].

However, one of the important aspects of PEMFC is to maintain ideal operating conditions, particularly temperature for its effective operation. The membrane and catalyst may deteriorate much more quickly at PEMFC stacks' high working temperatures, which would lower the stack's performance. Thermal management becomes more complicated for applications with high output power (>= 10 kW), as a large amount of heat is produced during their operation [7]. Hence, thermal management is very crucial for maintaining optimal performance and longevity of PEMFCs. This would ensure uniform distribution of temperature across the membrane, preventing hot spots and enhancing the overall efficiency of the fuel cells [8]. To ensure that the desired temperature is maintained inside the cell, the heat generated as the byproduct must be removed from the fuel cell stack.

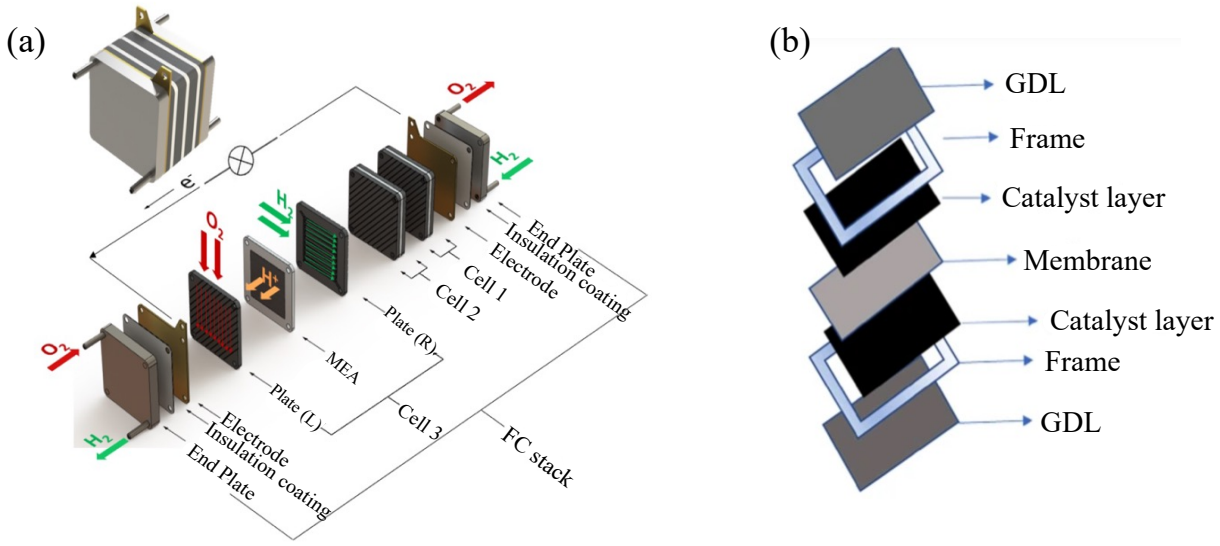



**Figure 1:** (a) Schematic of Proton Exchange Membrane Fuel Cell stack, (b) Components [4,5]

To achieve effective thermal regulation, several heat management strategies can be employed, including edge cooling, separate airflow cooling, air cooling, cooling via the cathode air supply, phase change cooling, and liquid cooling. These methods are crucial to maintain the optimal temperature of the PEMFC ensuring long-term durability [9]. The selection of cooling methods for PEMFCs depends on several key factors which include fuel cell power output, the complexity of the system, overall cost considerations, specific applications and the amount of heat that can be removed. Each of these factors plays an important role in determining the most suitable cooling strategy as it directly impacts the overall performance of the fuel cell system. For smaller applications, cost and complexity limits might call for simpler procedures, whereas larger fuel cells may demand more advanced cooling techniques [10]. The most common cooling technique employed in PEMFC systems involves either liquid or air as the cooling medium, with the implementation of forced circulation convection [11]. This is typically done through specially designed coolant plates or channels. In some cases, edge cooling methods are used with or without the addition of fins to enhance heat dissipation. In general, liquid coolants are more effective than air or gases in transferring heat at the same pumping power due to their higher thermal conductivity and greater heat capacity [12]. As a result, liquid cooling systems are more efficient at removing heat, making them the preferred choice in high-power PEMFC stacks, especially those exceeding 10 kW. This is particularly relevant in automotive applications, where effective thermal management is essential for maintaining the fuel cell's performance and durability under high load

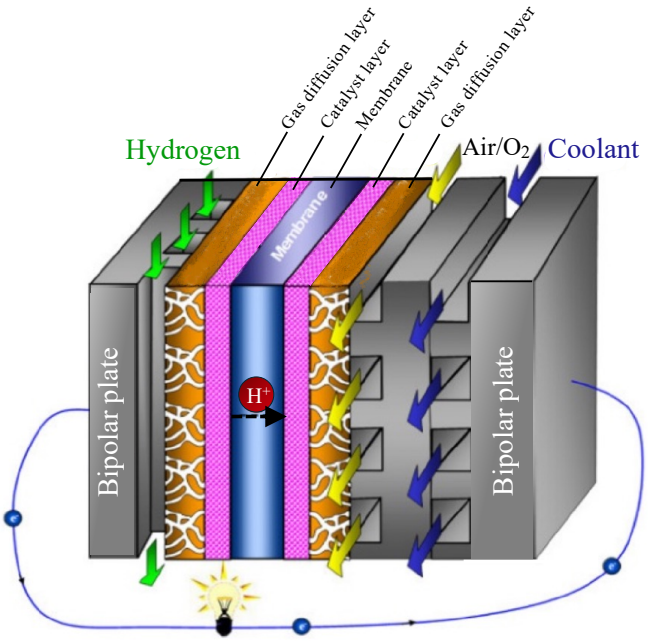
conditions. Liquid cooling ensures that the fuel cell operates within safe temperature ranges, minimizing the risk of overheating and extending the overall lifespan of the system [13].

In liquid cooling systems for PEMFCs, the heat transfer process begins at the MEA, where heat generated during the electrochemical reaction is transferred from the fuel cell to the bipolar plates [14]. The bipolar plates serve as a conductor of heat, allowing the generated heat to pass through and enter the cooling channels. These channels can either be designed in the bipolar plate or can be separate from the fuel cell's active components. Cooling channels carry the coolant- typically water or a coolant mixture through the stack. As the coolant flows through the channels, it absorbs the heat from the fuel cells, raising the temperature of the coolant. Once the coolant reaches its maximum temperature or thermal capacity, it is pumped out of the stack and directed to a heat exchanger. The heat exchanger is responsible for transferring the heat from the coolant to another medium, such as air or water, that can then dissipate the heat to the surrounding environment [15]. Water as a coolant is most commonly used to transfer heat from the fuel cell stack to the cooling channels, ensuring effective thermal management and therefore preventing overheating. Its heat transfer properties, like high thermal conductivity (0.644 W/mK) and specific heat capacity (4181 J/kgK), make it more effective than air or other gases in managing the heat generated in a fuel cell stack [16]. These advantages combined with less pumping power requirement, make water-based cooling systems particularly suitable for high-power PEMFC applications.

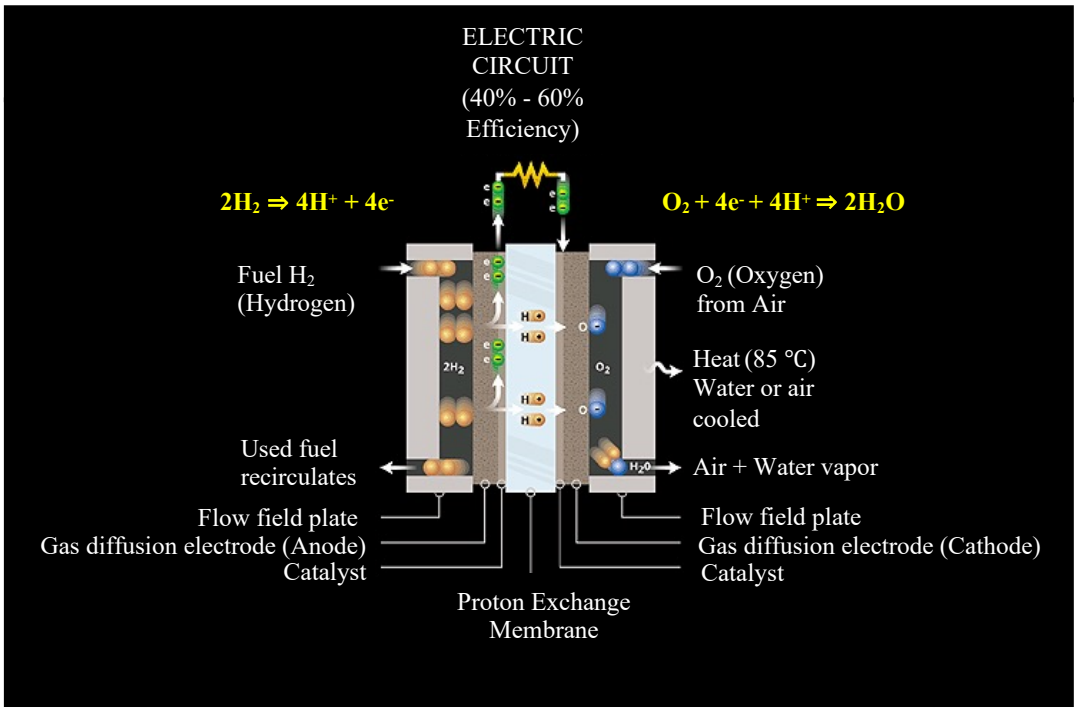
There have been multiple studies that have focused on improving liquid cooling performances by altering the flow field design and the cooling channel geometry. Among the various cooling channel designs, parallel channels are often preferred due to their ability to ensure uniform temperature distribution and reduce pressure drop [17]. While numerous studies explore the impact of different flow channel designs on heat distribution, few address the influence of the solid and liquid material distribution within the cooling plate and channels. This study focuses on examining how the thermal and physical properties of materials affect heat dissipation by strategically arranging parallel channels. Additionally, this study covers the effect of input and output geometry parameters that would influence the flow and the temperature uniformity of the cooling plate.

## 1.2 Principle of Proton Exchange Membrane Fuel Cells (PEMFCs)

PEMFCs are one of the main ways to lessen global reliance on fossil fuels, particularly in the transportation industry. PEMFCs operate based on electrochemical conversion of hydrogen and oxygen into electricity, water and heat.




(a)




(b)

**Figure 2:** Operating principle of PEMFC [18,19]

Multiple fuel cell units linked in series create a PEMFC stack. Each cell is composed of four main structural components: PEMs, CL, GDLs and bipolar plates from the center to both sides as shown in Figure 2 [18, 19]. In the working of a PEMFC, pressurized and humidified hydrogen ($H_2$) is

introduced into the anode side via specifically designed flow channels on the bipolar plate. At the anode catalyst layer, hydrogen molecules are split into protons ($H^+$) and electrons ($e^-$) through an electrochemical reaction facilitated by the platinum catalyst. Meanwhile, on the cathode side, humidified oxygen ($O_2$) or air is directed into the flow channels and reaches the cathode catalyst layer. Here, the oxygen reacts with the proton, which have crossed the membrane, and the electrons, which travel through an external circuit, to form water ($H_2O$) as the primary byproduct [20]. The proton exchange membrane in a fuel cell needs to remain fully hydrated to function effectively as electrolyte. To prevent the membrane from drying out due to water evaporation, both the fuel (hydrogen) and oxidant (oxygen or air) streams are typically humidified to 40% - 100% relative humidity. This ensures adequate moisture is maintained for optimal membrane performance and longevity.

At the anode catalyst layer, hydrogen undergoes electrooxidation with the production of protons and electrons.

$$H_2 \rightarrow 2H^+ + 2e^- \quad (1)$$

Protons are migrated from anode to cathode through proton exchange membrane in the form of hydronium ions $(H_2O)_\xi H^+$, where $\xi$ is the number of water molecules per proton. On the other hand, electrons generated at the anode are compelled to travel through an external electrical circuit. As the membrane electrolyte has high resistance to electron flow and very low resistance to proton motion, these electrons perform work on the load simultaneously [21].

At the cathode catalyst layer, oxygen or air molecules, which are supplied from the oxidant flow channels, react with the protons($H^+$) and electrons($e^-$) generated from the anode catalyst layer.

$$\frac{1}{2}O_2 + 2H^+ + 2e^- \rightarrow H_2O \quad (2)$$

This reaction results in the formation of water ($H_2O$) as the main product. The combination of oxygen, protons, and electrons at the cathode is a crucial part of the electrochemical process, completing the circuit and allowing the fuel cell to generate continuous electrical power [22].

Consequently, the overall cell reaction is obtained by combining the two half-cell reactions:

$$H_2 + \frac{1}{2}O_2 \rightarrow H_2O + \text{Electrical energy} + \text{Heat} \quad (3)$$

Water formed at the cathode catalyst layer in PEMFCs, seeps into the GDL, making water removal and control critical for optimal performance. Further, during the conversion process some energy is inevitably lost as waste heat. The energy released during this reaction at 298 K is referred to as the standard enthalpy of formation, which for a single cell is given by the following equation:

$$q'' = (E_{th} - E_{cell}) \times i \quad (4)$$

where $E_{th}$ is the thermoneutral voltage that gives the voltage at which all the chemical energy is converted into electrical energy without any heat generation, i is the current density ($A/cm^2$), and $E_{cell}$ is the cell working voltage (V) [23]. The power density, P in fuel cells is defined by Equation 5:

$$P = E_{cell} \times i \quad (5)$$

As can be seen from equations 4 and 5, at higher current densities, the heat generation rates in PEMFCs surpass that of power generation. This is also evident from Figure 3 [24].

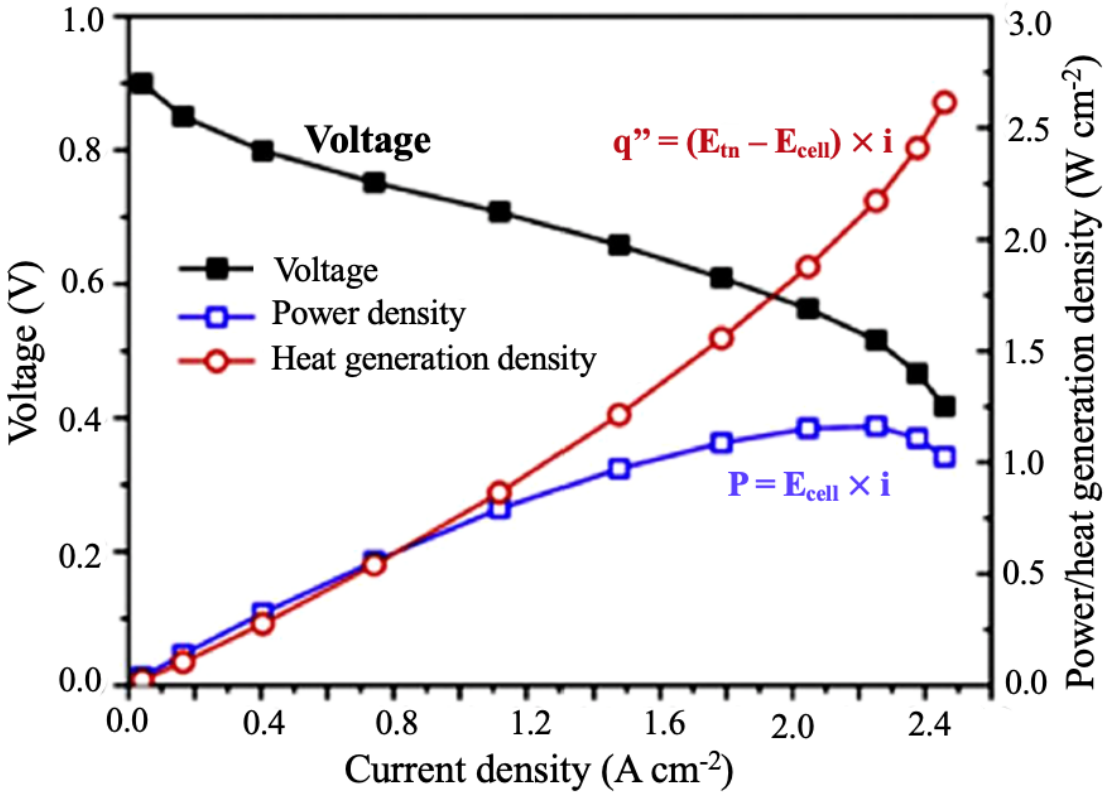



**Figure 3:** Variations of heat generation and power generation with current densities for a PEMFC [24]

Excessive temperature in a PEMFC can cause irreversible damage to the proton exchange membrane, leading to dehydration, or rupture, which reduces proton conductivity and disrupts the electrochemical reaction. While higher temperatures can reduce voltage losses and improve cell voltage, they can also create hotspots on the bipolar plates, accelerating the degradation of the CL and membrane. On the other hand, low temperatures slow down the reaction kinetics, reducing power generation efficiency and potentially causing water flooding due to low saturation pressure. High-temperature operation and localized hotspots are significant factors in material degradation, affecting the durability of the fuel cell [24]. This brings to light the importance of thermal management in a fuel cell stack. Thermal management focuses on keeping the stack's temperature within an optimal range while ensuring consistent temperature distribution across the stack and its components. Overall, an effective thermal management of PEMFCs is essential to ensure high performance and longevity, as it plays a significant role in determining the overall power output of the stack [25]. Hence, it is of utmost importance to explore and investigate various cooling techniques to regulate the temperature within the fuel cell stack. Evaluating multiple approaches, such as active and passive cooling systems, and the importance of flow field patterns in the cooling process can help develop more efficient strategies to enhance the overall functionality and durability of PEMFCs.

## 1.3 Heat Generation and Heat Removal

As mentioned earlier, one of the major challenges in PEMFCs is managing the heat generated during operation and efficiently removing it from the stack. This heat is result of the electrochemical reactions occurring within the fuel cells, where the actual operating voltage is often lower than the thermo-neutral voltage [26]. Given this heat production, the energy conversion efficiency of PEMFCs is practically limited to 50%, as part of the heat is lost as heat rather than being converted to usable electrical energy, as is mentioned in Figure 4 [9].

PEMFCs are usually made to operate at an average cell voltage, E of between 0.6 - 0.7 V. The thermal neutral cell voltage, $E_{tn}$ for pure hydrogen fuel reacting with oxygen to form product water is 1.48 V, if the product water is in liquid form (HHV) and 1.25 V if it is in vapor form (LHV). Consequently, the chemical to electrical energy efficiency is given by [22]:

$$\eta = \frac{E}{Etn} = 48\sim56\% \tag{6}$$

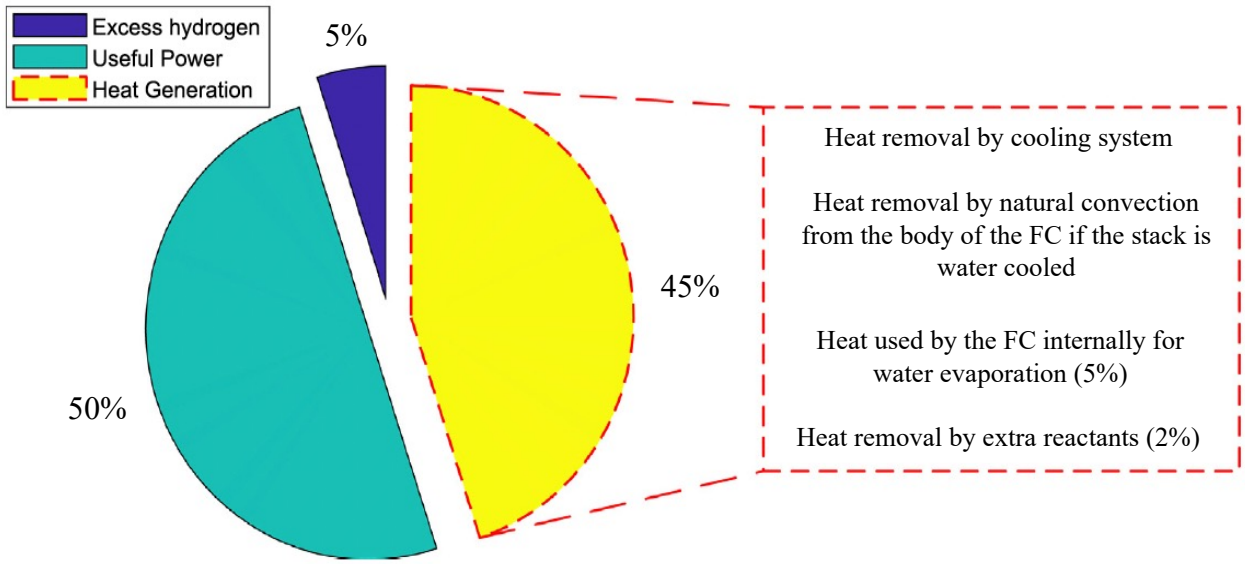



**Figure 4:** The output of PEMFC [9]

The remaining chemical energy is transformed into sensible thermal energy, also known as the fuel cell's waste heat. Hence, the amount of waste heat produced is approximately equal to the electrical power output of the stack.

Heat generation in PEMFCs occurs due to the following:

[1] Reversible heat of electrochemical reaction (entropic heat): The reversible heat in a PEMFC represents the difference between the total chemical energy contained in the reactants (hydrogen and oxygen) and the maximum amount of useful energy that can be extracted according to the second law of thermodynamics. To maintain a constant operating temperature during the fuel cell's operation, it is crucial to manage this heat effectively [27].

[2] Irreversibility of reactions: The irreversible heat in a PEMFC arises from the inefficiencies and losses that occur during the electrochemical reactions. In the fuel cell, the splitting of the overall chemical reaction into half-reaction at the anode and cathode creates local heat [24]. At the anode, hydrogen molecules are oxidized, releasing protons and electrons whereas at the cathode, oxygen reacts with protons and electrons to form water. However, due to various losses such as activation losses (energy required to initiate the reaction), the reactions at both electrodes are not perfectly efficient. These inefficiencies produce irreversible heat, which accumulates in the PEMFC stack.

[3] Ohmic resistance: Ohmic heat in a PEMFC primarily arises due to the resistance to the ions and electrons through the various cell components. High ohmic resistance not only increases

heat production but also reduces the overall efficiency of the PEMFC [28]. To minimize ohmic heat, it is crucial to design PEMFCs with materials that exhibit high electrical conductivity and high ionic conductivity.

[4] Heat from water vapor condensation: The heat released from water vapor condensation in a PEMFC occurs when water is produced as a byproduct of the electrochemical reactions at the cathode. As the hydrogen and oxygen combines to form water, some of this water exists in the form of vapor. When the water vapor condenses into liquid form within the cell, it releases latent heat. However, the heat generated from water vapor condensation is typically much less significant than other heat sources in PEMFC [29].

In general, the summation of entropic heat, irreversible heat and ohmic heat account for 55%, 35% and 10% of the total heat, which is comparable to the total power of stack [26]. To understand the heat generation in a fuel cell, an energy balance must be performed. This energy balance helps explain how the reactants chemical energy is transformed into waste heat and valuable electrical energy. In fuel cells several approaches can be used to establish this balance, depending on the level of detail and complexity required. The heat generated rate ($Q_{gen}$) can be mathematically represented using specific equations. In general, the total energy converted into heat and electricity is governed by the fuel cell's performance parameters as shown in equation 7:

$$\frac{I}{2F} \times H_{HHV}\, n = Q_{gen} + I\, V\, n \tag{7}$$

Hence, the heat generation rate ($Q_{gen}$) in a fuel cell can be determined using equation 8, which is based on the high heating value (HHV) of the fuel [30].

$$Q_{gen} = \frac{I}{2F} \times H_{HHV}\, n - I\, V\, n \tag{8}$$

I is the current density, V is the cell voltage, n is the number of cells in the stack, F is Faraday's constant (96485 C/mol).

Heat generation can also be calculated using the potential losses for the PEMFC stack. Figure 5 [31] shows a typical polarization curve for the cell potential as a function of current density. The cell potential stays equal to the reversible cell potential in the ideal VI relationship, regardless of the current extracted from the cell. It's been found that actual cell potential is smaller than reversible cell potential and decreases as the current drawn is increased due to the three mechanisms of irreversible losses: activation, ohmic and concentration. Activation polarization

($\eta_{act}$) occurs due to the slow rate of electrochemical reactions, and it requires additional energy to accelerate the reactions to meet the required current demand. Thus, a portion of the energy is lost in meeting the current demand, leading to voltage loss.

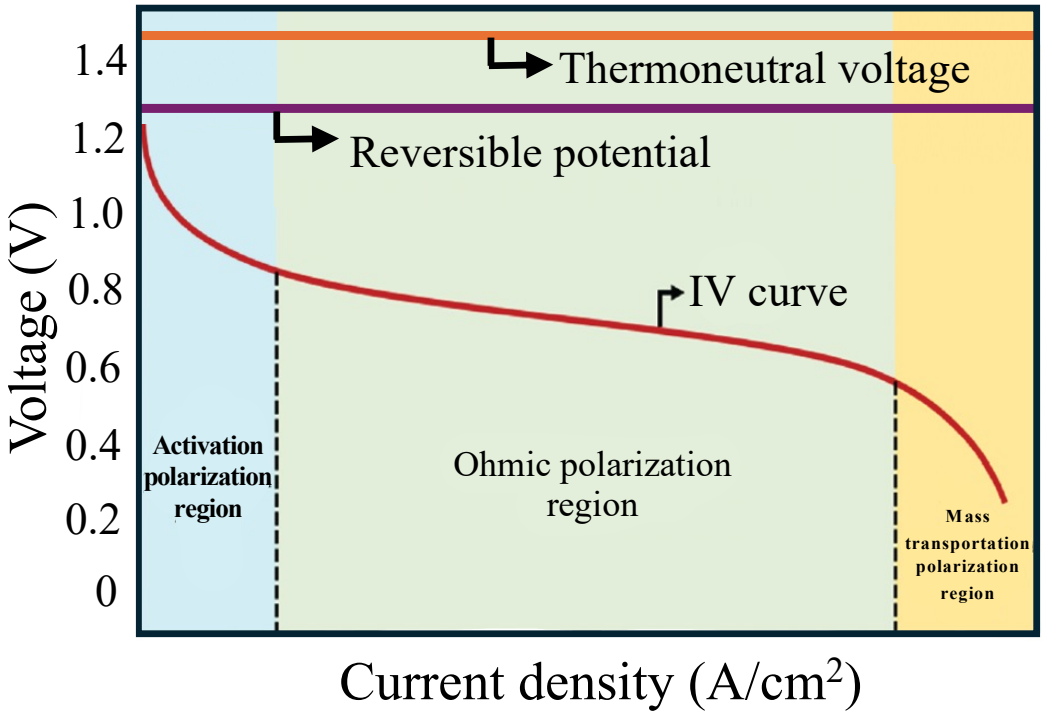



**Figure 5:** Polarization characteristics of a typical PEMFC [31]

Ohmic polarization ($\eta_{ohm}$), on the other hand, results from resistance to the flow of ions and electrons within the fuel cell. Ohmic losses are usually linearly proportional to the current flowing through the cell, and reducing these losses requires highly conductive materials and optimal hydration of the membrane for efficient ion flow [22]. Concentration potential ($\eta_{conc}$) arises due to limitations in mass transport. As the electrochemical reactions proceed, reactants like hydrogen and oxygen get consumed, and the products (such as water) can accumulate. If the supply of reactants to the reactant sites becomes insufficient or if the products block the access of fresh reactants to the reaction sites, the fuel cell performance suffers. This type of polarization typically occurs at higher current densities when the demand for reactants exceeds the rate at which they can be supplied, causing a reduction in voltage as the cell struggles to maintain reaction rates [32]. A schematic of the temperature profile in a PEMFC shows the non-uniform distribution across different components, highlighting localized variations in heat generation along the flow channel, as shown in Figure 6 [33]. The schematic is for a 50 $cm^2$ single cell operating at 1 A $cm^{-2}$ and

0.6 V. However, real world commercial systems nowadays typically achieve current densities in the range of 1.0 to 2.0 A/cm$^2$. As the current density increases, there could be various aspects that are needed to be considered. With increasing the current density, the fuel cell efficiency decreases along with the decreasing fuel cell voltage and the amount of heat which has to be removed from the system increases super proportionally, which poses challenge in the thermal management [34]. This highlights the need for continued research and technological advancements to enhance the performance of PEMFCs. The variations in components are critical for optimizing thermal management and ensuring efficient performances.

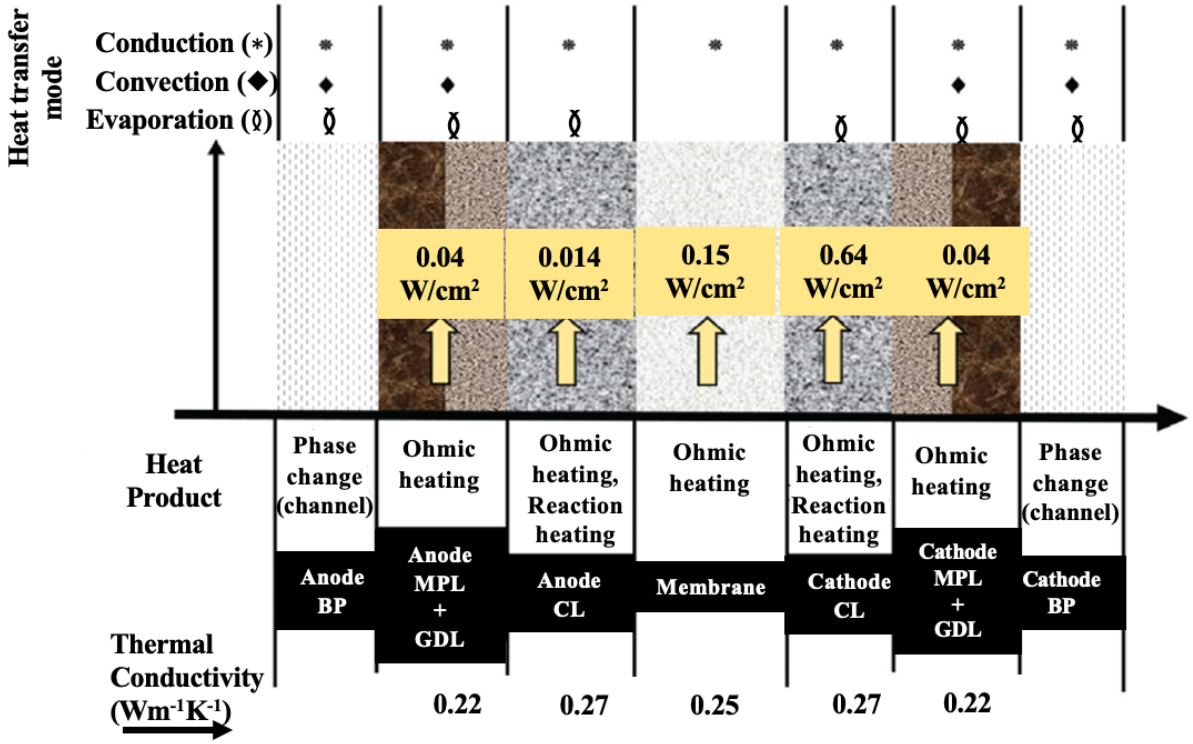



**Figure 6:** A representative temperature profile of different components of PEMFC with typical heat generation values along the channel region [33]

The above discussion shows that the actual cell potential E is lower than the reversible potential $E_r$ [35]. Therefore,

$$E = E_r - (\eta_{act} + \eta_{ohm} + \eta_{conc}) \quad (9)$$

The loss of potential leads to a decrease in the overall efficiency of the fuel cell. Effective cooling techniques can help reduce these losses by maintaining an optimal temperature, improving reaction kinetics, and decreasing resistive losses in PEMFC.

## 1.4 Cooling Techniques in PEMFC

Cooling systems are fundamentally designed to maintain the operating temperature and uniform temperature distribution inside the stack, as this directly affects the performance and durability of PEMFCs. Various cooling strategies are proposed to achieve this goal. Studies shows that thermal management systems account for around 8% of the cost of PEMFC stack [36]. Figure 7 [37] shows the classification of conventional PEMFC cooling system, and the choice of the cooling strategy depends on various factors. Some of the factors includes the power capacity of the system, the rate at which heat needs to be removed and the specific needs of the application.

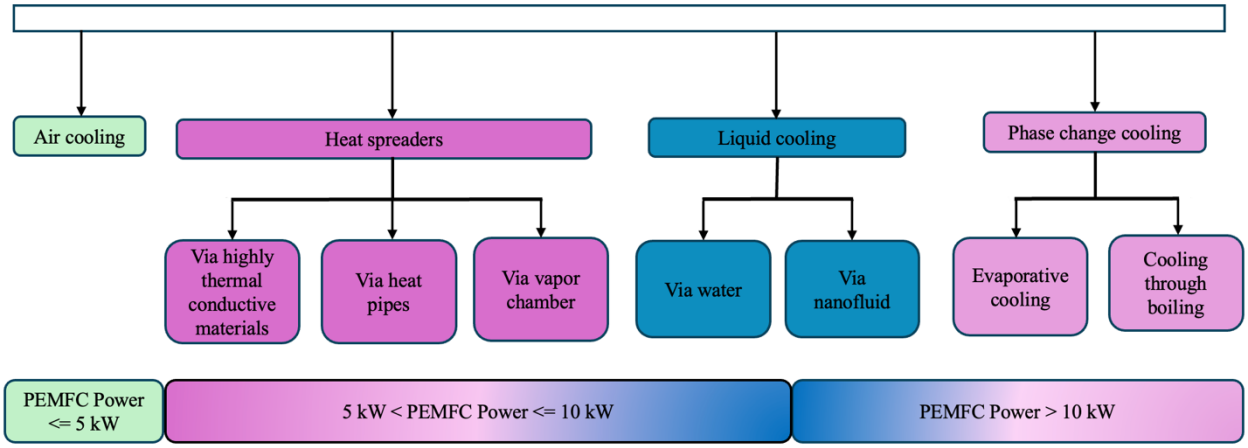



**Figure 7:** Main cooling strategies of PEMFC [37]

Additionally, the intensity of heat generation, environmental conditions and system integration all play a significant role in choosing the most effective thermal management approach. Overall, it could be said that there are two type of cooling techniques: Active and Passive techniques. Active cooling involves the use of external energy-driven components such as coolant pumps, fans or refrigeration systems to enhance the dissipation process. Whereas passive cooling refers to the use of natural heat transfer methods that rely on the principles of conduction, convection and radiation to dissipate heat. Although passive cooling is simple to execute and has high energy conversion efficiency, but it has low cooling efficiency as compared to active cooling [38]. Further, different thermal management techniques can be applied, including air cooling, heat spreaders, liquid cooling and phase change cooling.

### 1.4.1 Air Cooling

Air cooling represents one of the most straightforward methods of cooling in PEMFCs; however, it is less efficient compared to alternative cooling techniques. This inefficiency arises from the relatively low thermal capacity of air, which limits its ability to absorb heat in comparison to other coolants, such as water or specialized liquids. To mitigate the effects of this low thermal capacity, it is necessary to circulate a substantial volume of air to effectively dissipate heat, thereby increasing the pumping power required to transport the air throughout the system. Consequently, this also incurs an additional cost [39].

Moreover, if the cooling air is passed through the cathode flow channels, it can cause an excessive air flow rate at the cathode. This leads to several issues, such as the need for larger cathode flow channels, which can complicate the design and reduce the space for effective electrochemical reactions [40]. Additionally, the high air flow can carry away excessive electrolyte vapor, potentially harming the electrolyte balance and shortening the fuel cell's lifespan. In some cases, the electrolyte may need to be replenished more frequently.

To address these issues, a separate cooling plate with its own cooling channels may be incorporated into the design. However, even with this added complexity, air cooling is often used for smaller fuel cell stacks where the cooling demands are lower, and the simplicity of the system is more advantageous [41]. This method incorporates natural convection at the bipolar plate surface for heat dissipation. However, the size of air channels plays a significant role in determining the effectiveness of air cooling. Additionally, the study explored how different flow channel configurations, such as serpentine, parallel, spiral, divided spiral, and distributed spiral, impact the thermal characteristics of air-cooled PEMFCs. Modifications in these channel designs affect the uniformity of heat removal, influencing the overall performance and efficiency of the cooling system.

### 1.4.2 Heat Spreaders

This method, commonly referred to as edge cooling, presents numerous advantages, including a compact design, diminished parasitic losses, and the obviation of circulation systems. Edge cooling operates on the principle of heat dispersion, whereby heat is dissipated from the fuel cell through distribution across the edges or surfaces rather than employing more intricate cooling mechanisms such as pumps or fans. This approach renders the system simpler and markedly more energy efficient. Specifically, the implementation of thermal management utilizing heat spreaders proves

to be particularly effective for PEMFCs characterized by larger active areas and functioning at temperatures surpassing 373 K [42]. According to this study, as the operating temperature increases, heat management using spreaders or high-conductivity materials becomes more feasible, improving overall system performance. Bipolar plates, GDL, and MEA are typically made from highly thermally conductive materials, which allow heat to spread efficiently across the surface and are used as heat spreaders. Different materials with high thermal conductivity can be used for bipolar plates as heat spreaders. Copper is widely used for its exceptional thermal conductivity (400 W $m^{-1}$ $K^{-1}$) and is commonly employed as a heat spreader [43]. Aluminum, with a conductivity of 200 W $m^{-1}$ $K^{-1}$, is favoured for compact stacks due to its optimal conductivity and density. Graphene and carbon nanotubes (CNTs), with thermal conductivities ranging from 300 to 500 W $m^{-1}$ $K^{-1}$, are also used as high-rate heat spreaders [44]. Additionally, pyrolytic graphite (1000 W $m^{-1}$ $K^{-1}$) and low-density graphite (600 W $m^{-1}$ $K^{-1}$) provide excellent heat-spreading capabilities [45]. Hybrid materials like CNT/carbon fibre/graphite-filled polycarbonate are also utilized for low-temperature PEMFCs, offering improved thermal efficiency when the fillers approach their percolation threshold. The GDL in PEMFCs is crucial for heat management, but its anisotropic thermal and electrical conductivity makes it challenging to accurately measure and model the heat distribution within the cell [46]. The microporous layer (MPL), often integrated with the GDL, tends to experience higher temperatures, especially where product water undergoes phase transitions, which further complicates thermal regulation. Research has shown that increasing the filler content in GDLs, such as the addition of materials like carbon or graphite, can improve its thermal conductivity, but only within a certain range. Beyond this range, the benefits diminish or lead to material degradation [47]. Graphite/aluminum laminate composite-based GDLs have been developed for enhanced thermal performance, with microstructure properties depending on the fractional volume of graphite films. These composite materials show improved heat-spreading characteristics, providing better thermal management for the fuel cell.

Although thermally conductive materials offer advantages in heat dissipation, they also come with many disadvantages. Some of these materials are expensive as well as require complex manufacturing processes, which can increase the overall cost of the system. Further, metals like copper and aluminum are corrosive in nature and may corrode over time, which could compromise their structural integrity and thermal conductivity [48]. The utilization of these materials poses significant challenges, as numerous thermally conductive substances also exhibit electrical

conductivity. This may necessitate the inclusion of supplementary insulation layers when implemented in PEMFCs.

Apart from the thermally conductive materials, heat pipes and vapor chambers can be used for the transfer of heat. The heat pipe cooling technique offers more thermal conductance and is more effective when compared to metals. A conventional heat pipe is composed of an evacuated tube that houses a working fluid, which exists in both liquid and vapor phases, along with a wick structure that assists in the return of the condensed liquid to the evaporating section zone. Further, working fluid vaporizes in the evaporation section when the system is in operation and absorbs latent heat, which is transferred to the condensation section to condense. This condensed fluid is then returned to the evaporation zone via a capillary medium. The schematic of the working concept of the heat pipe is shown in Figure 8 [49].

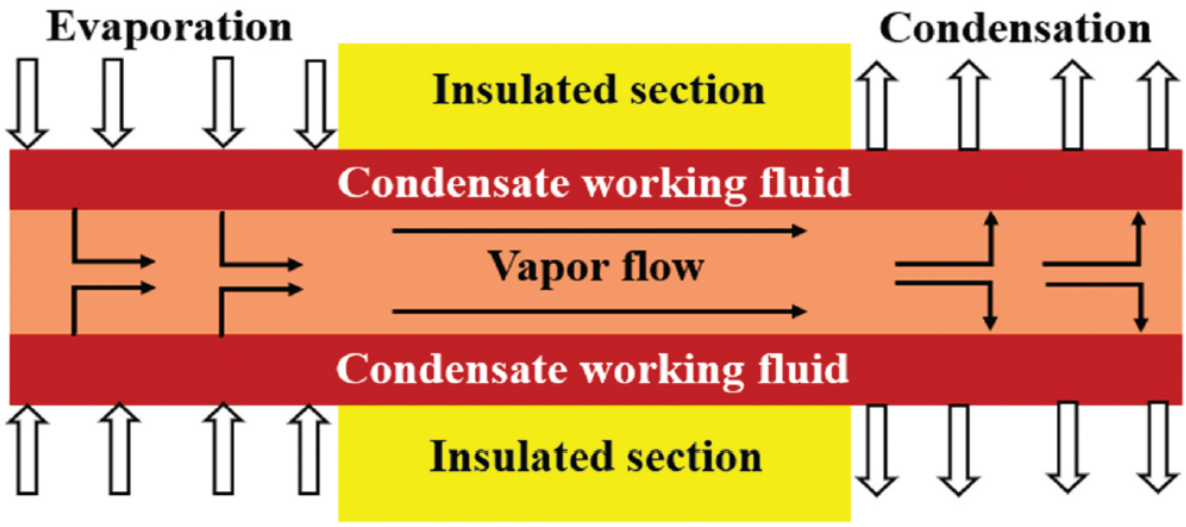



**Figure 8:** Schematic representation of working concept of conventional heat pipe [49]

This technique is particularly suitable for PEMFCs designed for portable fuel cells with low power outputs ranging from 10 to 100 Watts, utilizing micro passive heat pipes. However, for larger PEMFC systems, pulsating heat pipes are employed due to their enhanced efficiency. Hence, these heat pipe techniques help in maintaining optimal operating temperatures of the stack. Anyhow there is higher manufacturing costs linked to heat pipes and potential challenges in maintaining the consistent performance under varying operating conditions.

Vapor chamber is another passive cooling method that operates on the principle of evaporation and condensation. The chamber typically is a sealed and a flat device that contains a small amount of liquid. So, when heat is applied, the liquid inside the chamber absorbs the heat and gets

vaporized. This vapor travels to the cooler region where it condenses back into liquid and releases the heat to the surroundings. The condensed liquid is then dawn back to the heated region through a wick structure (capillary action), completing the cycle. There have been different studies focusing on vapor chamber techniques. Z. Huang et al. [50] investigated this cooling technique and point out the excellent heat dissipation properties of vapor chambers, especially with high power density PEMFC stacks. However, vapor chamber has its own disadvantages when it comes to long term performance degradation due to the working fluid and wick materials issues. The choice of material working fluid is very critical as its properties like boiling point and thermal conductivity should match the temperature range of PEMFC.

### 1.4.3 Phase Change Cooling

Phase change cooling is gaining attention as it does not require any additional circulation power like pump. Basically, cycle is completed using natural hydrophilic wicking. It can also be referred as a method that uses a liquid -to-gas- to- liquid cycle to transfer heat. This technique involves two basic mechanisms i.e. evaporation and condensation. Firstly, liquid water is injected directly into the reactant flow channels. Liquid then absorbs heat from the system and gets evaporated, this also humidifies the PEMFC stack. The exhaust vapor produced in this stage is then directed to a condenser, where it cools and transforms back into liquid form. This liquid is stored in a tank for later use, allowing the system to continuously recycle the cooling medium. This approach enhances efficiency and optimizes the humidification of the stack, which makes it an effective solution for thermal management of PEMFCs [51]. The materials that are used in this process are generally called phase change materials, also referred to as PCM. PCMs can absorb or release large amounts of energy when they undergo a phase change. Some common PCMs used in PEMFC cooling systems include paraffin wax and hydrated salts such as sodium sulphate decahydrate. Water (ice) is used for low temperature applications, while waxes and salts are used for high temperature applications. While this method offers efficient heat removal, it does come with certain challenges such as leaking of the working fluid. This phenomenon may result in a reduction of cooling capacity, ultimately leading to system failure. Furthermore, the instability of two-phase flow and the potential for corrosion of the components of the cooling system are significant concerns that could result in the degradation of materials over time. Additionally, selecting a fluid with suitable thermal properties to accommodate the fluctuating temperature range of the PEMFC presents a considerable challenge [52].

### 1.4.4 Liquid Cooling

As mentioned earlier, the cooling technique chosen for a PEMFC stack depends on its power output. For stacks up to 2 kW, air cooling is commonly used, but as the power output increases, air cooling becomes less efficient due to the higher heat generation associated with increased power. For stacks above 2 kW, liquid cooling techniques are typically employed, as they have proven to be more effective in removing heat and maintaining optimal operating temperatures. For the typical FCEV power output range of around 5 kW to 200 kW, liquid cooling is preferred due to its higher heat removal efficiency and compact design [53]. Additionally, liquid cooling offers better control over the fuel cell's operating temperature, which is crucial for maintaining stack performance and ensuring a uniform temperature distribution. Figure 9 [54] represents the schematic of a typical liquid-cooled PEMFC system. Liquid cooling can be further categorized based on the type of coolant used in the process, such as deionized water and antifreeze liquids or nanofluids. The coolant is typically circulated through channels incorporated within the bipolar plates or through dedicated cooling channels, which are connected to liquid pumps for efficient circulation. Water has a specific heat capacity that is approximately four times greater than air. The higher specific heat of water allows it to effectively manage the heat generated in the fuel cell and maintain optimal operating temperatures.

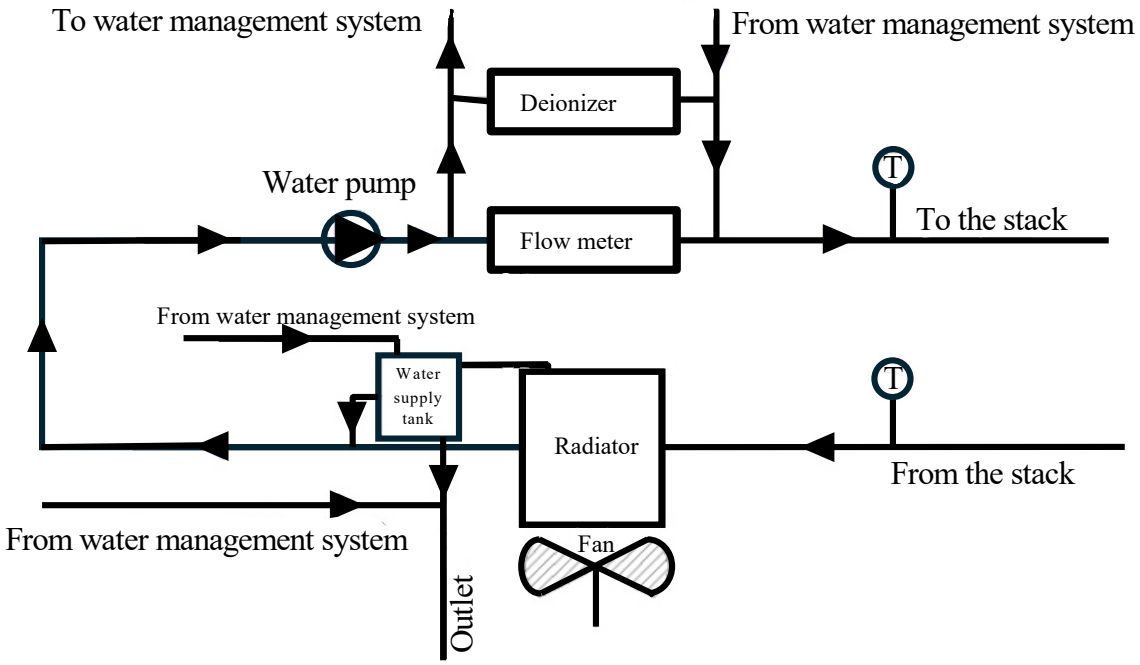



**Figure 9:** The liquid cooling circuit schematic of a PEMFC [54]

Further, nanofluids have gained attention from researchers because of their favourable properties as coolant. Nanofluids are suspensions of nanoparticles in a base fluid such as water or ethylene glycol that can be used for liquid cooling to improve heat transfer. An example of a nanofluid is the addition of 0.5 vol% of $Al_2O_3$ in a water-ethylene glycol mixture. It has been found that this enhances the heat transfer rate by 13.87% [55].

Nanofluids offer benefits such as a low freezing point, making them advantageous for PEMFCs operating in subzero temperatures. The nanoparticles in nanofluids increase the coolant's surface area, improving the convective heat transfer between the coolant and fuel cell components. However, challenges remain in understanding the electrical conductivity of nanofluids, as well as standardizing their synthesis and characterization methods [56]. The selection of nanoparticles and base fluids must be done carefully to avoid issues like clogging or degradation of fuel cell materials over time. Additionally, nanoparticles should be handled with care, as they can penetrate human skin and pose health risks.

Overall, cooling methods, including liquid and air cooling, play a crucial role in regulating the heat produced in PEM fuel cells. However, their effectiveness is greatly influenced by the design of the cooling channels. The geometry of these channels has a direct effect on the heat dissipation process, which in turn affects temperature uniformity and the overall performance of the fuel cell.

## 1.5 Cooling Channel Geometry

Numerous efforts have been made to enhance the performance of the PEMFC liquid cooling system, including the optimization of coolant flow field design, channel geometry, and coolant properties. The design and configuration of the cooling channels play a critical role in heat removal efficiency, as the geometry and flow patterns directly influence the heat transfer rates. By refining these aspects, it is possible to improve the overall thermal management and ensure more effective temperature control across the fuel cell stack.

Numerous studies have explored the impact of flow field designs and coolant channel geometry on enhancing the thermal performance of PEMFC stacks. Figure 10 [57] is a schematic representation of a PEMFC with parallel cooling channel. The primary objective has been to remove fuel cell overheating by minimizing pressure losses across the field while achieving a uniform temperature distribution. This is done by lowering the maximum temperature and reducing temperature variations within the active area of the fuel cell stack [58]. There are studies that highlight the critical role of coolant flow field design in improving the cooling efficiency of

liquid-cooled PEMFC systems. In PEMFCs, cooling channels can either be incorporated directly into the bipolar plates or designed as separate cooling plates. Separate cooling plates are placed between bipolar plates which allow for larger and more flexible channel designs. This does give better heat dissipation; however, they increase the overall size and weight of the stack. On the other hand, when integrated into the bipolar plates, cooling channels offer a compact design and efficient heat transfer [59]. This reduces stack size and simplifies the system but can increase manufacturing complexity. Both approaches serve to maintain optimal operating temperatures, with the choice depending on different applications and convenience.

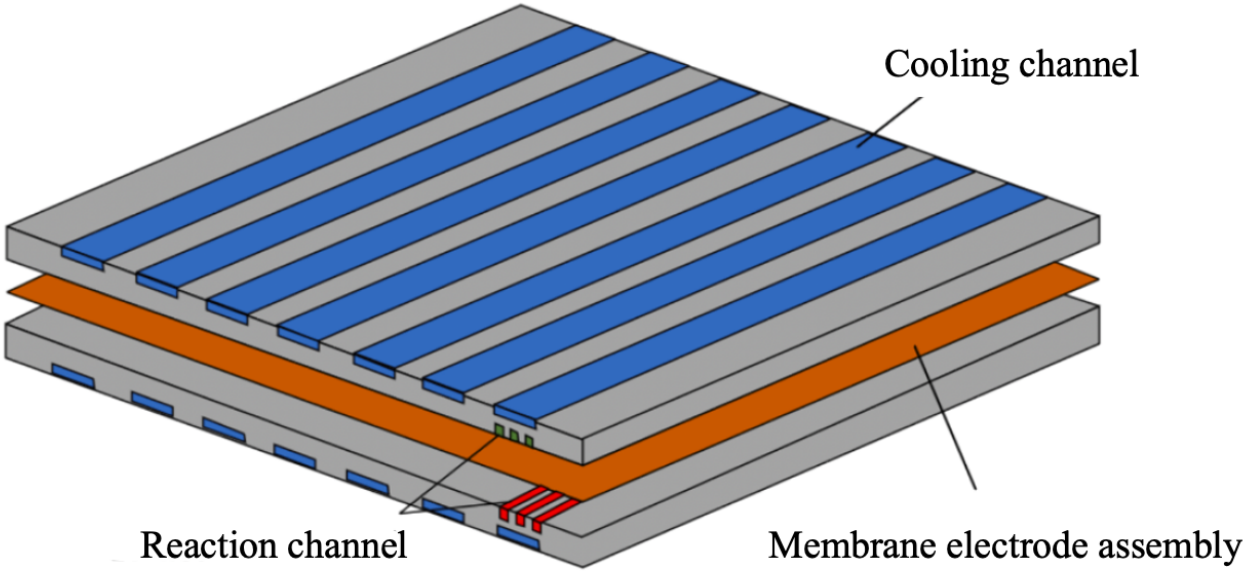



**Figure 10:** Cooling channel geometry of a PEMFC [57]

Several flow field configurations have been developed and designed on bipolar plates, including parallel, serpentine, interdigitated, and radial designs. Each flow field design significantly influences the PEMFC's performance, with multiple strategies available to optimize cooling and overall efficiency. In parallel flow fields, multiple coolant channels run in parallel across the surface of the bipolar plate. These are relatively simple to design and manufacture [60].

They provide a lower pressure drop and can provide an even distribution of coolant across the cell, when designed properly. Further, zig-zag flow channels by varying the geometry of parallel channels have been studied by E. Afshari et al. [61]. It is discovered that the cooling performance of fuel cells at high flow rates and higher heat fluxes has been improved using zig-zag channels,

but the pressure drop increases significantly as compared to straight channels. Further, serpentine cooling channels enhance the heat transfer by their long winding paths for the coolant to flow through. There have been various studies that compare serpentine flow field channels with different modifications [62].

Further, multiple-pass serpentine flow fields, which involve using multiple passes within the serpentine flow field design, have been shown to significantly improve the uniform distribution of temperature in a cooling plate. A study by S.M. Baek et.al. investigated the surface temperature distribution in cooling plates with six different coolant flow field designs and compared the maximum surface temperature and pressure drop at various volume flow rates [63]. The results highlight the importance of multiple-pass flow fields in enhancing the thermal performance of cooling plates, demonstrating a notable improvement in temperature uniformity and efficiency. However, one of the main drawbacks is the complexity of design and manufacturing processes for multi pass serpentine flow fields, leading to higher production costs. Furthermore, the intricate flow paths increase the risk of clogging, especially when using coolants containing particulates or nanoparticles, potentially affecting the system's long-term performance.

## 1.6 Objectives and Scope of Thesis Research

Thermal management in PEMFCs plays a critical role in enhancing their performance, longevity, and overall efficiency, particularly in automotive applications where high reliability and durability are paramount. Nevertheless, achieving a uniform temperature distribution and efficient heat dissipation presents a challenge due to the intricate nature of PEMFCs, particularly under varying operational conditions. As a result, there is an increasing demand for research on the thermal management of PEMFCs to develop advanced cooling techniques, improve temperature gradients, and enhance the performance of the fuel cell stack. This study aims to investigate cooling strategies with a focus on the geometry of coolant channels to optimize the thermal behavior of PEMFCs. Specifically, the objectives of this thesis research are:

- To develop a numerical model for the simulation of various coolant channel designs, with an emphasis on critical parameters including the temperature differential, temperature uniformity index, and pressure drop, in order to evaluate their influence on the thermal performance of the fuel cell system.

- To establish a computational framework for assessing the impact of geometric variables, such as channel width, rib width, and header width, on the heat transfer characteristics and pressure drop within the coolant channels of PEMFCs under diverse operational conditions, employing advanced numerical techniques including computational fluid dynamics (CFD).
- To assess the thermal management efficiency of various coolant channel designs via numerical simulations by analyzing the temperature gradients, the uniformity of temperature distribution across the cooling plate, and the pressure drop associated with each design. This effort aims to contribute to the optimization of thermal management strategies for fuel cell systems.

To achieve the above objectives, thesis will be focused on developing a comprehensive numerical model to examine the geometry of cooling channels in PEMFC, specifically parallel channels. The research will involve modifying the width of the channels and the ribs, and the model's variations will be analyzed to determine what factors contribute to achieving a uniform temperature distribution. The findings from this study will provide insights into optimizing cooling channel designs and improving overall performance of PEMFC.

# 2. Literature Review

PEMFCs are extensively used in aerospace, auto mobiles, power generation and other applications due to their various advantages. They are usually employed because of their compact size, non - polluting operation, high efficiency and low operation temperature [64] Although PEMFC's are known for their high energy conversion efficiency, they produce a significant amount of waste heat during the electrochemical reactions [65]. The heat generated as a byproduct of electrochemical reactions in the fuel cell stack must be efficiently removed to maintain the desired operating temperature, which is critical for both the performance and longevity of the PEMFC. The operating temperature and the temperature uniformity within the stack significantly influence the fuel cell's performance and durability. Cooling methods for PEMFCs are influenced by factors such as stack size, application, system complexity, cost, and the amount of heat that needs to be managed. One of the commonly employed heat removal techniques is forced convection using liquid cooling, as liquids have higher thermal conductivity and heat capacity than gases like air [66]. For PEMFC stacks with a power output greater than 5 kW, liquid cooling is widely used to manage the heat generated. In this method, coolant fluid flows through specially designed channels on cooling plates or bipolar plates, depending on the stack's design. The heat is transferred from the cell through the bipolar plate to the coolant, which then flows through separate coolant channels within the stack. The heated coolant is subsequently pumped to a heat exchanger, where the heat is rejected to the surrounding medium or used for alternative purposes such as cogeneration. Given the extensive use of liquid cooling, especially for the automotive PEMFC stacks, numerous studies have been conducted to enhance the performance of the PEMFCs using liquid cooing systems through modifying systematic design of cooling channels and optimizing the properties of the coolants used in the systems [67].

To mitigate the fuel cell overheating, studies are mainly focused on lowering the pressure drop across the flow field and providing the uniform temperature distribution by reducing the maximum temperature and temperature variations within the active area of the stack. This highlights the critical role of coolant flow field design and coolant channel geometry in enhancing the performance of PEMFCs. Many of these studies use numerical 3D models to study the thermal management in PEMFCs particularly by analyzing the effects of coolant channel geometries. These simulations allow to evaluate various flow fields and channel configurations and then predict temperature distribution, assess pressure losses and optimize the coolant flow to achieve

more efficient heat removal. A study by S.A. Atyabi et al. [68] showcases the importance of cooling channels by comparing a PEMFC design with and without cooling channels as shown in Figure 11 [68]. By calculating and comparing the fuel cell temperature under varying air velocities, the water content and concentration across the GDL and catalyst membrane interface, and the polarization curves for both configurations, the study demonstrates that the presence of cooling channel improves the cooling capability of the fuel cell. However, despite the improved cooling performance, the net power output was decreased due to high pressure loss, leading to substantial parasitic power consumption.

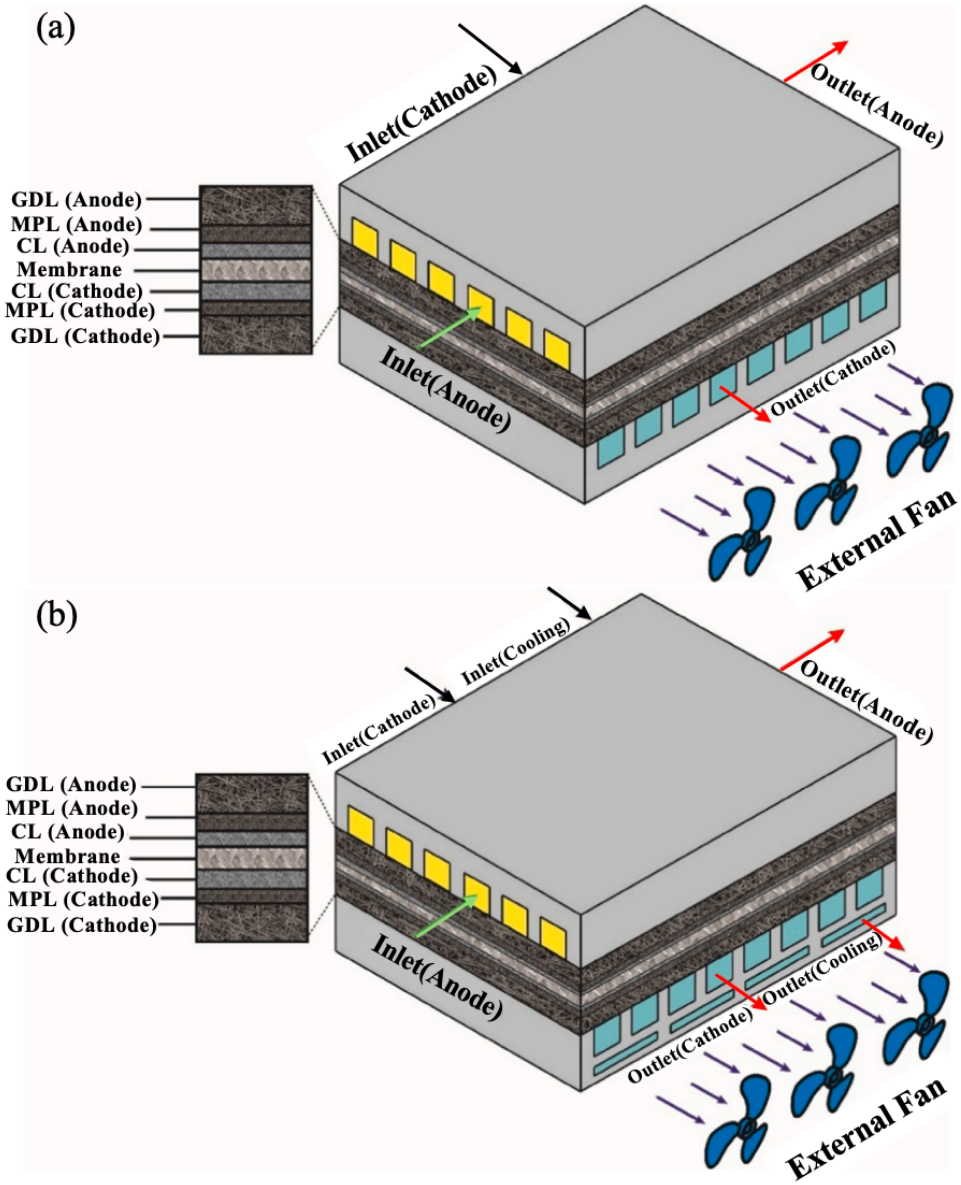



**Figure 11:** Schematic view of cross-flow PEMFC design (a) without and (b) with cooling channels and main components [68]

Several studies including a study by K. Mogorosi et al. [69] have addressed the impact of cooling channels on the performance of PEMFCs in terms of current density and temperature distribution. Comparing the geometry with no cooling and with cooling channels Figure 12 [69], showed that presence of cooling channel reduces the local temperatures on the cathode side by about 10 ℃ .The non cooled cell had a higher temperature of 333 K and remained almost constant with the change in flow rate whereas the presence of a cooling channel provided an average temperature of the cell at 323 K. This clearly highlights the fact that the temperature of the cell is greatly influenced by the introduction of cooling channels.

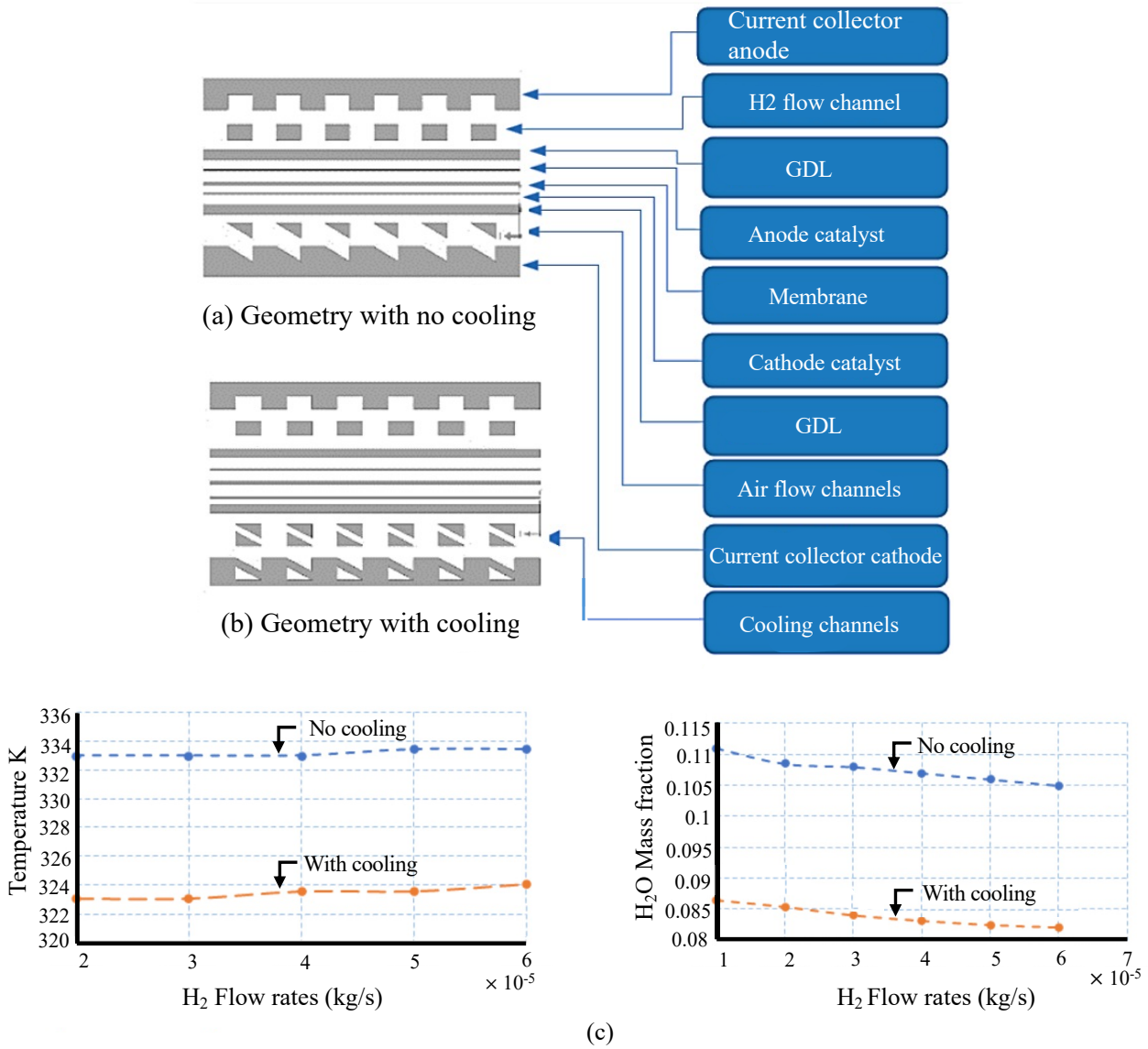



**Figure 12:** (a) Cross section representation of geometry with no cooling, (b) Geometry with cooling, (c) Variation of temperature and $H_2O$ mass fraction with $H_2$ flow rates [69]

S. Asghari et al. [70] designed a thermal management subsystem for 5 kW PEMFCs, with flow field designs on cooling plate. Figures 13(a) [70] illustrate the parallel serpentine flow field design employed to achieve uniform temperature distribution through the inlet and outlet manifolds of the reactant gases. The number of parallel channels in the design and coolant flow rate was the design parameter of the study. Figure 13(b) [70] shows the results obtained, which clearly indicate that the maximum temperature difference within the bipolar plate is a function of the coolant flow rate at the operational voltage underscoring the significance of uniform temperature distribution throughout the bipolar (cooling) plates.

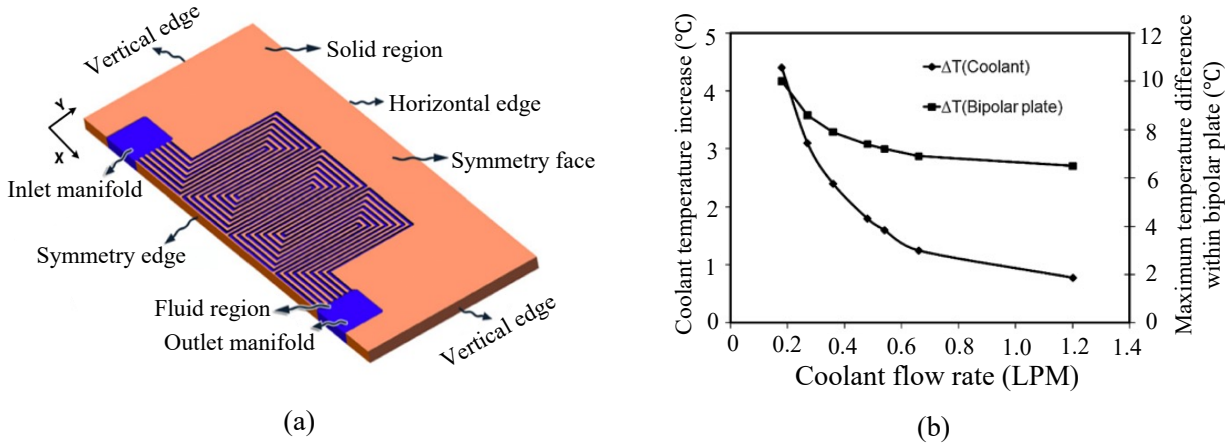



**Figure 13:** (a) Schematic of a developed geometric model of parallel serpentine design, (b) Coolant temperature increment and maximum temperature difference within the bipolar plate versus coolant flow rate per cell [70]

Further, to study the influence of cooling channel geometry and flow field designs, different types of flow fields have been developed. E. Afshari et al. [61] embarked on a study to examine the influence of cooling channel geometries, specifically concentrating on straight parallel channels and zigzag flow channels, as illustrated in Figure 14 [61]. Their research, which employed three-dimensional numerical simulations, sought to assess key performance metrics, including maximum surface temperature, temperature uniformity, and pressure drop from the inlet to the outlet of the cooling channels. The results, as shown in Figure 15(a) [61] indicated that the zig zag channels exhibited lower maximum temperature than the parallel channels with respect to the heat flux. A similar trend was observed for the change of maximum temperature against the coolant flow rate as can be seen in figure 15(b) [61]. So, their study indicated that variations in cooling channel geometry have a considerable influence on temperature management within the fuel cell stack.

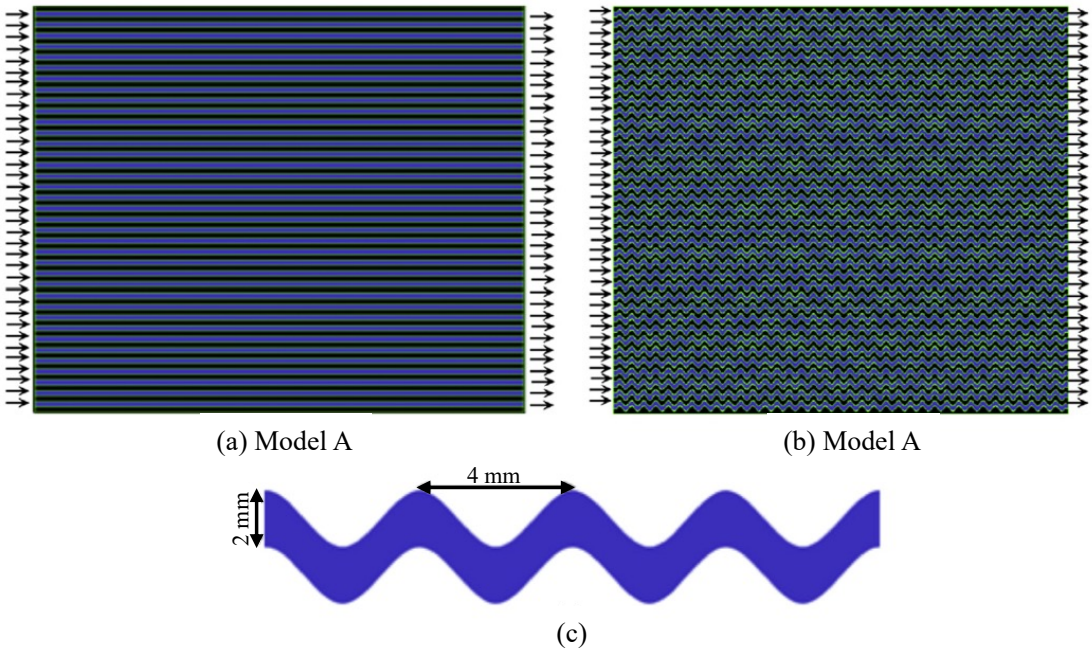



**Figure 14:** Two flow field designs for a cooling plate (a) straight channel, (b) zigzag channels, (c) close view of a zigzag configuration [61]

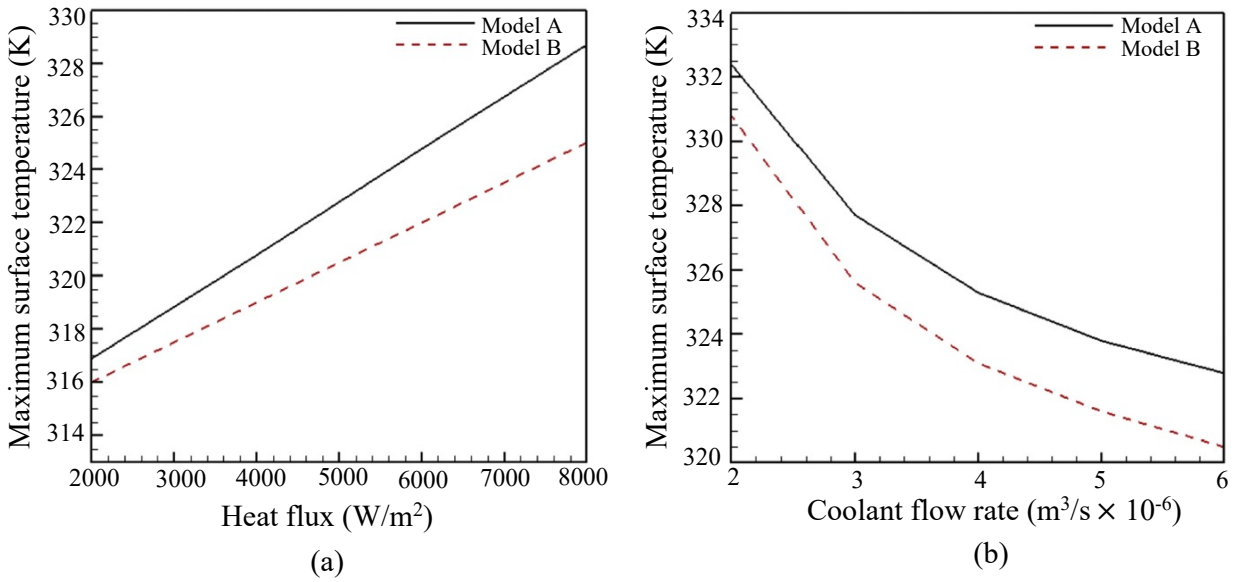



**Figure 15:** (a) Maximum surface temperature of models A and B at the center-plane of the cooling plate (Re = 330, volume flow rate = $6 \times 10^{-6}$ $m^3/s$), (b) Maximum surface temperature of models A and B at the center-plane of the cooling plate with heat flux = 4255 $W/m^2$ [61]

By adjusting the geometry of the flow field, it is possible to maintain a more uniform temperature distribution, which is vital for optimizing the performance and longevity of fuel cells. Specifically, the study demonstrated that both the maximum surface temperature and the temperature uniformity index were improved in the zigzag channel model, achieving reductions of approximately 5% and

8%, respectively, in comparison to the straight channel model. These findings underscore the potential of various flow field designs to enhance thermal management PEMFCs.

Studies such as those previously mentioned present additional opportunities to explore various designs. Thermal investigation done by S.M. Rahgoshay et al. [71] on serpentine and parallel types of the flow field of cooling plates, when compared with the typical isothermal model (without cooling flow field), shows a 24% improvement for serpentine cooling flow field than parallel one. This signifies that changing the heat transfer rate can directly influence the performance of PEMFC. This comparison also shows that the pressure drop for parallel type configuration had a lower value than serpentine type configuration. Consequently, the increase in pressure necessitates the implementation of a compressor or pump, leading to increased risk and cost. With this in mind, these type of conventional designs were further modified to address the related challenges. M. Ghasemi et al. [72] simulated and compared six different cooling field designs e.g. conventional serpentine, typical of multi-pass serpentine flow field (MPSFF), typical of serpentine, parallel-serpentine, conventional spiral and conventional parallel as shown in Figure 16 [72].

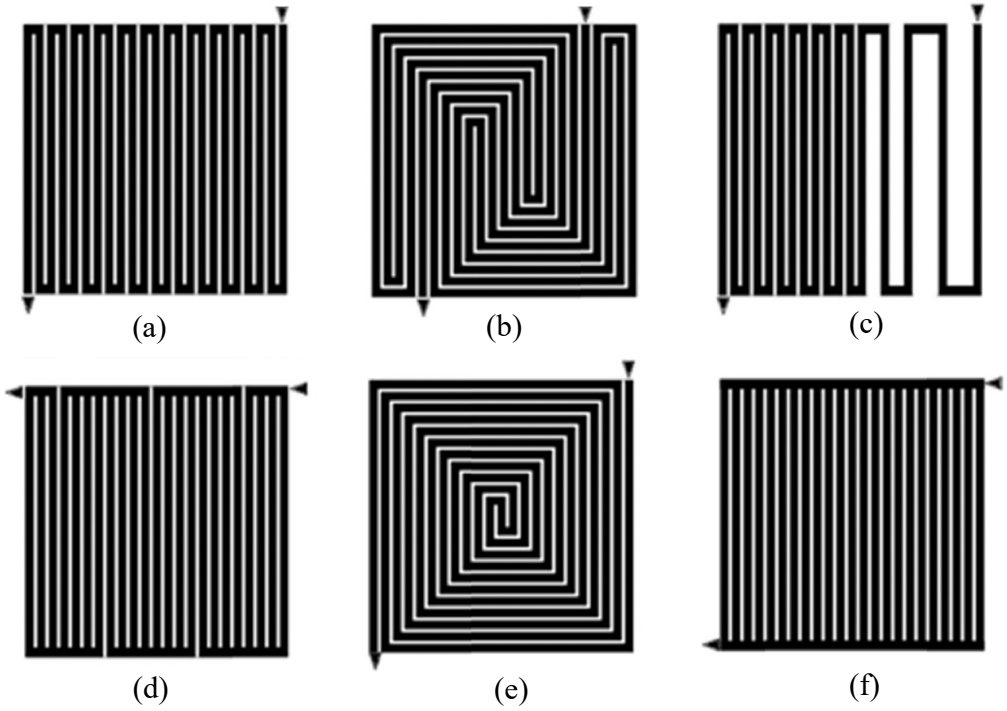



**Figure 16:** Six cooling channel flow fields: (a) conventional serpentine, (b) typical of MPSFF, (c) typical of serpentine, (d) parallel serpentine, (e) conventional spiral, (f) conventional parallel [72]

Based on the minimum and maximum temperature gradient and temperature uniformity index, the results in Figure 17 [72] indicate that conventional spiral design has a good temperature

distribution with temperature uniformity index, $U_T$ = 0.58 ℃ and temperature difference, ΔT = 3.38 ℃, whereas serpentine design had $U_T$ = 0.72 ℃ and ΔT = 4.51 ℃. However, the spiral design also showed a higher pressure drop, whereas the typical serpentine design demonstrated better performance in terms of pressure drop. It is important to note that typical of serpentine design involved adjustments in the width of channel and rib, highlighting the importance of dimensional changes to achieve better temperature distribution while minimizing pressure drop.

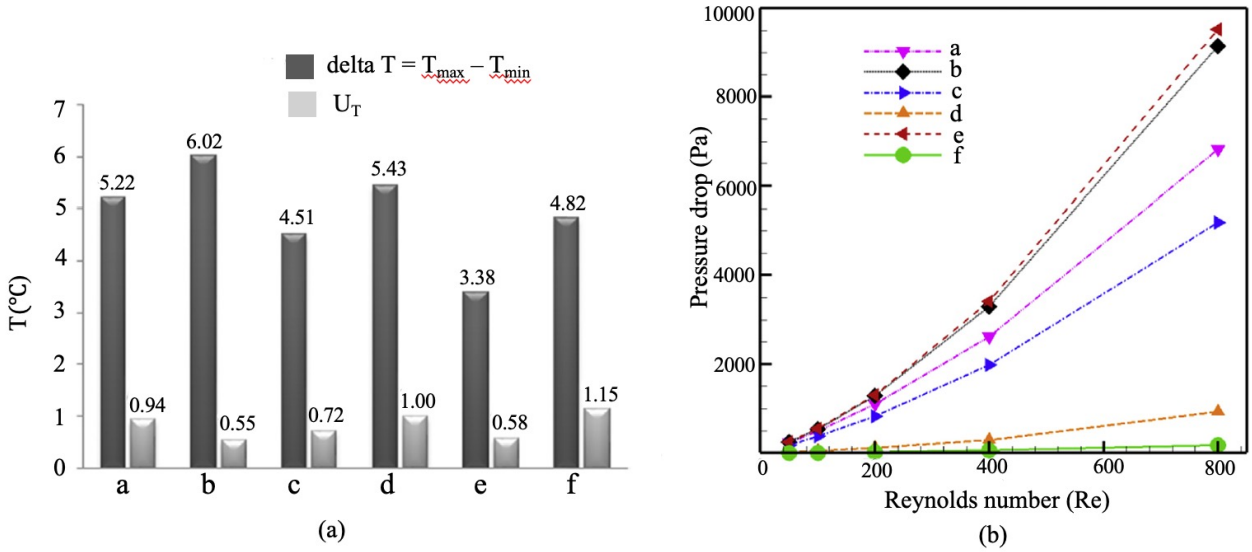



**Figure 17:** (a) Temperature uniformity indices and catalyst-membrane interface temperature ranges for different cooling plates at V= 0.6 V and Re= 400, (b) Pressure drop through the cooling plate versus Reynolds number [72]

Nevertheless, these findings have inspired fellow researchers to explore various designs of channels. S. Li and B. Sunden [73] implemented wavy channels within cooling plates and conducted a comparative analysis against parallel channels to evaluate heat transfer properties. Their findings indicated that the utilization of wavy channels, characterized by reduced wavelength and augmented amplitude presented better heat transfer performance in comparison to parallel channels. These types of studies lead to greater possibilities for the enhancement of thermal management in PEMFCs. Various channel designs and configurations present opportunities to identify the optimal arrangement for achieving the lowest maximum temperature. Six distinct channel configurations were examined by J. Choi et al. [74]. The configurations of flow channels within the cooling plate are illustrated in Figure 18 [74] and feature both conventional and modified serpentine as well as parallel channel designs aimed at enhancing the thermal reliability of PEMFCs. To know the impact of different design modifications, the performance of cooling plate was checked by simulating maximum surface temperature and temperature difference

between the inlet and outlet of the cooling plate according to the Reynolds number, as can be seen in Figure 19 [74].

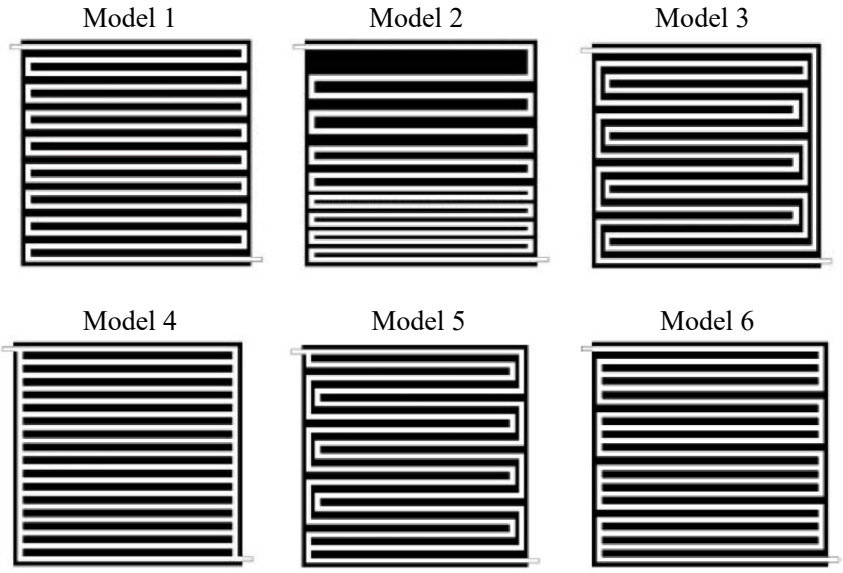



**Figure 18:** Configurations of flow channels in the cooling plate [74]

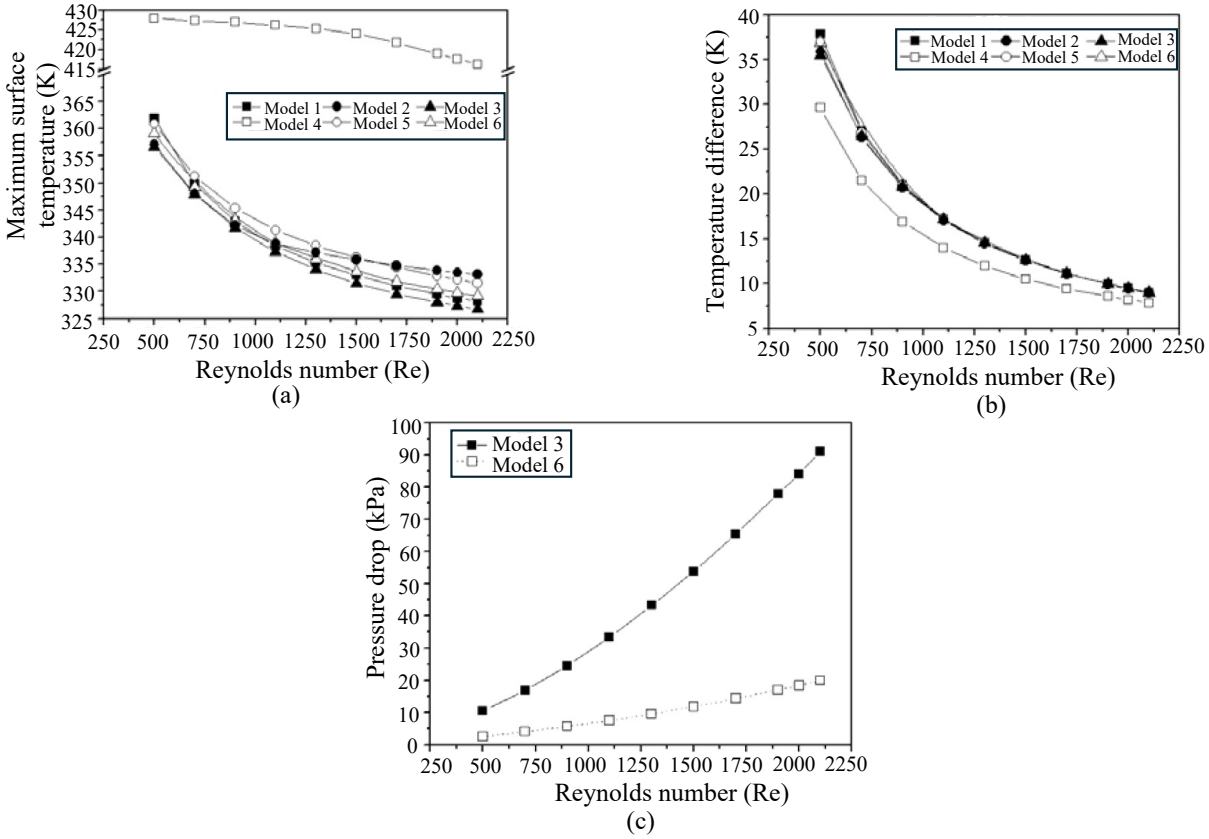



**Figure 19:** (a) Variation of maximum surface temperature according to Reynolds number, (b) Temperature difference between the inlet and outlet of the cooling plate according to Reynolds number, (c) Pressure drop through the cooing plate as a function of Reynolds number [74]

For serpentine channels, the modified configurations that were developed to enhance the cooling performance of other conventional serpentine channels exhibited a lower maximum temperature; however, they demonstrated a higher uniform temperature across the entire area.

In the case of parallel channels, the modified channels, which were specifically designed to enhance the non-uniform distribution of fluid flow within a typical parallel cooling plate, also demonstrated a reduction in maximum temperature. Nevertheless, upon comparison of the optimal models of parallel and serpentine channels, it was observed that the enhancement in thermal performance for the serpentine channels exceeded that of the parallel channels. But the pressure drop for serpentine was higher (Figure 19 (c)) [74] because those channels had relatively high flow velocity through them and a greater number of bends than parallel channels. To address this issue, various configurations of serpentine channels have been introduced and analyzed. By modifying factors such as the implementation of multi-pass serpentine flow field designs, numerous researchers aim to enhance the overall thermal performance of the cooling plates. This approach ensures a more uniform temperature distribution while simultaneously minimizing energy losses within the system.

S.H. Yu, et al. [75] performed computation fluid dynamics (CFD) simulations of fluid flow and heat transfer in the cooling plates with several MPSFF. As the role of the cooling plate is to release heat from electrochemical reactions and to maintain a uniform temperature distribution within the MEA, a study of uniform temperature distribution at the interface between the cooling plate and anode or cathode plate is desirable. This study emphasizes that making changes to the conventional designs can help reduce indices like maximum temperature and the temperature difference. Figure 20(a) [75] shows the design of channels provided by the study and indices like temperature uniformity index and the temperature difference were calculated. Figure 20(b) [75] shows the plot of temperature difference and $U_T$ against Reynolds number, and plots suggest that the conventional serpentine flow field (Model A) gives the largest temperature difference and $U_T$ of the six flow fields whereas the four MPSFFs (Model B-E) and the conventional spiral flow field (Model F) exhibits small temperature difference and $U_T$. These configurations employing MPSFF demonstrated a reduction in the uniformity indices of temperature difference and $U_T$ ranging from 40% to 60% compared to conventional designs. However, Model B to Model F are found to require a larger pressure drop than the conventional design (Model A), emphasizing on more research to be done.

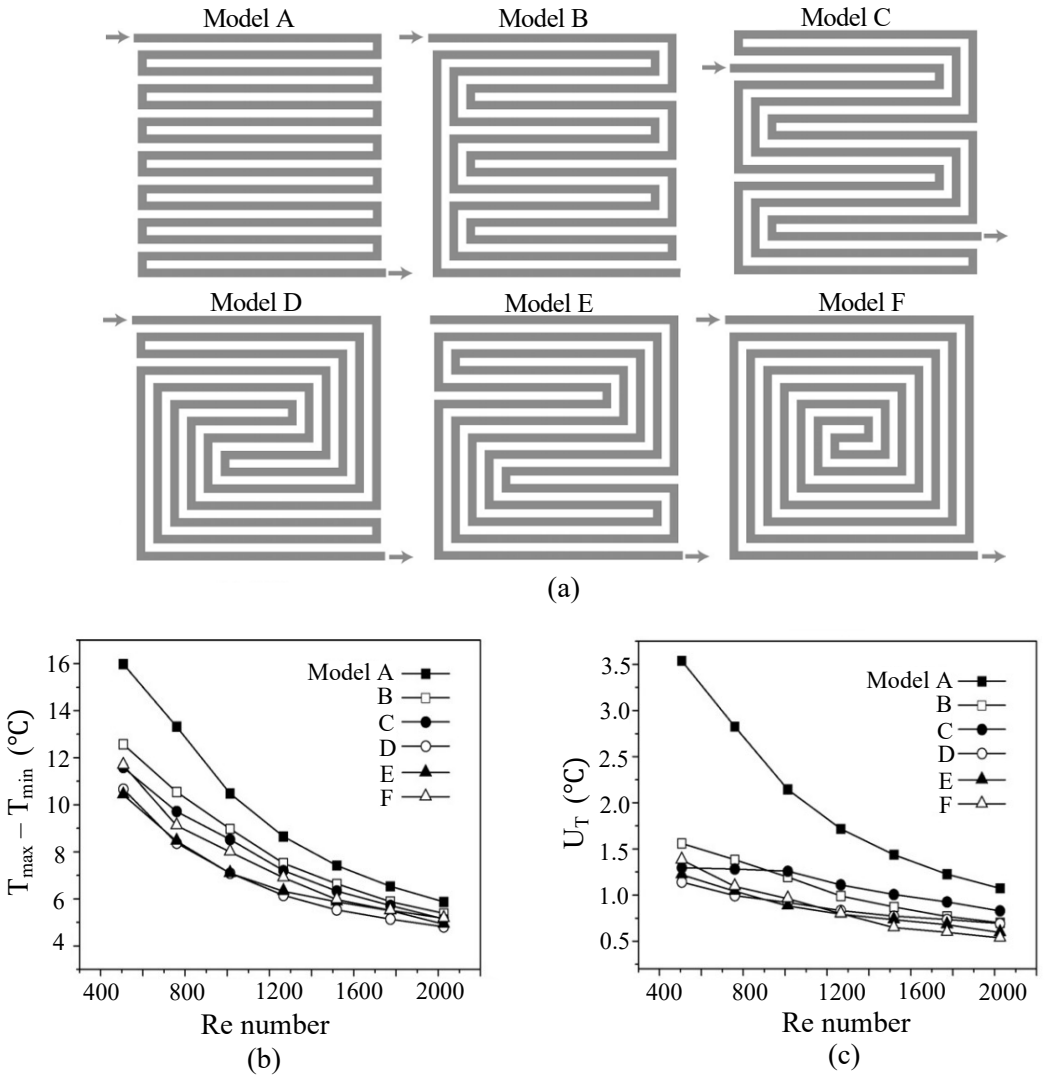



**Figure 20:** (a) Six serpentine flow-fields used as coolant channels, effect of flow velocity on performance of cooling plates: (b) surface temperature difference, (c) temperature uniformity index, $U_T$ [75]

On similar grounds, a study by S.M. Baek, et.al. [63] shows that MPSFF designs could significantly improve the uniformity of temperature distribution as compared to its conventional design. The MPSFFs maintains about 60% of $U_T$ for the conventional parallel and serpentine flow fields, however the pressure drop was found to be increased with the design with lower number of parallel channels. It is mainly because of the fact that both the fluid velocity and the channel length are inversely proportional to the number of parallel channels when the coolant flow rate is fixed. Nevertheless, the increased pressure drop in serpentine channels continues to pose challenges. Consequently, researchers have investigated several alterations to conventional designs to enhance the analysis of various channel configurations. A numerical investigation by S.M.M. Joibary et al. [76] studies the influence of six different cooling flow channels on the thermal distribution in a

PEMFC. Figure 21 [76] depicts the different configurations of the designs including parallel, serpentine in the beginning, serpentine in the middle, serpentine at the end, horizontal serpentine and four section serpentine cooling channel fields. To enhance the understanding of the performance and process of the fuel cell, thermal distribution in different parts of the fuel cell was assessed.

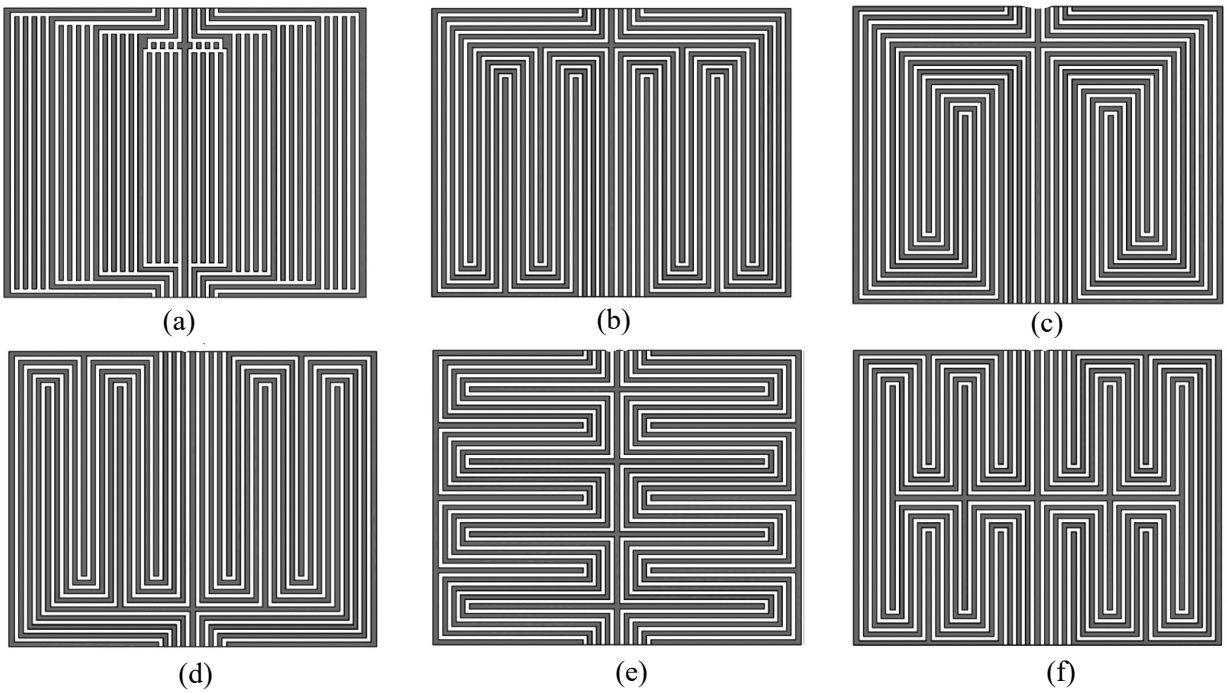



**Figure 21:** Six different cooling channel fields: (a) parallel, (b) serpentine in the beginning, (c) serpentine in the middle, (d) serpentine at the end, (e) horizontal serpentine, (f) four section serpentine [76]

The results shown in Figure 22 [76], suggests the highest (357.9 K) and lowest (354 K) average temperature of the membrane mid-plane for parallel and four section serpentine geometries, respectively. Further interestingly, the temperature on both the cathode and anode surfaces of parallel and serpentine in the middle geometries shows almost equal temperatures, and a 1℃ difference for the other geometries. Accordingly, in terms of temperature, the four-section serpentine design had the $U_T$ and temperature range compared to the other geometries, however it was found that in terms of absorbed heat and output power the serpentine in the beginning had better performance. This trend underscores the importance of thoroughly examining all parameters that could influence the temperature distribution when evaluating the performance of PEMFCs. In this context, parallel channels offer a more straightforward solution, as their simpler structure

facilitates a reduction in pressure drops across the channels while ensuring a more uniform distribution of flow.

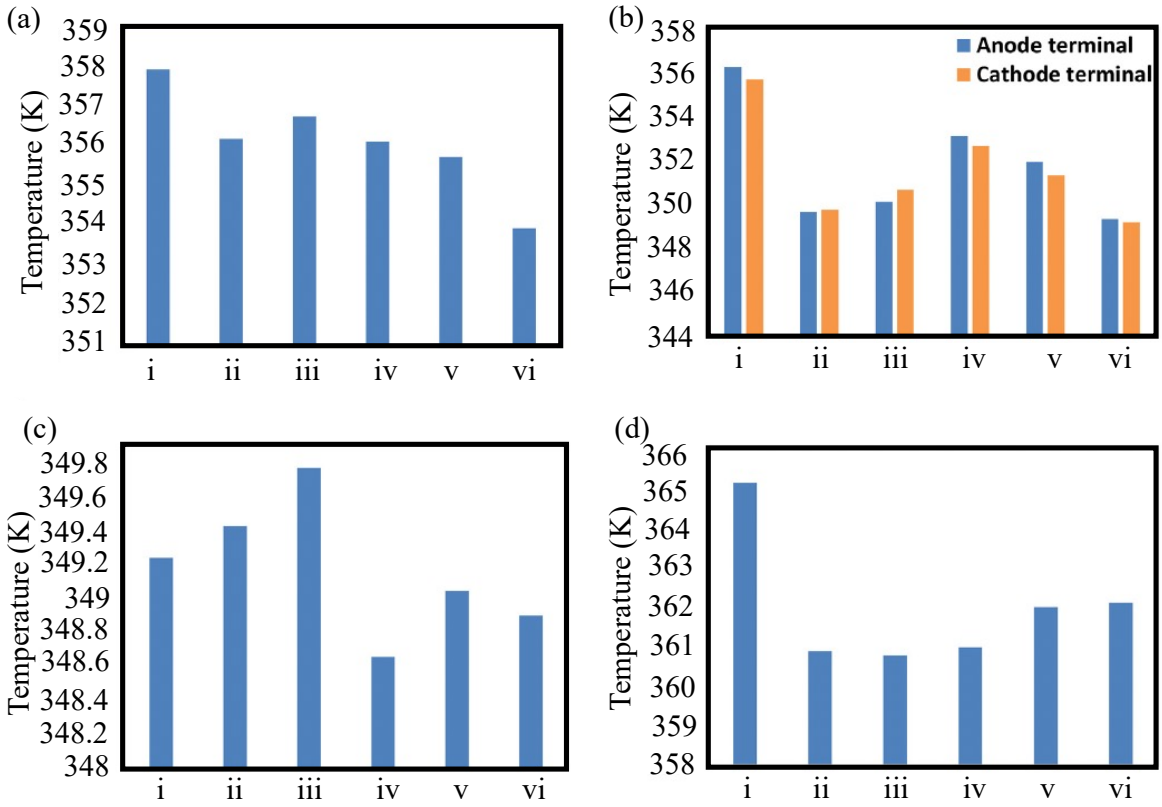



**Figure 22:** (a) Average temperature of the membrane mid-plane, (b) Average temperature of the anode and cathode terminals, (c) Outlet temperature of the cooling fluid, (d) Maximum temperature of the membrane mid plane. (i) parallel, (ii) serpentine in the beginning, (iii) serpentine in the middle, (iv) serpentine at the end, (v) horizontal serpentine, (vi) four section serpentine [76]

Different researchers have further tried to address the heat removal problem by making modifications in parallel channels that aim to maintain the benefits of conventional design while reducing its drawbacks. E. Afshari, et al. [54] studied the geometric model of parallel design cooling flow fields by varying the width of the channel (channel depth constant) and varying the depth of the channel (channel width constant). Modifying the dimensions while maintaining the constancy of other parameters is regarded as an effective approach for examining the impact of the alterations implemented. It has been observed that increasing the channel depth correlates with an increase in indices such as maximum and average surface temperature; conversely, a decrease in pressure drop was found to be decreasing with the rising channel depth. Furthermore, as the channel width increases, the desired indices tend to diminish, which aligns with the intended outcome. A significant takeaway from the study was to be wise with the choice of the dimensional

alterations, as the efficiency of the cooling plate depends on a well-balanced design. Although expanding the width can enhance heat removal by augmenting the coolant flow capacity, exceeding an optimal threshold may not yield the anticipated results. Consequently, to prevent system inefficiencies and to sustain optimal thermal performance, the careful selection of channel dimensions is important. It has been observed that effective cooling is crucial for the stability, longevity, and optimal thermal performance of PEMFCs. One method to accomplish this objective is through the optimization of cooling flow field designs.

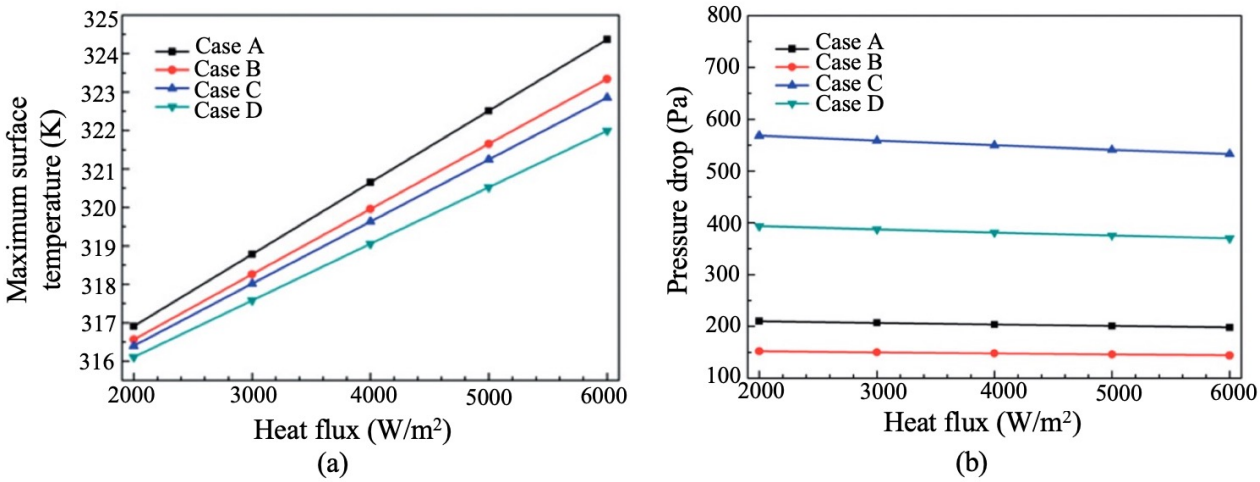
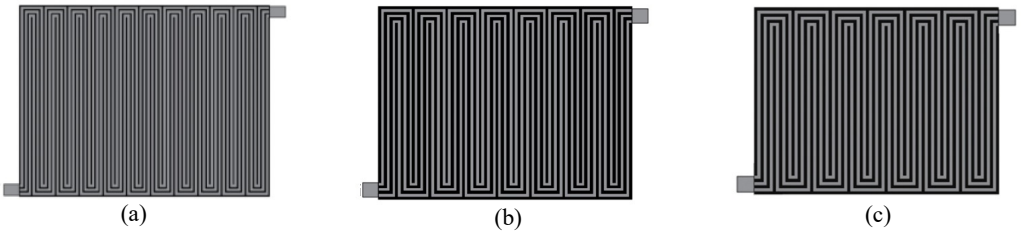



**Figure 23:** Effect of heat flux on (a) maximum temperature, (b) pressure drop [77]

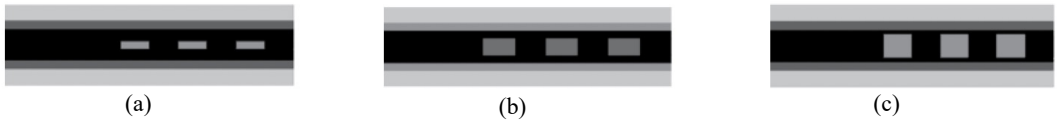
S. Li and B.Sunden [77] studied and compared their study with S.M. Baek et al. [63] and their study incorporated a non-uniform cross-section for the parallel channels by varying the width and height of the channels at the inlet and outlet. Similarly, the temperature difference between maximum and minimum surface temperature decreased in the range of 10 to 20% as compared to novel designs. In addition to alterations in geometry, various other factors may impact heat transfer, such as heat flux and the inlet Reynolds number. An increase in heat flux will result in a more significant temperature gradient across the PEMFC. As can be seen in Figure 23(a) and Figure 23(b) [77], author found out that maximum temperature linearly increased with increase in the heat flux and pressure drop is slightly decreased. However, the maximum temperature is significantly reduced as the inlet Reynolds number increases. An increase in the Reynolds number enhances the mixing of the coolant and elevates the heat transfer coefficient. Although a higher Reynolds number improves heat transfer, it simultaneously leads to increased frictional losses within the flow paths, resulting in a greater pressure drop across the cooling channels, as evidenced

by the study. Consequently, effective flow management becomes crucial in balancing all these effects.

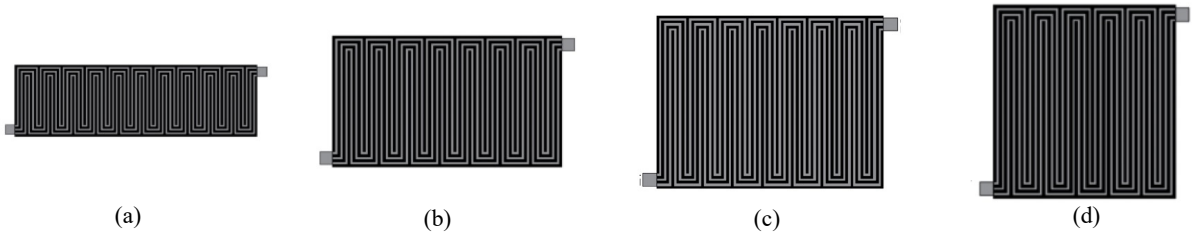
To further highlight the importance of change in coolant channel geometry to control the working temperature, a study by W. Wang et al. [78], presents the influence of different ridge widths, cooling channel depth and length to width ratio on cooling performance of PEMFC. Figure 24 [78] shows the structure of cooling channels with varying geometrical parameters, and to check for the variation design with better heat transfer, maximum temperature difference and average temperature of cells are compared with respect to the heat flux density.




Cooling runner geometries with different ridge widths (a) 0.5 mm, (b) 1.5 mm, (c) 2.0 mm




Enlarged view of cooling runner inlet at different depths (a) 0.5 mm, (b) 1.0 mm, (c) 1.5 mm




Cooling runner geometry with different aspect ratios (a) 3.40:1, (b) 1.75:1, (c) 1.32:1, (d) 0.95:1

**Figure 24:** Variations in cooling channel geometry [78]

Results as shown in Figure 25 [78] underscores that the optimal cooling channel form among the variation of ridge width is the one with 2 mm ridge width, and the lowest maximum temperature difference is achieved for channel depth of 0.5 mm. However, for the variation in aspect ratio for the given geometry, it was observed that the aspect ratio did not significantly affect the temperature distribution of the fuel cell. It can be concluded from the study that there could be numerous ways to change the geometrical parameters and study their effects on the heat transfer, but a strategic decision while selecting the parameters is important.

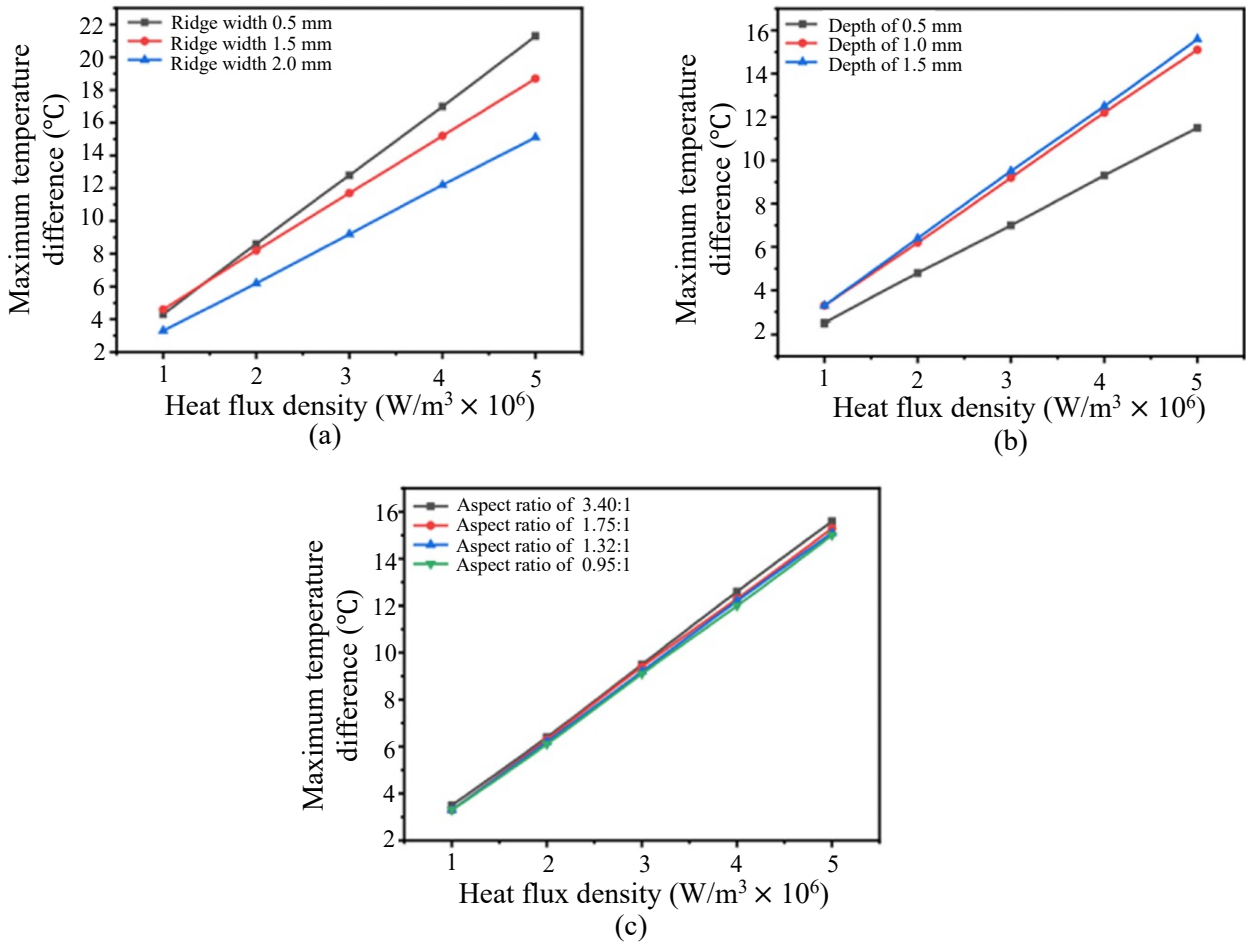



**Figure 25:** (a) Maximum cell temperature difference variation with different ridge width and heat flux densities, (b) Maximum cell temperature difference variation with different channel depth and heat flux densities, (c) Maximum cell temperature difference variation with different aspect ratios and heat flux densities [78]

Another numerical simulation of various coolant channel geometry studied by A.P.Sasmito et al. [79] integrated existing designs to create an innovative hybrid cooling channel as shown in Figure 26 [79]. To check on the thermal management of the system, temperature distribution at the middle of the cathode catalyst layer for all the design variations was compared. The results from Figure 27 [79] indicates that the serpentine channel design yields the best thermal management, demonstrating lower pumping power requirements compared to conventional channels. However, the net efficiency of the serpentine channel decreases due to higher pressure drop and increased parasitic losses. The novel hybrid parallel-serpentine-oblique-fins channel design, delivers the highest net power output, primarily due to much lower pressure drop. This highlights the significance of optimization to refine the design and enhance the overall performance of the stack.

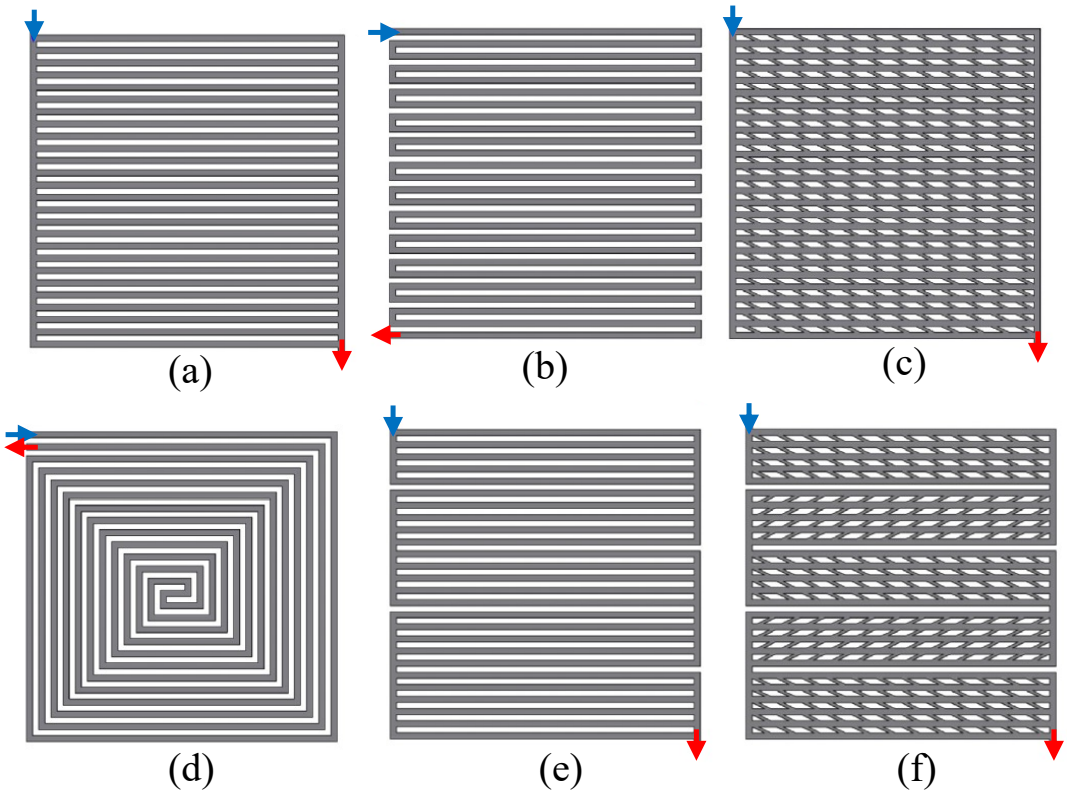



**Figure 26:** Coolant channel designs: (a) conventional parallel, (b) conventional serpentine, (c) oblique-fins, (d) coiled, (e) parallel-serpentine, (f) novel hybrid parallel-serpentine-oblique-fins channel designs [79]

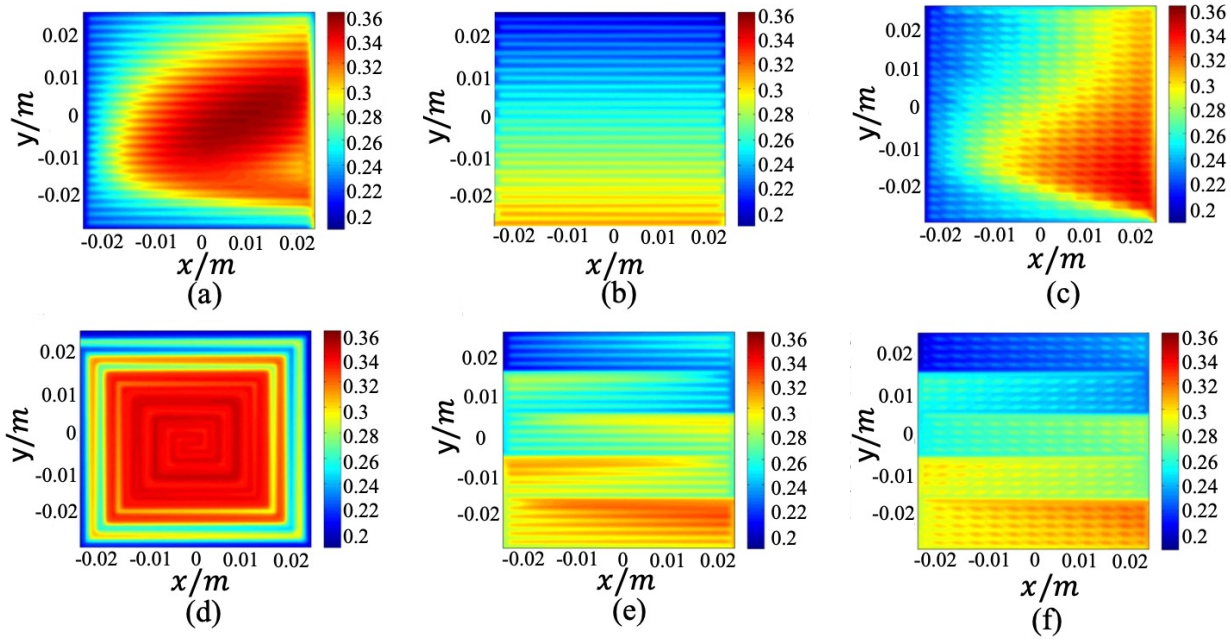



**Figure 27:** Temperature distribution at the middle of the cathode catalyst layer (a) conventional parallel, (b) conventional serpentine, (c) oblique-fins, (d) coiled, (e) parallel-serpentine, (f) novel hybrid parallel-serpentine-oblique-fins channel designs at coolant inlet Reynolds ~600 and cell voltage = 0.7 V [79]

The importance of the geometrical change can also be explored by studying the factors like the coolant inlet temperature, coolant flow direction and the coolant volume flow rate. X. Liu et al. [80] studied three different channel geometries, namely parallel channels, parallel serpentine along Y axis and parallel serpentine along X axis as shown in Figure 28 [80]. The study demonstrates the influence of coolant inlet temperature and coolant flow direction on the PEMFCs operating temperature and temperature gradient, respectively. Moreover, the coolant flow rate significantly impacts the magnitude of the temperature gradient in the PEMFC. The research findings indicate that the implementation of a parallel serpentine channel oriented along the x-axis significantly regulates the temperature distribution within the catalyst layer, thereby enhancing temperature uniformity.

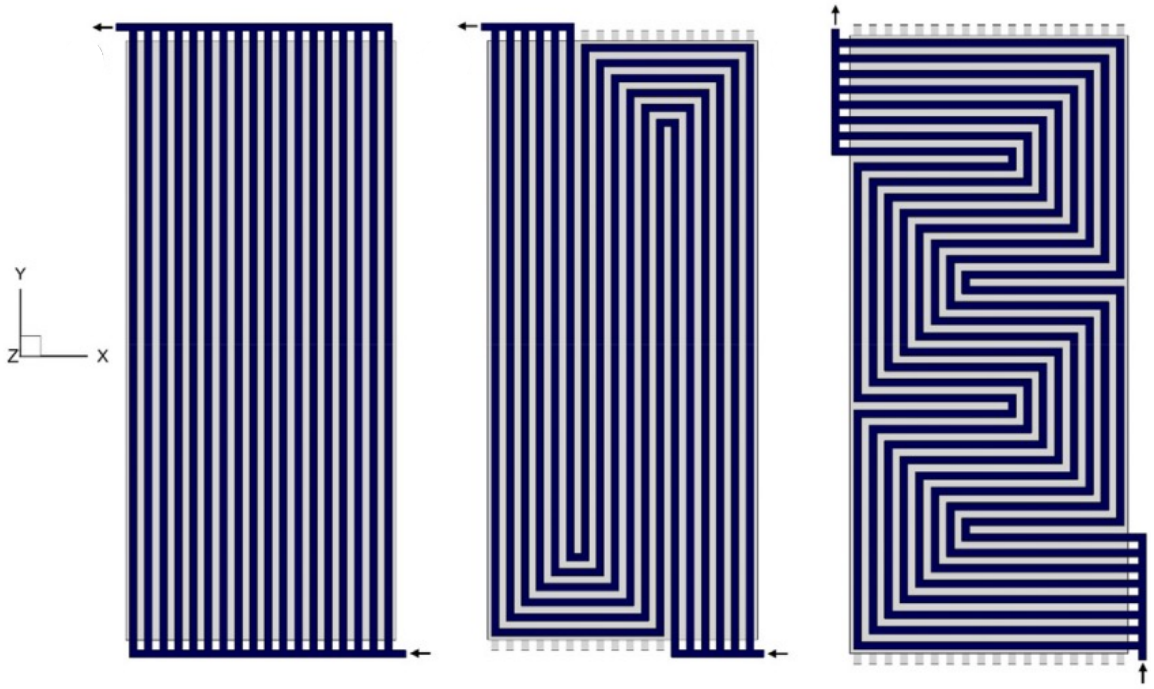



**Figure 28:** Three coolant flow field designs for a large-scale cooling plate. (a) parallel flow field, (b) parallel serpentine flow field along Y-axis, (c) parallel serpentine flow field along X-axis [80]

Looking ahead, there is significant potential for variations that can be done to achieve more efficient thermal management. The development of innovative designs based on the existing cooling channel design also presents a viable approach for optimization. X. Xu et al. [81] proposed a 3D PEMFC model for two novel designs of coolant channel geometry (Figure 29), inspired by serpentine and parallel topologies. The novel A and B coolant channels were designed and evolved

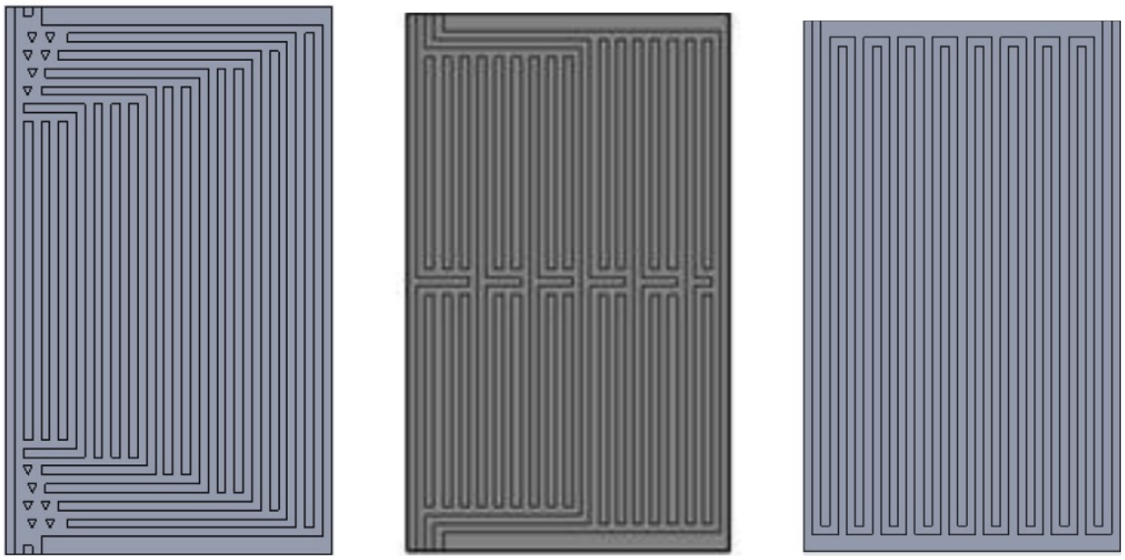



**Figure 29:** Different configurations of flow fields (a) Novel A, (b) Novel B, (c) serpentine channel [81]

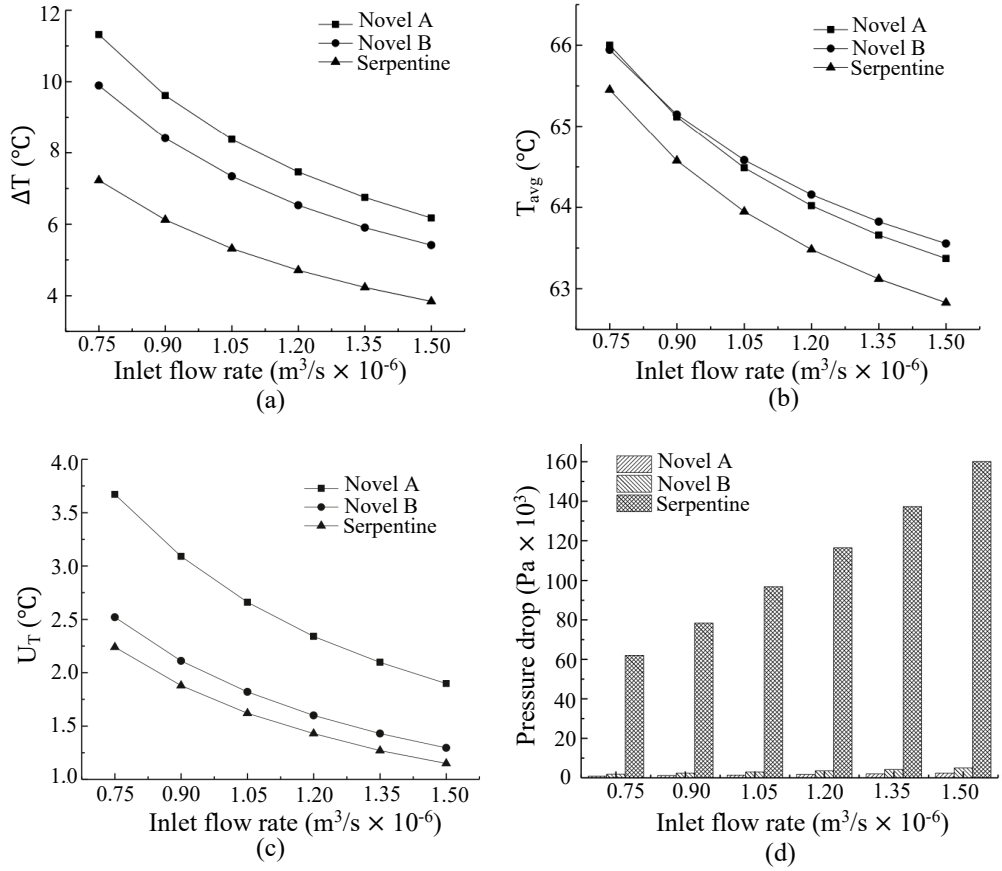



**Figure 30:** (a) Variation of temperature difference of different cooling channels with varying flow rate, (b) Variation of average temperature of different cooling channels with varying flow rate, (c) Variation of temperature uniformity index of different cooling channels with varying flow rate, (d) Variation of pressure drop of different cooling channels with varying flow rate [81]

from traditional multi-passes parallel coolant channel and the single pass serpentine coolant channel. The different configurations of the novel designs and serpentine flow fields was then compared to conclude that the stack with novel A cooling channels showed better cooling performance compared with the other two types of channels, under the same conditions of the form of gas flow rate and the form of MEA and bipolar channel. As can be seen from the results, shown in Figure 30 [81], for the flow rate of $1.5 \times 10^{-6}$ $m^3/s$, the ΔT of the novel A channel was 6.8 ℃, $T_{avg}$ was 63.6 ℃ , $U_T$ was 1.9 ℃ and pressure drop was 2379 Pa, which was the lowest among the three configurations. Besides, the flow field is one of the key factors that determines the temperature uniformity in the cell to improve the power generation of the fuel cell.

These studies draw attention to the importance of coolant channel geometry and thermo-physical properties of coolant plate materials. When the channel geometry is modified by altering the dimensions of the channels, the geometry itself plays a significant role in improving heat transfer. However, the thermophysical properties of the coolant plate material also have a crucial impact on heat transfer performance. These properties, such as thermal conductivity, specific heat capacity, and density, influence the material's ability to conduct and store heat, which can either enhance or limit the cooling efficiency. Therefore, while the geometry of the channels is important for optimizing fluid flow and heat dissipation, the thermophysical characteristics of the coolant plate material also contribute significantly to the overall heat transfer performance.

# 3. Methodology

## 3.1 Geometric Model

Generally, a PEMFC is composed of several key components that each serve essential functions for efficient operation. PEMFC consists of a MEA for the ion conduction and enables the electrochemical reactions to take place. Surrounding the MEA are two GDLs which ensure the uniform reactant diffusion, and additionally two bipolar plates are used for the electron conduction and distributing the flow of reactant gases and coolant in some cases [82]. An enlarge view of typical unit cell of a PEMFC can be seen in Figure 31 [61], with dimensions of cooling channels and reactant gas channel in few millimeters. Further, by stacking such unit cells repeatedly, a stack with desired level of output power is obtained.

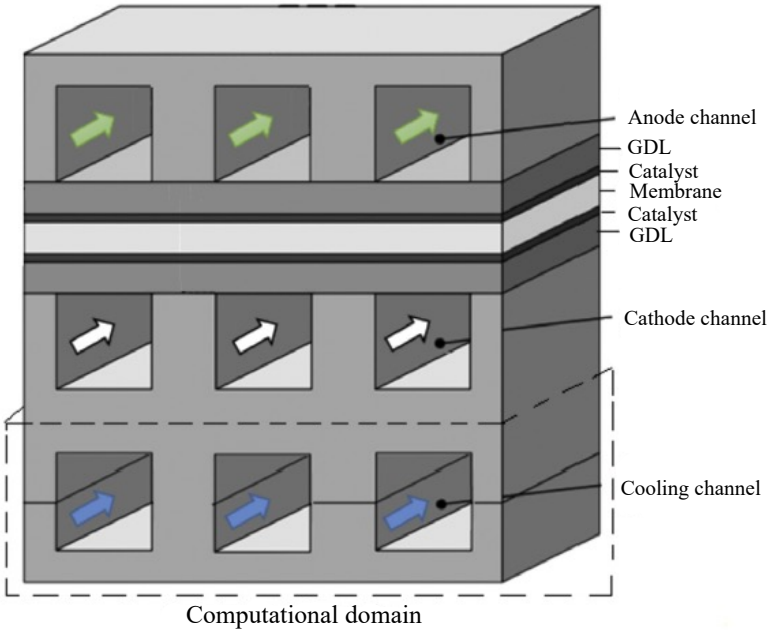



**Figure 31:** Typical unit cell of PEMFC and computational domain [61]

Evidently, effective cooling is important for the operation of a PEMFC stack to dissipate the heat generated. This cooling process is typically achieved using liquid water that circulates through the cooling channels. These channels are either integrated into the bipolar plates or located in separate cooling plates [8]. For this study, a section of the cooling plate has been selected, in which the cooling channels are constructed. The structure used for the cooling plate simulations is illustrated in Figure 32, where the plate is discretized into either fluid cells for coolant channel regions or solid cells for bounding structure regions.

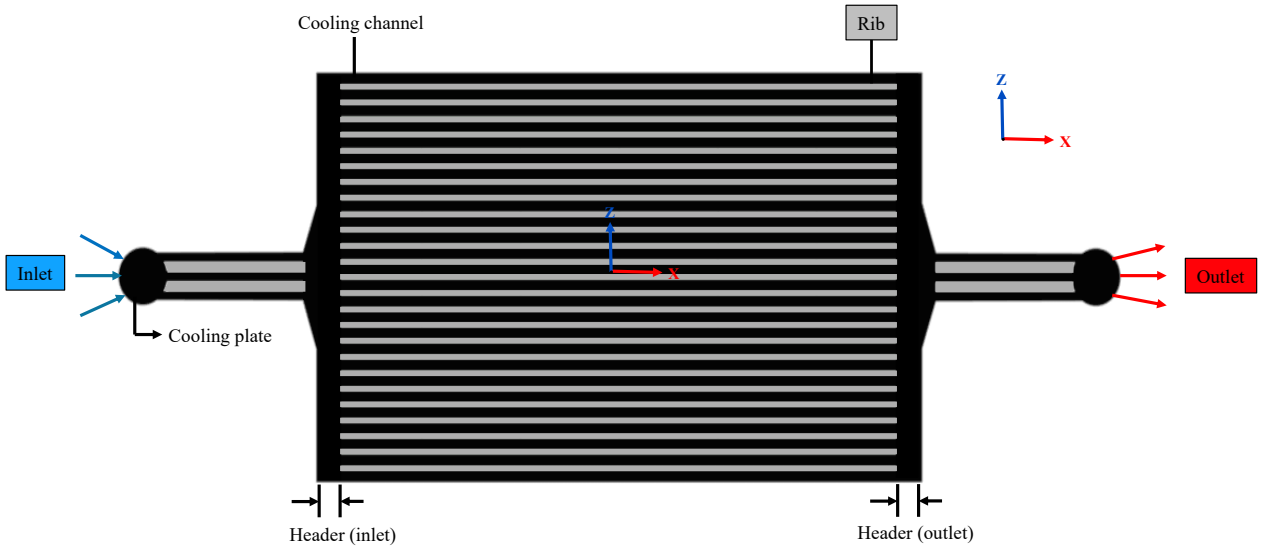



**Figure 32:** Geometry of cooling plate used in the numerical simulation

It is important to note that the rate of heat generation in a PEMFC is generally comparable to the electrical power output of the system. This is because the thermal efficiency of PEMFC is usually around 40% to 50 % [22]. So, managing this heat becomes critical as it can impact the performance and durability of the fuel cell. In this study, a heat slab as illustrated in Figure 33 is used to mimic the heat generated in PEMFC. However, it is difficult to maintain a constant heat flux condition at the surface of the cooling plate during the actual operation of PEMFC, nevertheless the insights gained from these idealized simulations are expected to provide valuable information regarding the performance of cooling plates in real situations.

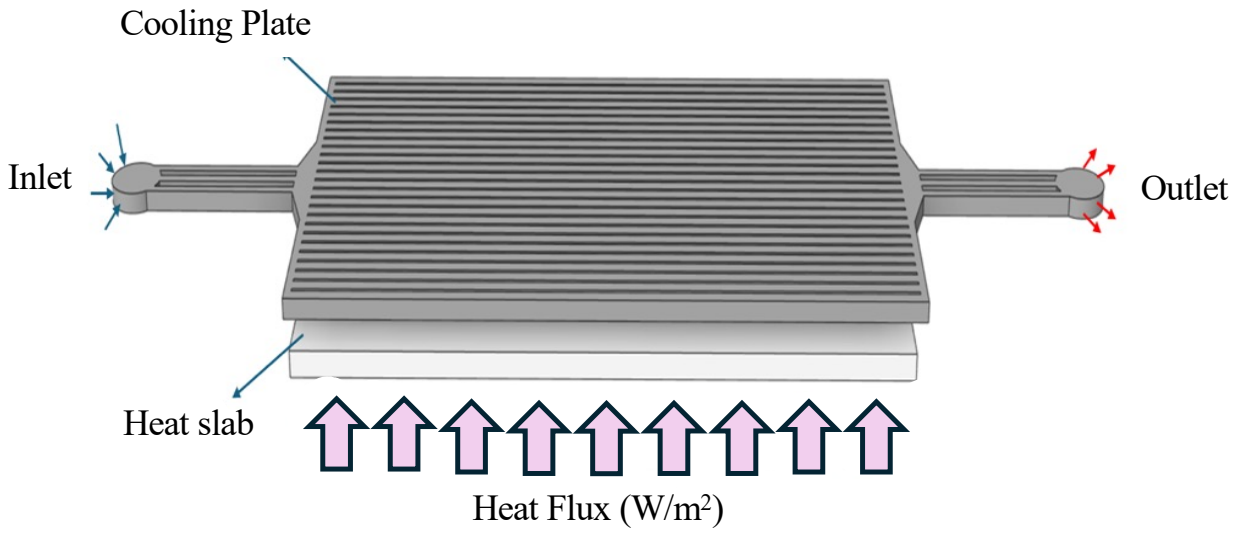



**Figure 33:** Schematic representation of cooling plate and heat slab

For the steady state operation of a PEMFC, the average heat flux at the surface of a dedicated cooling plate is calculated as the amount of heat energy being transferred per unit area. This heat flux denoted as q, represents the rate at which heat is being removed from the fuel cell stack through the cooling plate. It reflects the ability of the cooling system to dissipate the heat generated by the electrochemical reactions [74].

Heat flux, q is determined from the fundamental expression:

$Q_{gen}$ = Total energy from fuel (hydrogen) – Electrical energy output

which can be also written in the form of Equation 8

$$Q_{gen} = \frac{I}{2F} \times H_{HHV}\, n - I\, V\, n. \tag{8}$$

Further, heat flux, q is expressed as :

$$q = \frac{Q_{gen}}{A}$$

Setting the value of $Q_{gen}$ from Equation 8,

$$q = \frac{I\, n}{A} \left( \frac{H_{HHV}}{2F} - V \right)$$

The higher heating value of hydrogen is approximately related to its standard enthalpy of formation: $\Delta HHV \approx -\Delta h_f°$. Hence, q is determined as

$$q = \frac{n\, I \left( \left( \frac{-\Delta hf°}{2F} \right) - V \right)}{A} \tag{10}$$

where n is the number of unit cells per cooling plate, I is the cell current, V is the output cell voltage, A is the total cell area, $\Delta h_f°$ is the formation enthalpy of water (241.8 kJ/mol for LHV, 285.8 kJ/mol for HHV), and F is the Faraday constant (96,487 C/mol). As can be seen from Equation 10, heat flux depends on the cooling system's design, the temperature difference between the cooling fluid (water) and the fuel cell, and the thermophysical properties of the cooling plate material. For the current study, the number of unit cells per cooling plate, n, is one since the model is tested for a single unit cell. However, in practical applications, n, of approximately 3 to 5 is typically used [60].

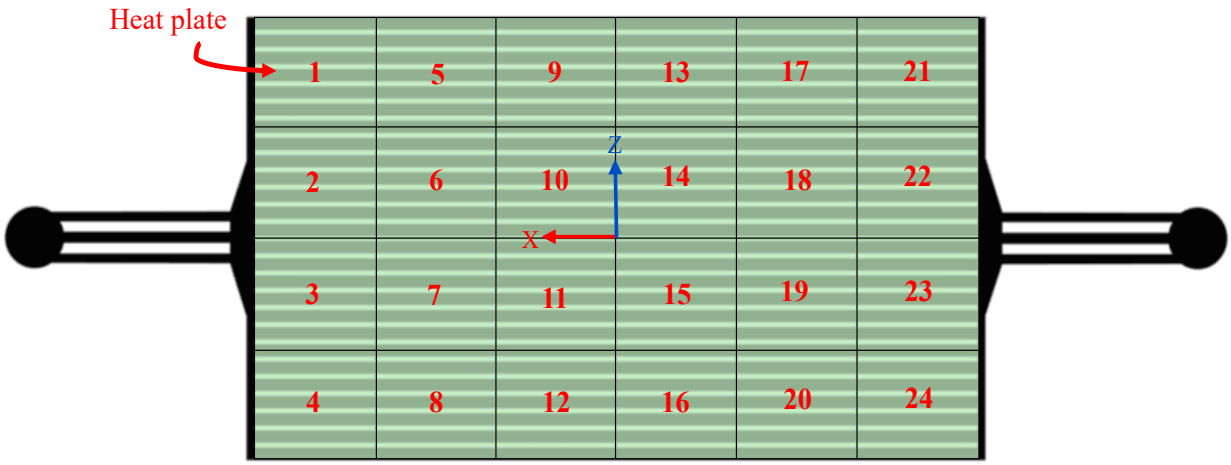



**Figure 34:** Heat slab for the heat flux boundary

For further calculations, the heat slab of a minimum thickness of 0.1 mm, as shown in Figure 34 was considered. The slab was then divided into 24 equal sections to calculate the area-averaged temperature for each region, as well as for the entire plate to check on the uniformity of the distribution of temperature. A constant heat flux boundary condition was then applied at the bottom surface (the heat flux surface) to simulate heat transfer across the plate. The cooling plates have an active area of 87 mm × 51 mm with machined 26 parallel channels, one inlet and one outlet for the cooling fluid (water). The channel depth is 1 mm, and channel width, rib width and the hydraulic diameter are subjected to change in different cases. The surface heat flux, q, is calculated by setting n = 1, V = 0.7 V, J = 1 A/cm$^2$, A = 4437 mm$^2$ in Equation 10 and was prescribed to be 7820 W/m$^2$.

At the outset, there are fifteen cases characterized by variations in geometrical parameters such as the channel to rib width (CR) ratio and the header width. These configurations are designed to provide a detailed understanding of how these parameters affect the thermal and hydraulic performance of the fuel cell system. Every scenario includes twenty-six parallel channels, each with a length of 87 mm. Table 1 illustrates various configurations of CR ratios and header widths, and the coolant flow field designs considered in this study are shown in Figure 35(a), (b), (c), (d) and (e). The consideration of parallel channels with differing CR ratios and header widths is advantageous, as it facilitates a more precise regulation of coolant distribution and heat dissipation. Elaboratively, to provide insight into the scenarios considered, case 1, 2 and 3 have CR ratio of 1, with the channel width and rib width of 1mm. These three cases are taken to be as the base case to study the impact of change in geometrical parameters for correspondingly same header width.

| Cases | CR= $\frac{\text{Channel Width in mm}}{\text{Rib Width in mm}}$ | Header width(mm) |
|---|---|---|
| 1 | 1=1/1 | 1 |
| 2 | 1 | 2 |
| 3 | 1 | 3 |
| 4 | 3.125 = 1.5/0.48 | 1 |
| 5 | 3.125 | 2 |
| 6 | 3.125 | 3 |
| 7 | 0.329 = 0.5/1.52 | 1 |
| 8 | 0.329 | 2 |
| 9 | 0.329 | 3 |
| 10 | 1.69 = 1.25/0.74 | 1 |
| 11 | 1.69 | 2 |
| 12 | 1.69 | 3 |
| 13 | 0.14 = 0.25/1.78 | 1 |
| 14 | 0.14 | 2 |
| 15 | 0.14 | 3 |

**Table 1:** Different cases with variation in CR ratio and header width

For cases 4,5 and 7 the ratio is increased significantly to 3.125, indicating a channel width of 1.5 mm and rib width of 0.48 mm. Subsequently, for cases 7, 8 and 9 CR ratio is taken to be 0.329 with the channel width of 0.5 mm and rib width of 1.52 mm. As the cases progress, with cases 10, 11 and 12, CR further is taken to be 1.69 with channel width of 1.25 mm and rib width of 0.74 mm. For the cases 13, 14 and 15, CR ratio is considered to be 0.14 with the channel width of 0.25 mm and rib width of 1.78 mm. The appropriate values of channel and rib width is chosen in such a way that the number of channels remains constant for each case. Header width for cases 1,4,7,10 and 13 is 1 mm, with varying CR ratios corresponding to each case. Cases 2, 5, 8, 11, and 14 exhibit the diverse range of CR ratios with a specified header width of 2 mm. Finally, cases 3, 6, 9, 12, and 15 demonstrate a range of CR ratios, all maintaining a header width of 3 mm. So, these different geometrical configurations are studied to explore the impact of varying CR ratios and header width, enabling the identification of the optimal configuration.

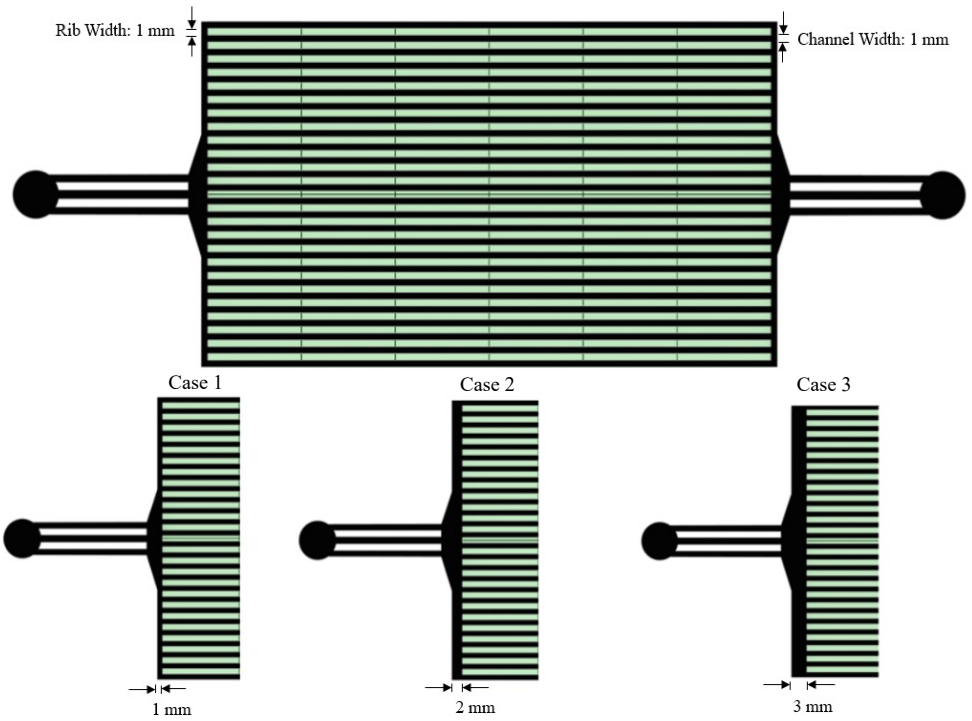



**Figure 35(a):** Coolant flow field design with CR = 1

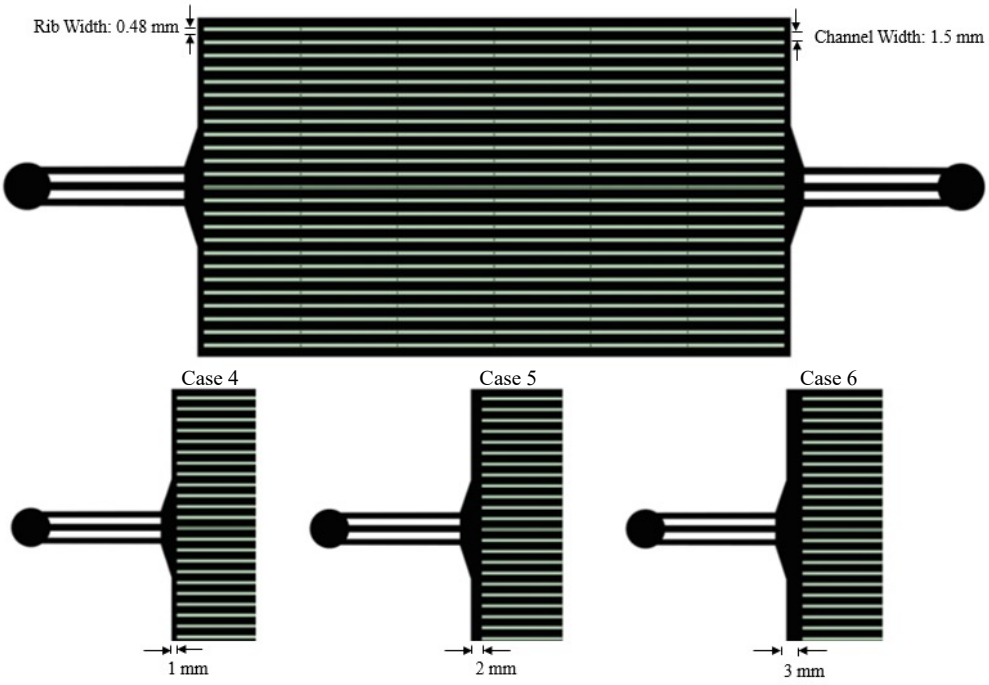



**Figure 35(b):** Coolant flow field design with CR = 3.125

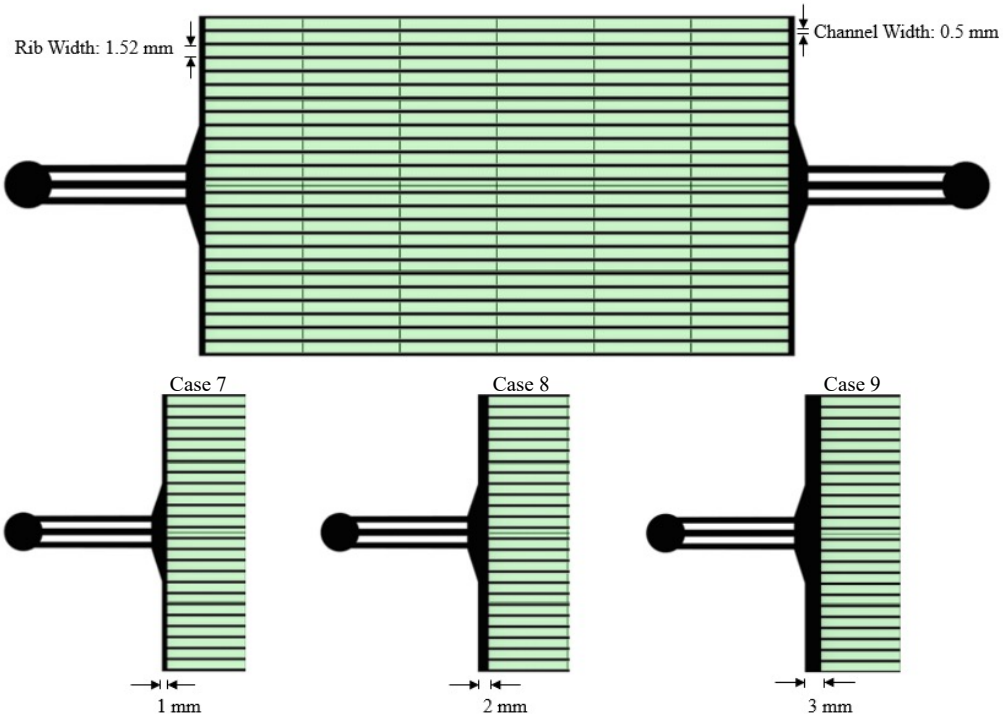



**Figure 35(c):** Coolant flow field design with CR = 0.329

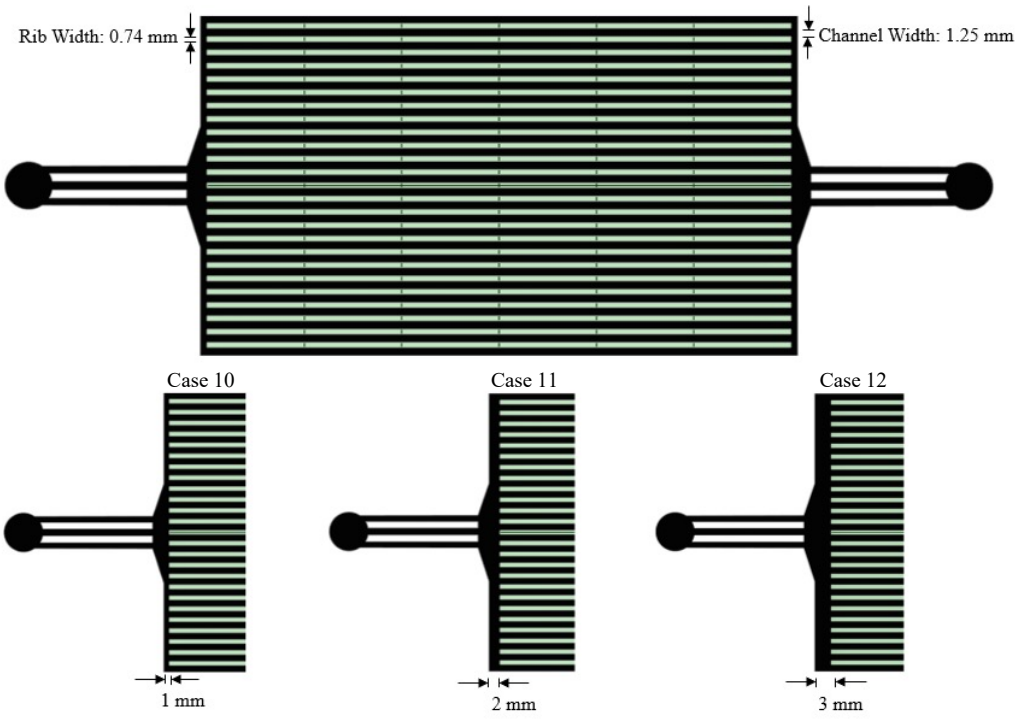



**Figure 35(d):** Coolant flow field design with CR = 1.69

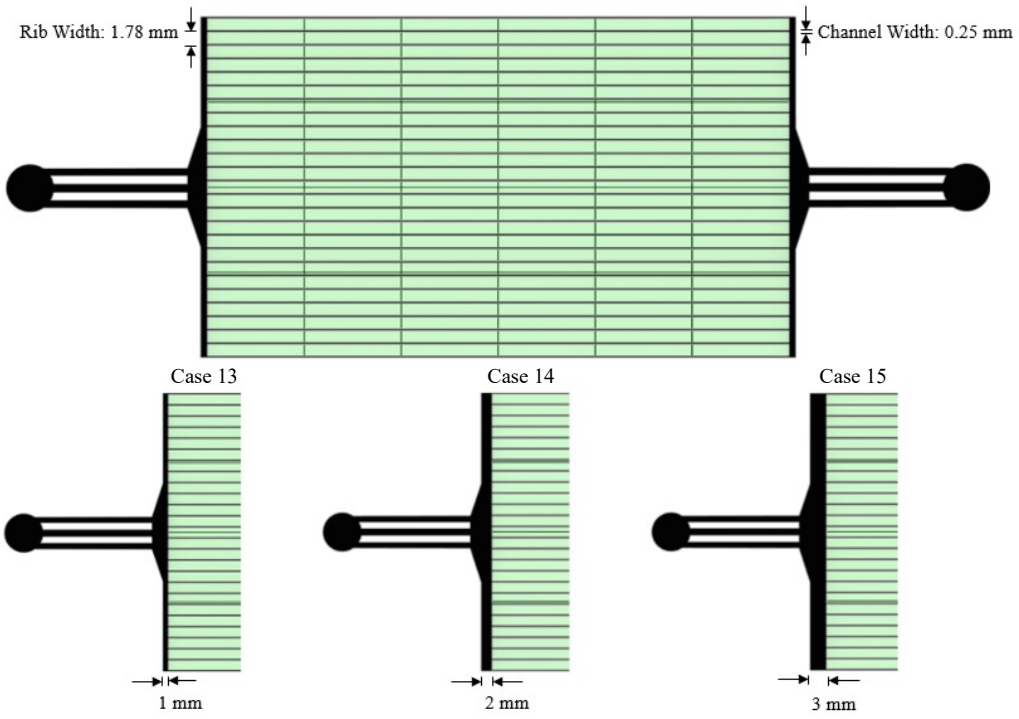



**Figure 35(e):** Coolant flow field design with CR = 0.14

Subsequent to the selection of the optimal case from the initial scenarios, characterized by a CR ratio of 3.125, the model is subjected to further refinement through the incorporation of pins at both the inlet and outlet.

| Cases | $CR = \frac{\text{Channel Width in mm}}{\text{Rib Width in mm}}$ | Header width(mm) | Pins Location |
|---|---|---|---|
| 1 | 3.125 = 1.5/0.48 | 1 | 1 |
| 2 | 3.125 | 2 | 1 |
| 3 | 3.125 | 3 | 1 |
| 4 | 3.125 | 1 | 2 |
| 5 | 3.125 | 2 | 2 |
| 6 | 3.125 | 3 | 2 |
| 7 | 3.125 | 1 | 3 |
| 8 | 3.125 | 2 | 3 |
| 9 | 3.125 | 3 | 3 |

**Table 2:** Different pin locations with CR ratio of 3.125 and varying header width

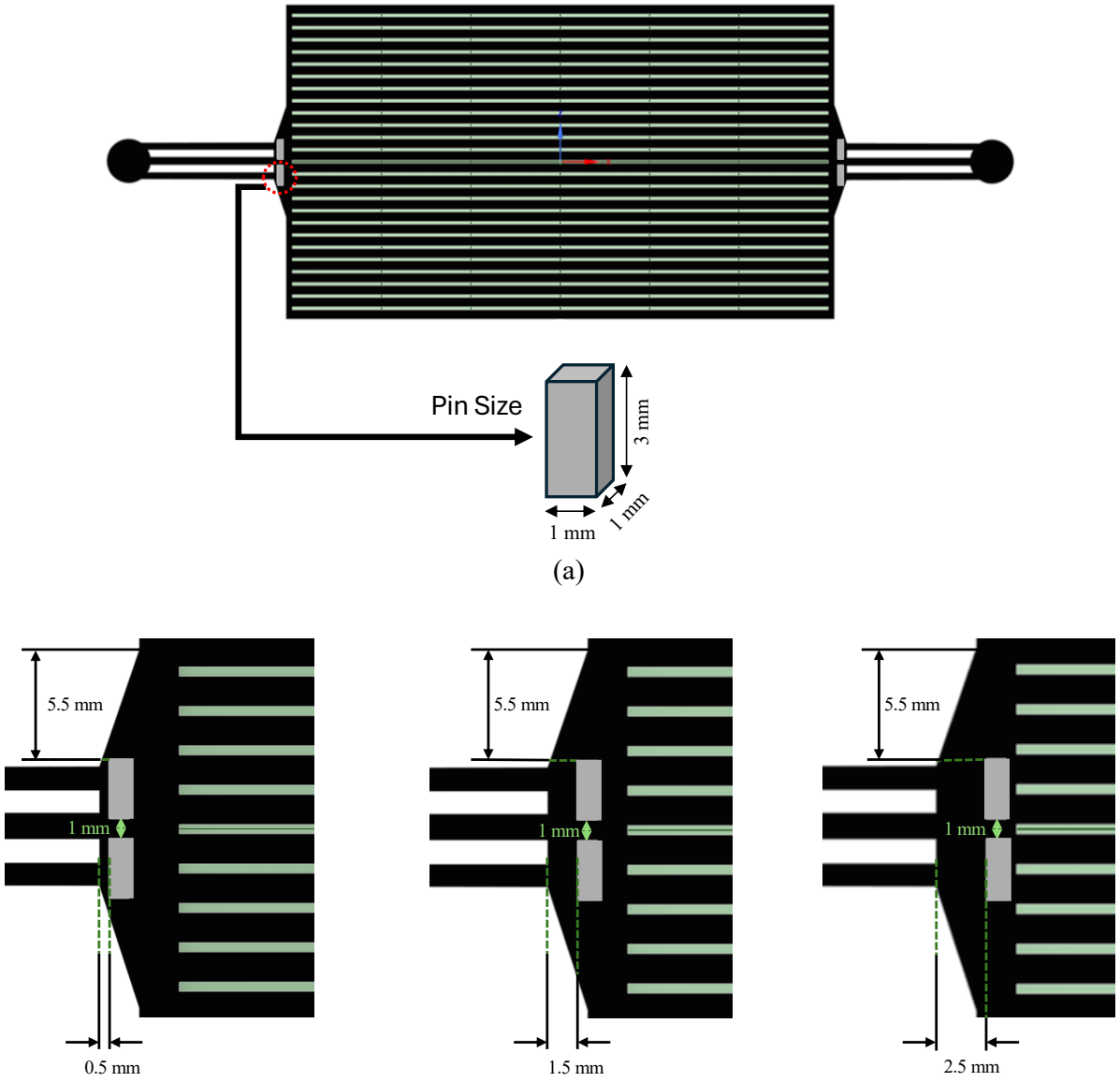



**Figure 36:** (a) Location of pins with CR ratio of 3.125, (b) pin location 1, (c) pin location 2, (d) pin location 3

These pins are strategically positioned at three distinct locations within three different header configurations to enhance the thermal performance and fluid dynamics of the coolant flow. The modifications are intended to optimize heat transfer and minimize thermal gradients within the system. Pin location 1 is positioned at the far left of the inlet side header and the far right of the outlet side header. Pin location 2 is at the middle point of both the inlet side header and outlet side header. Pin location 3 is established at the far right of the inlet side header and the far left of the outlet side header. Rectangular pins incorporated with size of 2 mm × 1 mm. Table 2 provides a detailed overview of nine distinct configurations that have resulted from the application of the

aforementioned modifications. Each case presents unique characteristics that contribute to the overall analysis of the proposed system. Moreover, the spatial arrangement of the pins, which vary in header sizes, is illustrated in Figure 36.

## 3.2 Assumptions

In this model, certain fundamental assumptions have been established to simplify the simulation and concentrate on the essential physical phenomena associated with cooling plate performance. Firstly, the flow is assumed to be in a steady state, indicating that all variables, including velocity, pressure, and temperature, remain constant over time. This assumption enables the simulation to emphasize the equilibrium behavior of the system, while excluding transient effects. The fluid flow is characterized as laminar, which indicates that the coolant moves in smooth, parallel layers with minimal mixing between them. Laminar flow is commonly observed at low Reynolds number and is comparatively simpler to model than turbulent flow. The coolant is regarded as a Newtonian fluid, signifying that its viscosity remains constant and is not influenced by shear rate, thereby assuring a linear relationship between shear stress and shear rate. This simplification facilitates the analysis, given that numerous real-world fluids exhibit such behavior under standard cooling conditions. Furthermore, the coolant is regarded as incompressible, signifying that its density remains constant even when subjected to fluctuating pressure conditions. This premise is widely accepted for liquid coolants due to the inherent low compressibility, and this assumption simplifies the fluid dynamics calculations.

A uniform heat flux is distributed across the surface of the cooling plate. It is assumed that heat is transferred at a constant rate across the entire surface, irrespective of local temperature fluctuations or flow conditions. This assumption simplifies the thermal analysis while offering valuable insights into the overall cooling performance. A no-slip boundary condition is implemented at the walls of the cooling channels, indicating that the fluid velocity at the walls is zero. This assumption is crucial for the accurate representation of boundary layer effects as well as the comprehensive heat transfer dynamics between the fluid and the channel walls. In this model, the influence of gravitational effects is regarded as negligible. Given that the primary emphasis lies on forced convection within the cooling channels, the buoyancy forces resultant from gravity are deemed insignificant. This consideration permits the simulation to concentrate on alternative forces that drive the fluid flow.

Lastly, the top boundary of the cooling plate is modelled as adiabatic, indicating that no heat transfer occurs through this surface. This assumption ensures that the cooling system exclusively transfers heat via the designated cooling surfaces, thereby isolating the effects of the coolant channels and ensuring that heat loss through other surfaces is excluded from the simulation. These assumptions enhance the model's efficiency while preserving the accuracy of the cooling performance analysis. By concentrating on essential parameters such as fluid flow, heat transfer, and boundary conditions, the model can yield significant insights into its behavior system.

## 3.3 Model Formulation

For laminar, Newtonian and incompressible flow of liquid coolant (water) through the cooling plate, as per the aforementioned assumptions, the governing equations are expressed as follows. The general continuity equation for a compressible liquid(water) in three dimensions is written as:

$$\frac{\partial \rho}{\partial t} + \nabla \cdot (\rho u) = 0 \tag{11}$$

where $\rho$ is density of water (kg/m$^3$), u is velocity vector of water (m/s), t is time (s) and $\nabla \cdot (\rho u)$ is the divergence of the mass flux. The fluid density ρ is constant for incompressible flow, so the term involving $\frac{\partial \rho}{\partial t}$ becomes zero. Further, in the cartesian coordinates, the velocity vector u has three components: u, v and w, which represent velocity in x, y and z directions, respectively. So, expanding the divergence operator gives the continuity equation expressed as:

$$\frac{\partial u}{\partial x} + \frac{\partial v}{\partial y} + \frac{\partial w}{\partial z} = 0 \tag{12}$$

The general momentum conservation (Navier – Strokes) equation for an incompressible fluid, derived from Newton's second law, can be expressed as:

$$\rho\left(\frac{\partial u}{\partial t} + u \cdot \nabla u\right) = -\nabla p + \mu \nabla^2 u + F \tag{13}$$

where ρ is the density of the fluid, u is the velocity vector of the fluid, p is the pressure (Pa), $\mu$ is the dynamic viscosity of water (Pa s), $\nabla^2 u$ is the Laplacian operator, and F is external body forces (gravity). For incompressible flow and considering all the assumptions, the momentum conservation in cartesian coordinates can be expressed as:

$$\rho\left(u\frac{\partial u}{\partial x}+v\frac{\partial u}{\partial y}+w\frac{\partial u}{\partial z}\right)=-\frac{\partial p}{\partial x}+\mu\left(\frac{\partial^2 u}{\partial x^2}+\frac{\partial^2 u}{\partial y^2}+\frac{\partial^2 u}{\partial z^2}\right) \quad (14)$$

$$\rho\left(u\frac{\partial v}{\partial x}+v\frac{\partial v}{\partial y}+w\frac{\partial v}{\partial z}\right)=-\frac{\partial p}{\partial y}+\mu\left(\frac{\partial^2 v}{\partial x^2}+\frac{\partial^2 v}{\partial y^2}+\frac{\partial^2 v}{\partial z^2}\right) \quad (15)$$

$$\rho\left(u\frac{\partial w}{\partial x}+v\frac{\partial w}{\partial y}+w\frac{\partial w}{\partial z}\right)=-\frac{\partial p}{\partial z}+\mu\left(\frac{\partial^2 w}{\partial x^2}+\frac{\partial^2 w}{\partial y^2}+\frac{\partial^2 w}{\partial z^2}\right) \quad (16)$$

The general energy equation in fluid dynamics describes the conservation of energy for a fluid flow. The equation in its general form for an incompressible liquid can be written as:

$$\rho C_p\frac{\partial T}{\partial t}+\rho C_p v\cdot\nabla T=k\nabla^2 T+Q_{source} \quad (17)$$

where, $C_p$ is specific heat capacity of water (J/kgK), T is temperature (K), k is thermal conductivity of water (W/mK), $Q_{source}$ is heat source term. However, for steady state incompressible flow, the energy equation in cartesian coordinates can be expressed as:

$$\rho C_p\left(u\frac{\partial T}{\partial x}+v\frac{\partial T}{\partial y}+w\frac{\partial T}{\partial z}\right)=k\left(\frac{\partial^2 T}{\partial x^2}+\frac{\partial^2 T}{\partial y^2}+\frac{\partial^2 T}{\partial z^2}\right) \quad (18)$$

Further, for solid regions, the energy equation is revised by setting u = v = w = 0. This represents the pure conduction equation.

The geometrical parameters and material properties utilized in this simulation are listed in Table 3. The cooling plates are composed of aluminum ($\rho$ = 2700 kg/m³ and k = 235 W/mK) and the primary reason to choose aluminum for this investigation is to assess the effect of the thermophysical properties of the plate, alongside its geometry, on the heat dissipation in a PEMFC. Aluminum exhibits exceptional thermal conductivity, thereby facilitating efficient heat transfer when accompanied by an increased surface area of the channel. Additionally, aluminum's lightweight nature is advantageous in applications requiring reduced weight, particularly in the automotive sector. Furthermore, it is recognized that water possesses a high specific heat capacity (4181 J/kgK) and commendable thermal conductivity (k = 0.644 W/mK), rendering it an ideal working fluid for this study; specifically, liquid water ($\rho$ = 988.1 kg/m³) is employed. The inlet temperature of the coolant (water) is established at 323 K and the heat flux generated per cell at a working voltage of 0.7 V and a current density of 1 A/cm² has been determined to be 7820 W/m².

| Properties of Water @323K | |
|---|---|
| Density | 988.1 kg/m$^3$ |
| Specific heat capacity | 4181 J/kg K |
| Thermal conductivity | 0.644 W/m K |
| Viscosity | 0.000547 Pa s |
| **Properties of Aluminium** | |
| Density | 2700 kg/m$^3$ |
| Specific heat capacity | 900 J/kg K |
| Thermal conductivity | 235 W/m K |

**Table 3:** Parameters used for cooling plate simulation

The thermal energy produced by the fuel cell has been modeled as a heat flux applied to the lower surface of the cooling plate, as depicted in Figure 33. While determining the comprehensive heat generation in a PEMFC is a relatively straightforward process, the precise evaluation of the local heat generation rate presents a considerable challenge. This complexity arises from the significant impact that local heat generation exerts on the performance of the cell. Nevertheless, due to the inherent irregularity of local heat generation, quantifying it accurately remains a difficult task. Uneven heat generation may result in localized hot spots and complicate the temperature distribution more complicated. Despite these difficulties, the outcomes of simulations that assume the constant heat flux remain significant. These idealized simulations yield critical insights into the performance of cooling plates and can serve as a benchmark for the design of cooling systems in practical applications [83].

The operating conditions are outlined in Table 4, and the computational domain of the plate can be seen in Figure 32. The mass flow rate at the inflow boundary of the fluid region is set to be constant ($\dot{m}$ = 0.00165 kg/s). The mass flow rate is calculated using the relation [84]:

$$Q = \dot{m}\, C_p\, \Delta T \tag{19}$$

where Q is the heat transfer rate(W), $\dot{m}$ is the mass flow rate of the fluid(kg/s), Cp is the specific heat capacity of the fluid(J/kgK) and ΔT is the temperature change of the fluid. The calculated heat flux is 7820 W/m² for a plate area of 4437 mm² with a temperature difference between inlet and outlet of the coolant of 5℃. Using Equation 19, the mass flow rate is determined to be 0.00165 kg/s under constant pressure at the outflow boundary. Precisely, Table 5 provides a comprehensive summary of the boundary conditions

| **Operating Parameters** | |
|---|---|
| Inlet temperature of water ($T_{inlet}$) | 323 K |
| Inlet mass flow rate ($\dot{m}_{in}$) | 0.00165 kg/s |
| Inlet velocity ($v_{in}$) | 1.1132 m/s |
| Heat flux | 7820 $W/m^2$ |

**Table 4:** Operating conditions of the computational domain

| **Boundary Conditions** | |
|---|---|
| Inlet flow | $u = v_{in}$ , $T = T_{in}$ |
| Outlet flow | $P = P_{atm}$, $\Delta P = P_{inlet} - P_{outlet}$ |
| Interface walls | u = 0, v = 0, w = 0<br>$q_{conduction} = q_{convection}$ |
| Bottom walls | u = 0, v = 0, w = 0<br>Heat Flux = q |
| Top walls | u = 0, v = 0, w = 0<br>Adiabatic |

**Table 5:** Boundary conditions of 3D model

## 3.4 Calculations and Numerical Procedure

The primary role of cooling plates in PEMFC is to mitigate the risk of overheating. While it is imperative to effectively dissipate the heat generated during electrochemical reactions, it is equally essential to maintain a uniform temperature distribution across the active area. Consequently, a comprehensive understanding of the temperature distribution on the surface of the cooling plate is of utmost importance. To quantitatively evaluate cooling performance, several critical parameters necessitate meticulous analysis. This study identifies various factors that may assist in the assessment of cooling performance, which are outlined below.

### 3.4.1 Temperature Difference between Minimum and Maximum Temperature

The variation in temperature between the maximum and minimum readings is an important measure of how evenly heat is distributed across the cooling plate. Keeping track of this temperature variation offers valuable information about the consistency of the temperature distribution.

Temperature difference, ΔT is given by:

$$\Delta T = T_{max} - T_{min} \tag{20}$$

A larger temperature difference suggests uneven cooling, which can negatively impact the performance and life of the fuel cell. However, a smaller surface temperature signifies more effective cooling, ensuring a uniform temperature distribution. Analyzing the variations in maximum temperature difference for mass flow rate and heat flux offers valuable insights into determining the optimal design. This approach helps in identifying which configuration performs better in terms of maintaining uniform temperature distribution and effectively managing the heat load [74].

### 3.4.2 Temperature Uniformity Index, $U_T$.

Temperature Uniformity Index, $U_T$ indicates the quantitative measure of how evenly the cooling system is managing the heat generated during the operation of the cell. It is a key tool for comparing different cooling channel designs, mass flow rates and heat flux conditions and helps identify the best configuration for thermal management. Temperature Uniformity Index, $U_T$ is defined as [63]:

$$U_T = \frac{\int_A |T - Tavg| dA}{\int_A dA} \text{ and } T_{avg} = \frac{\int_A T dA}{\int_A dA} \quad (21)$$

where A is the surface area, T is the surface temperature, $T_{avg}$ is the average temperature of the cooling. It is to be noted that integration in Equation 21 is done only for the surface area at the constant heat flux boundary. $U_T$ quantifies the degree of deviation of the surface temperature, T from the average temperature, $T_{avg}$. A low $U_T$ value indicates that the temperature distribution across the cooling channels is highly uniform, as the local temperatures are closer to the average temperature. It could also be said that the temperature distribution is perfectly uniform if $U_T$ becomes zero.

### 3.4.3 Pressure Drop

The pressure drop across the coolant flow field designs is an essential factor in maintaining an even coolant flow. It serves as an indicator of the ease with which the fluid moves through the channels. A uniform pressure drop throughout the entire flow field typically suggests that the fluid is distributed evenly across all channels, ensuring consistent heat removal from every part of the cell. If there are notable differences in the pressure drop throughout the flow field, it indicates an uneven distribution of flow. As a result, certain areas may encounter higher fluid velocities, which can lead to overcooling, while other regions may experience lower velocities or stagnant flow, resulting in inadequate cooling. These inconsistencies degrade the membrane, reduce reaction efficiency and cause long-term damage to the cells. A study by S.M. Baek et al. [63] supports this relationship by demonstrating that the parallel straight flow field showed a smaller pressure drop but, at the same time, the most non-uniform temperature distribution.

### 3.4.4 Numerical Procedure

The discretization of the governing partial differential equations is conducted utilizing the finite volume method, implemented on a staggered grid layout within the computational domain. Variables such as velocity and pressure are computed on distinct grids to enhance the accuracy of the solution. This methodology guarantees that the control volumes for varying variables, including pressure and velocity, are offset from one another, enhancing accuracy. The comprehensive simulation of fluid flow and heat transfer within the cooling plates was conducted using commercially available CFD software: ANSYS FLUENT, release 2023 R2. Software uses the finite volume discretization method to solve the conservation equations for mass, momentum and energy. FLUENT numerically solves the fundamental equations governing fluid flow and heat

transfer to predict the behaviour of the system. To ensure the proper coupling between the pressure and velocity fields, the coupled scheme is employed. The coupled algorithm addresses low convergence rates by implicitly handling both terms. This is achieved by coupling the momentum equations with the pressure and velocity fields through a series of coefficients that represent their interdependent effects on the continuity equation [85]. Furthermore, the convective terms in the equations are approximated using a second order upwind scheme, providing greater stability of the solution.

The convergence of a simulation is determined based on the averaged absolute value of the residual for each conservation equation. The scaled residual for the continuity equation is $10^{-4}$, indicating that the mass conservation is well satisfied within the specified tolerance. The residual for the velocity and energy components is $10^{-6}$. It is to be noted that the maximum allowable relative mass residual based on inflow mass is $10^{-4}$.

## 3.5 Grid Independency

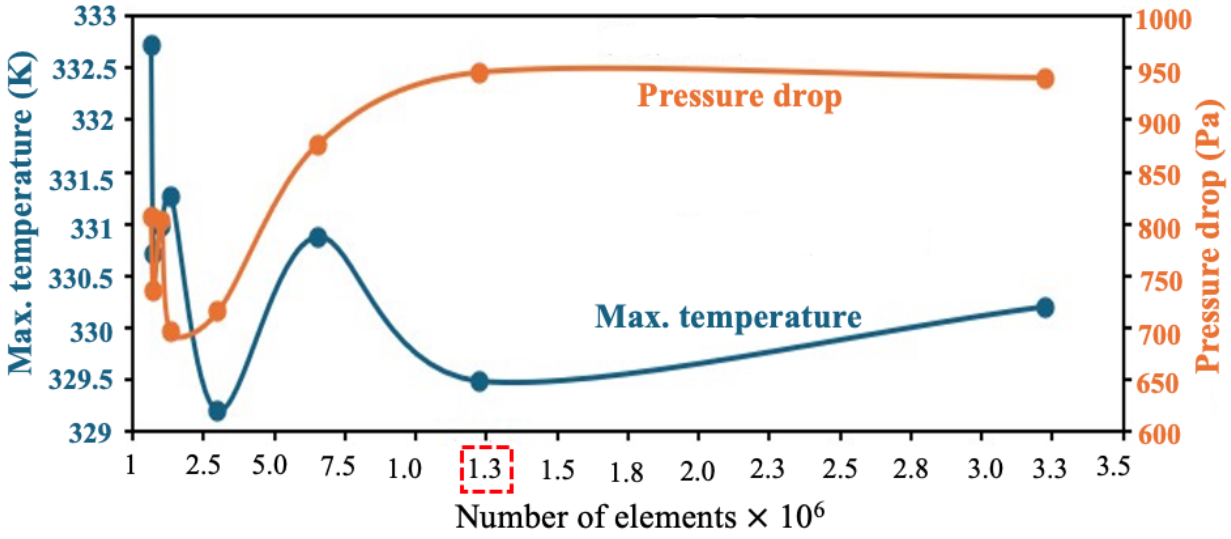



**Figure 37:** Grid independency for channel width 1.5mm against maximum temperature and pressure drop

To ensure the precision and reliability of the numerical findings, an investigation into grid independence is conducted in this section. This step is crucial for validating that the simulation results remain largely unaffected by additional grid refinement. The grid independence was assessed for the flow field design, characterized by CR ratio of 3.125 and a header width of 1 mm. The test examined the correlation between the number of discretized volume cells and the calculated pressure drop as well as the maximum surface temperature. Similar parameters were

studied by S.M. Baek et al. [63] to verify grid independence and confirmed that these parameters yield accurate results. Figure 37 illustrates the results derived from the grid dependency test for a parallel flow field design. The findings indicate that the pressure drop, and maximum temperature exhibit less dependency once the cell number exceeds 1,300,000. Beyond this point, fluctuations in pressure drop and temperature stabilize, indicating minimal changes with further increases in element numbers. Consequently, the optimal cell count for all scenarios was chosen to be 1,226,003. This ensures that the numerical model maintain its reliability without increasing unnecessary computational cost.

## 3.6 Model Validation

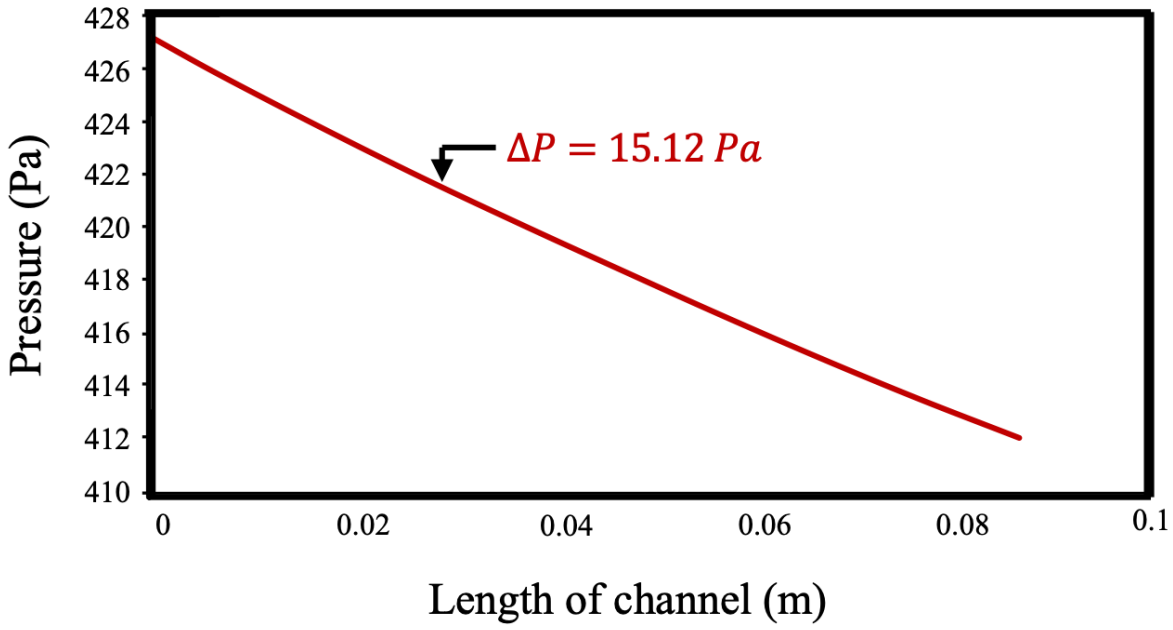



**Figure 38:** Evolution of pressure along the channel length

Validating cooling channel geometries in PEMFC simulations is necessary to ensure the accuracy of the model's predictions to match the real-world scenarios. To validate the present CFD calculations, the static pressure along the length of the channel is checked for the parallel straight flow field. Figure 38 shows the evolution of water pressure along the first straight channel from top. Empirically, the pressure drop across straight channels can be estimated using the Darcy-Weisbach equation for fully developed flow in channels:

$$\Delta P = f \frac{L}{D_h} \frac{\rho v^2}{2} \tag{22}$$

where, ΔP is the pressure drop across the channel, f is the friction factor dependent on the flow regime: laminar or turbulent, L is the channel length, $D_h$ is the hydraulic diameter of the channel, $\rho$ is the coolant density and v is the average flow velocity in the channel. For laminar flow, the friction factor f is given by:

$$f = \frac{64}{Re} \tag{23}$$

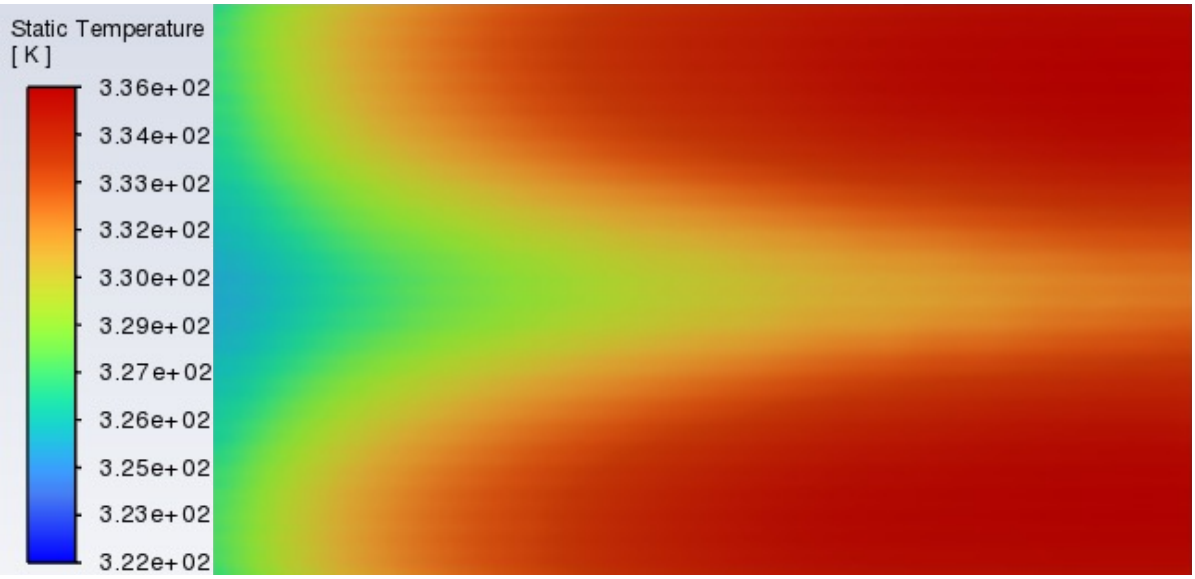
where Re is the Reynolds number.

In Figure 38, the simulated pressure drop is reported as 15.12 Pa. The average velocity of water within the channel measures 0.015743 m/s. Based on this data, the Reynolds number has been determined to be 34.126, which yields a friction factor value of 1.8754 when employing Equation 23. Consequently, utilizing Equation 22, the pressure drop value is calculated to be 16.64 Pa. The percentage deviation is 9.13%, which verify the reliability of the numerical simulation method used in this study.

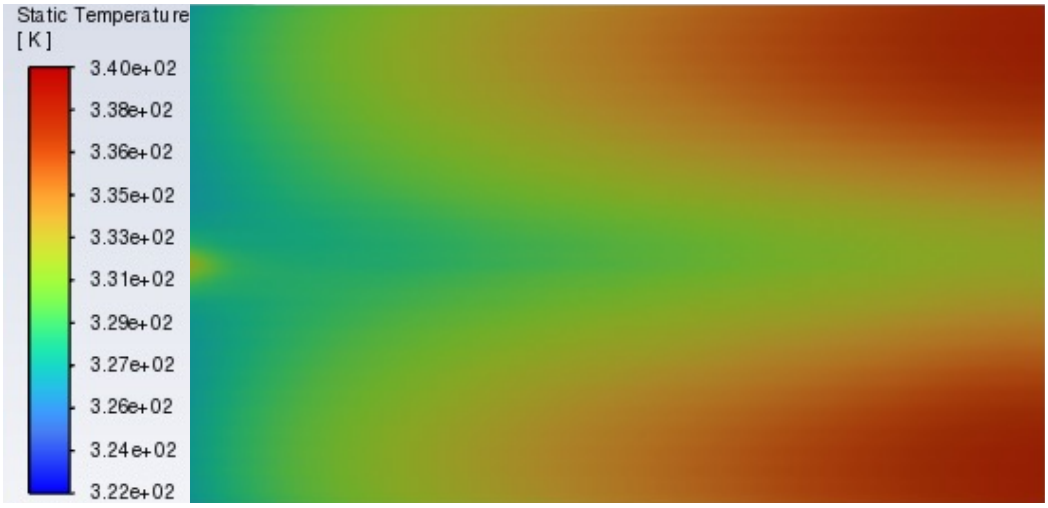
# 4. Results and Discussion

## 4.1 Temperature Distribution and Pressure Drop

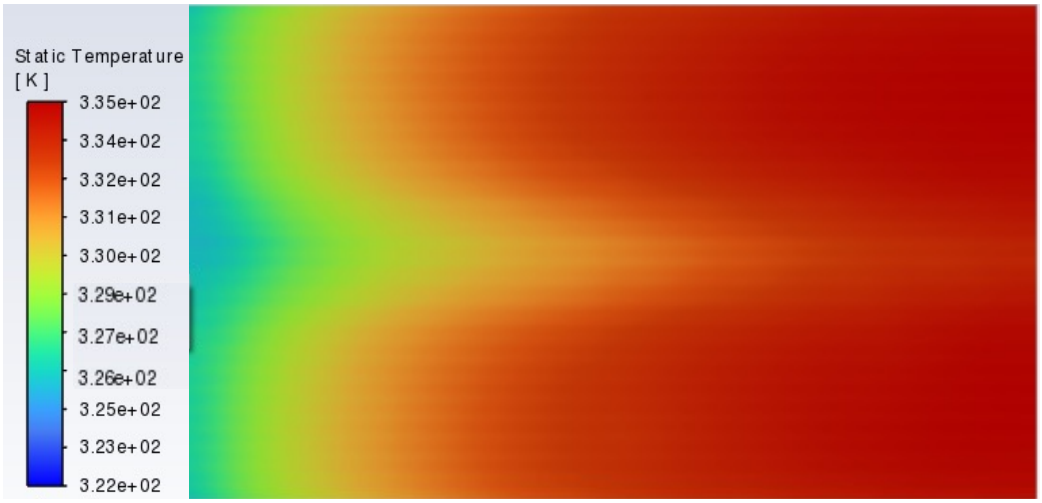
The simulated temperature distribution at the mid-plane of the cooling plate is calculated, with the mass flow rate of liquid water and the heat flux fixed at 0.00165 kg/s and 7820 W/m$^2$ respectively for the simulations. Figures 39 illustrate the temperature distribution across the solid plate region as the coolant water flows through the channel, corresponding to CR ratios of 1, 3.125, 0.329, 1.69, and 0.14 for header widths of 1 mm, 2 mm, and 3 mm. Table 1 depicts the configurations of different designs considered in the study. Cases 1, 2, and 3 exhibit more significant temperature variations, particularly around the inlets and outlets. In contrast, cases 4, 5, and 6 show a more evenly distributed gradient, resulting in minimal temperature variation. Cases 7, 8, and 9 have less pronounced temperature gradients due to the narrower width of the channels. Cases 10, 11, and 12 demonstrate a uniform cooling effect across the surface, while cases 13, 14, and 15 display the most uneven distribution of temperature. Overall, the trend indicates that wider channels lead to a more even temperature distribution, and cases 4,5 and 6 could be considered as the best among all the scenarios.



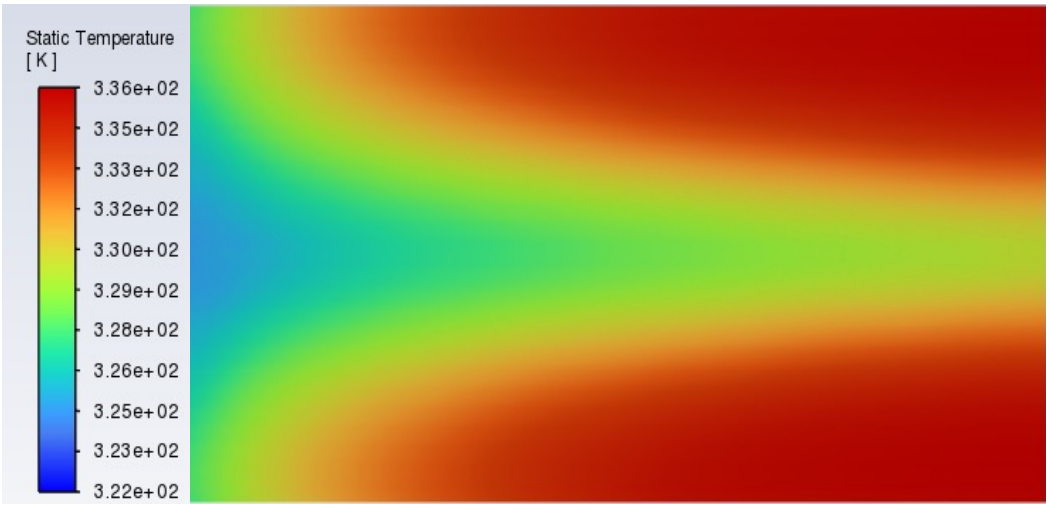

Case 1



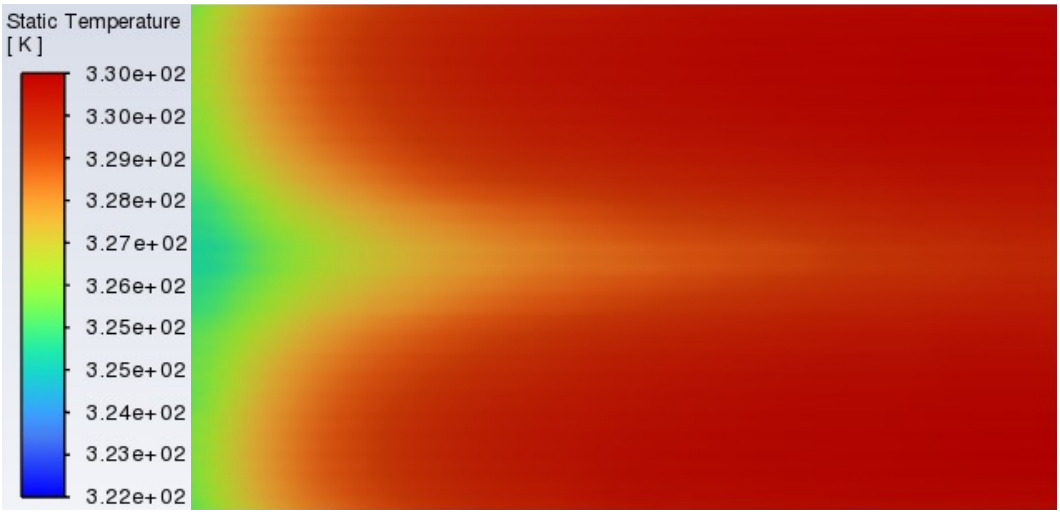

Case 2



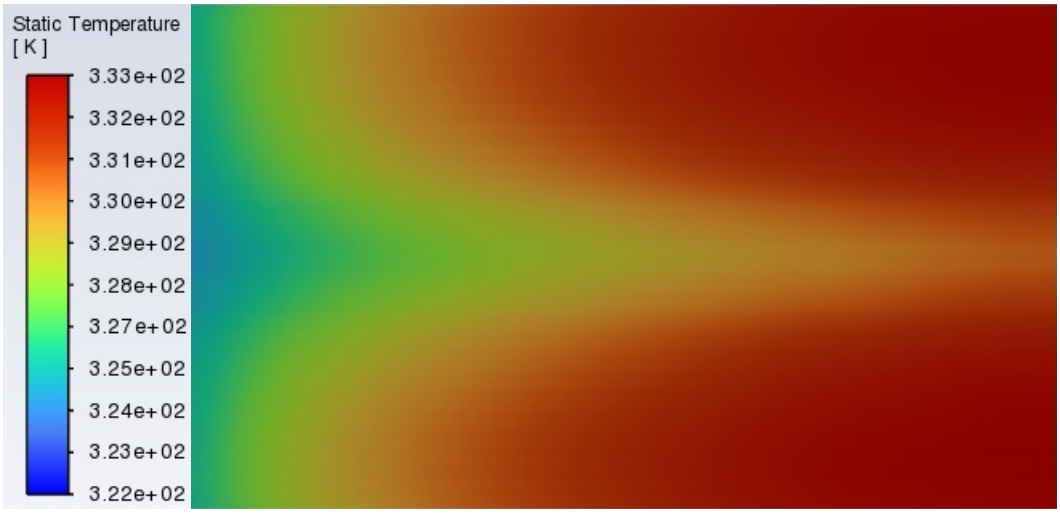

Case 3



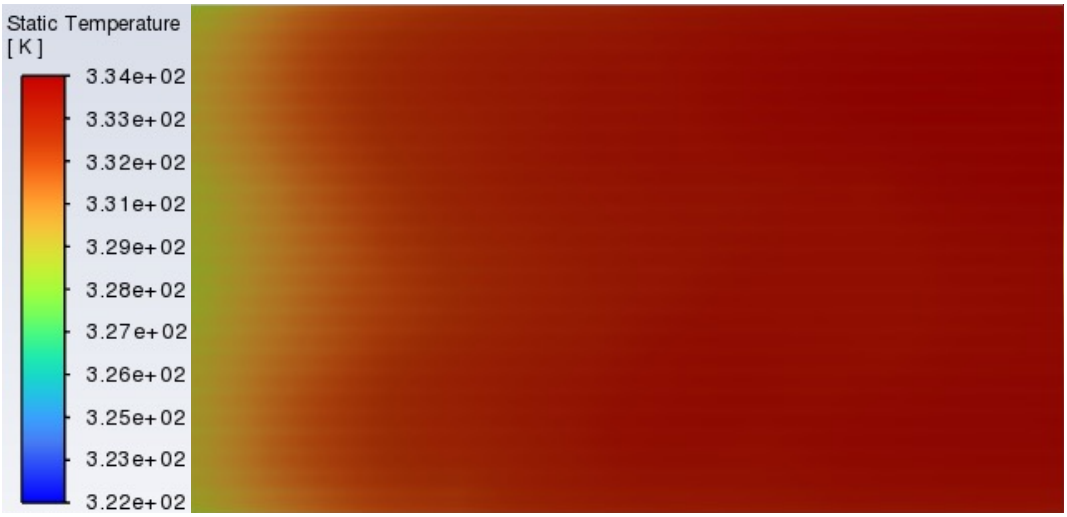

Case 4



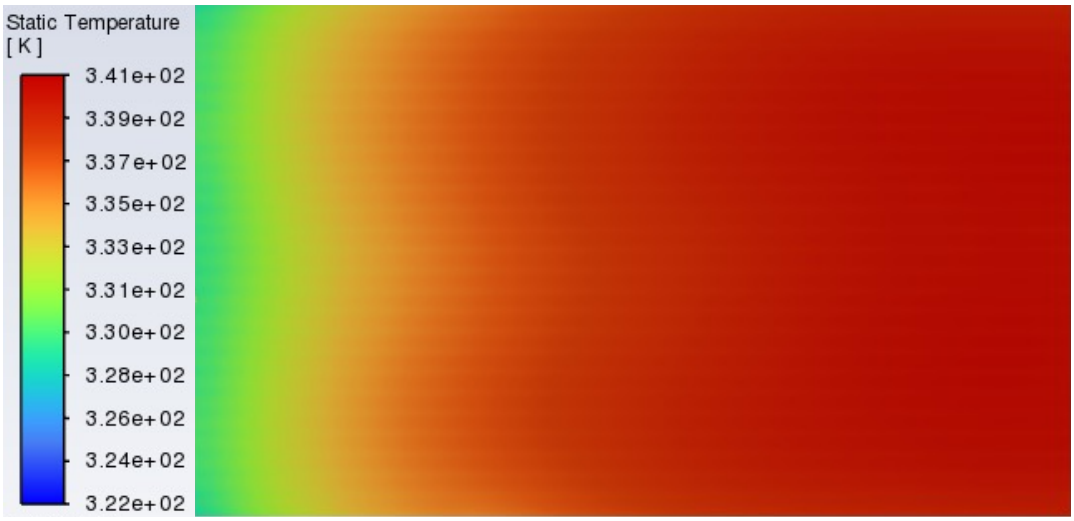

Case 5



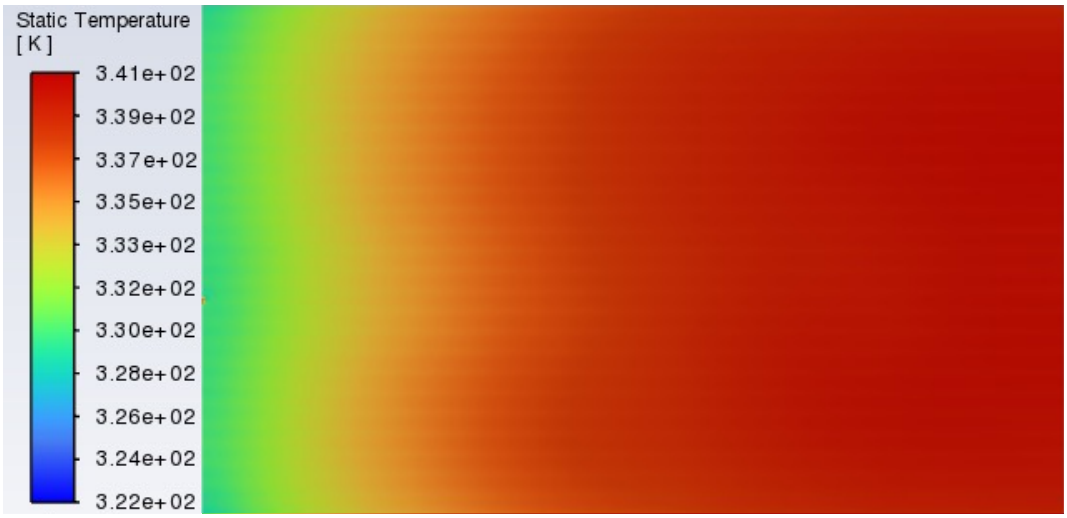

Case 6



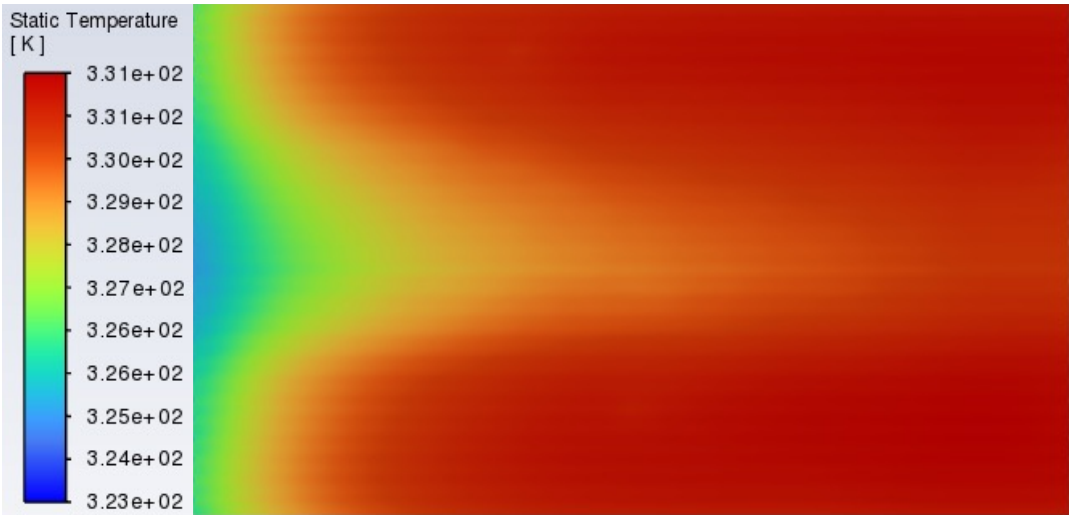

Case 7



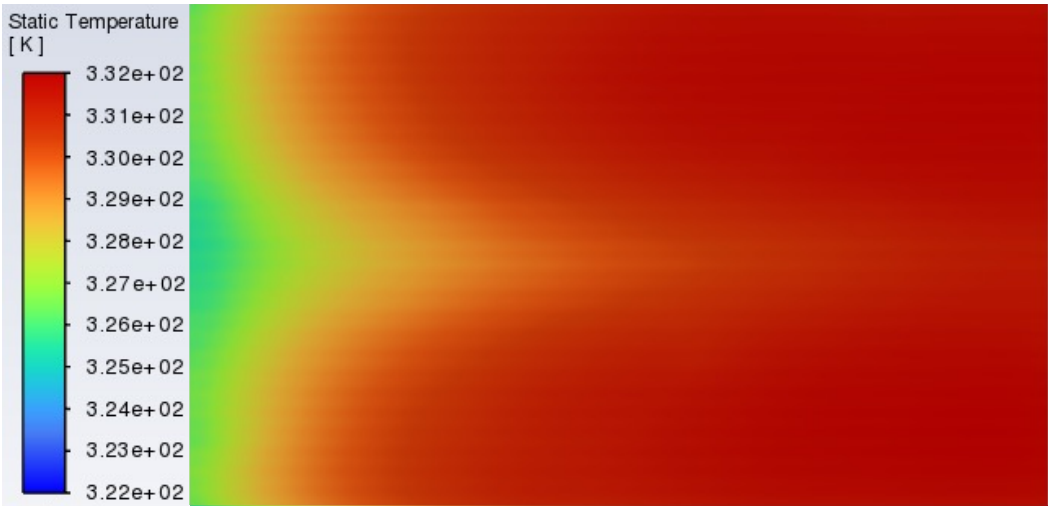

Case 8



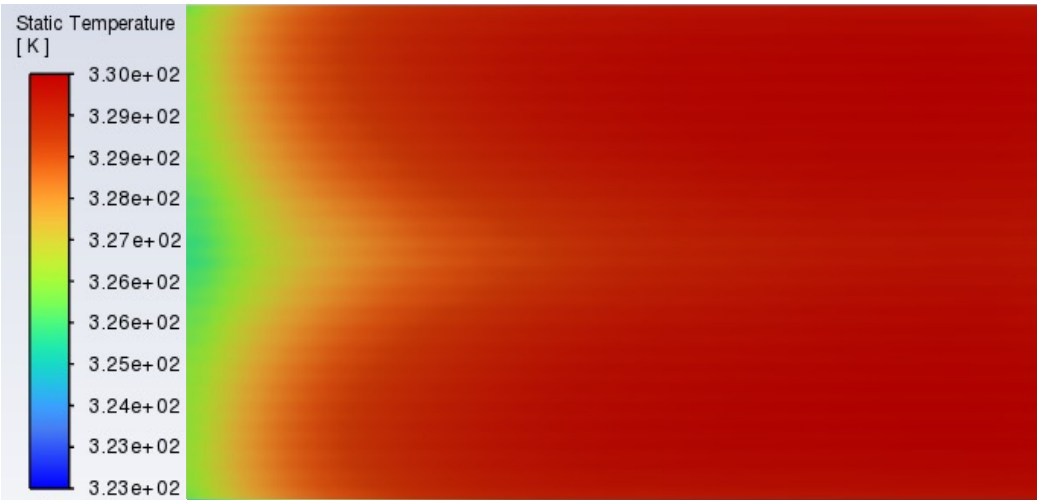

Case 9



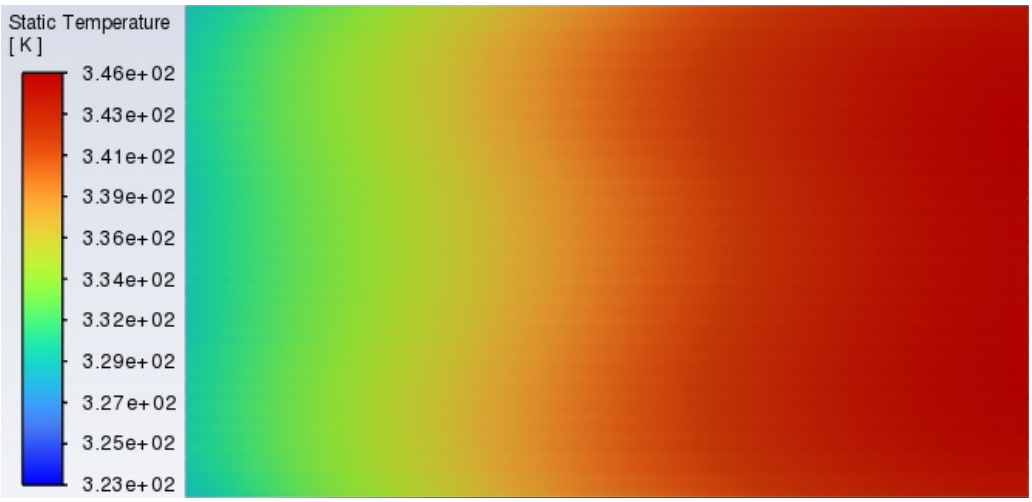

Case 10



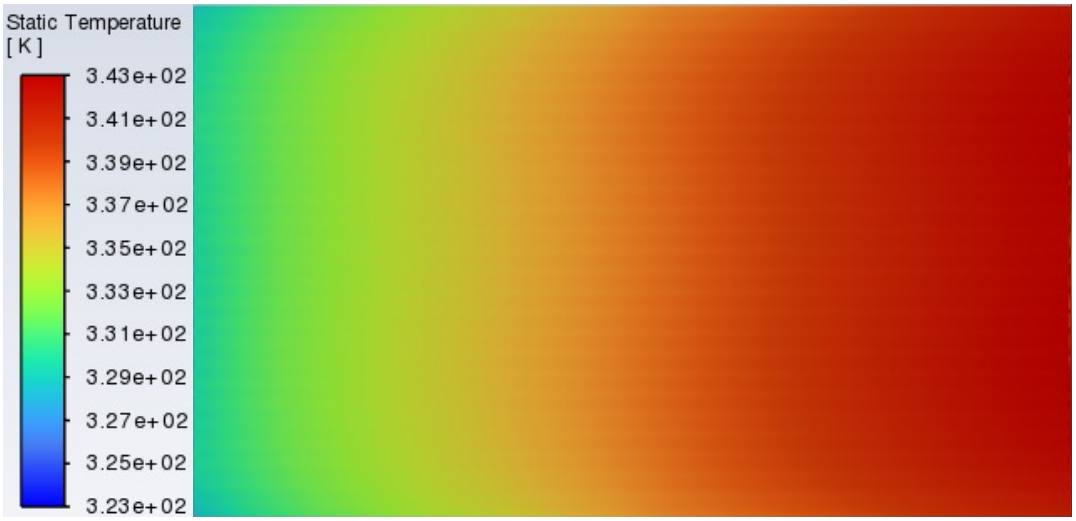

Case 11



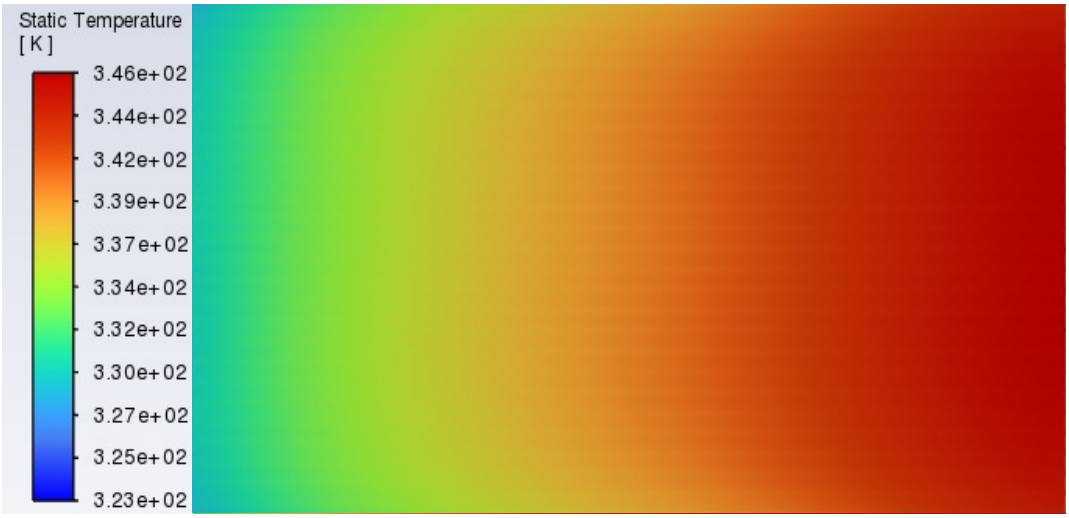

Case 12




Case 13




Case 14




Case 15

**Figure 39:** Temperature distribution for case 1 to case 15

It is observed that the temperature is typically lower near the coolant flow field's inlet and higher near its outflow because temperature tends to rise along the flow channel by collecting reaction heat (constant heat flux). The smoother gradient also suggests a steady increase in temperature along the coolant flow path.

The distribution of temperature in the cooling channels is closely related to the velocity of the flow field, as the cooling fluid's movement is crucial for effective heat transfer. Increased fluid velocity typically boosts convective heat transfer, which minimizes localized temperature variations and helps prevent the formation of hotspots. In contrast, areas with slower flow velocity may suffer from lower cooling efficiency, resulting in uneven temperature distribution and possible thermal

imbalances within the system [77]. The normalized distribution of mass flow is depicted in Figure 40, which directly relates to the velocity distribution. It is to be noted that for cases 13, 14 and 15, since the channel width is considerably smaller than that of the rib width, a velocity profile attained was not sufficiently informative for the analysis. The velocity is calculated at the mid plane of the bipolar plate and at the midpoint of each channel. The variations in velocity distribution could suggest areas where heat transfer might not be as efficient, and a higher normalized velocity indicates a faster flow, while a lower value indicates a slower flow. Channels with lower velocities could be underperforming in terms of heat removal or fluid movement. The graph in Figure 40 also indicates opportunities for design improvements.

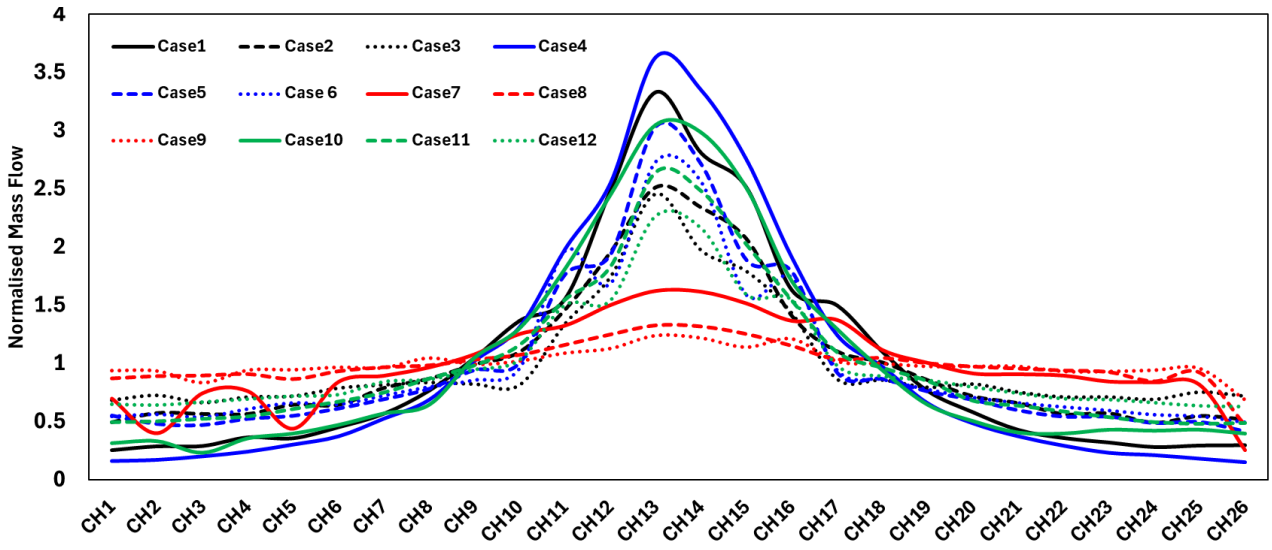



**Figure 40:** Normalized mass flow distribution for different cases

To further quantify the results, Figure 41 illustrates the temperature differences relative to varying channel widths and header widths. A lower temperature difference indicates that the thermal management system successfully disperses heat throughout the entire surface. The plot in Figure 41 shows that channels with higher CR ratio lead to reduced temperature differences, likely due to their larger surface area facilitating heat exchange between the coolant and the walls of the channel. These results align well with findings from the study conducted by E. Afshari et al. [54]. To draw a comparison among the cases, the scenario with CR of 1, is taken to be the base case with temperature difference of ~6 °C. Channel with the CR ratio of 3.125 showed the lowest temperature difference (~4 °C) and channel with the CR ratio of 0.14 had the highest temperature difference (~14 °C).

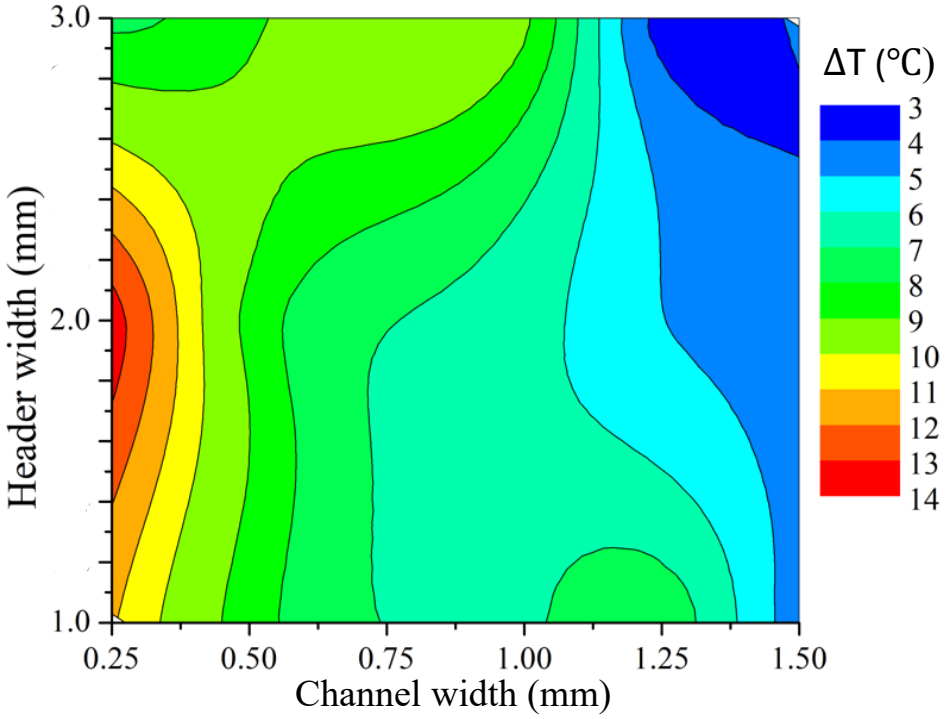



**Figure 41:** Temperature difference against channel width and header width

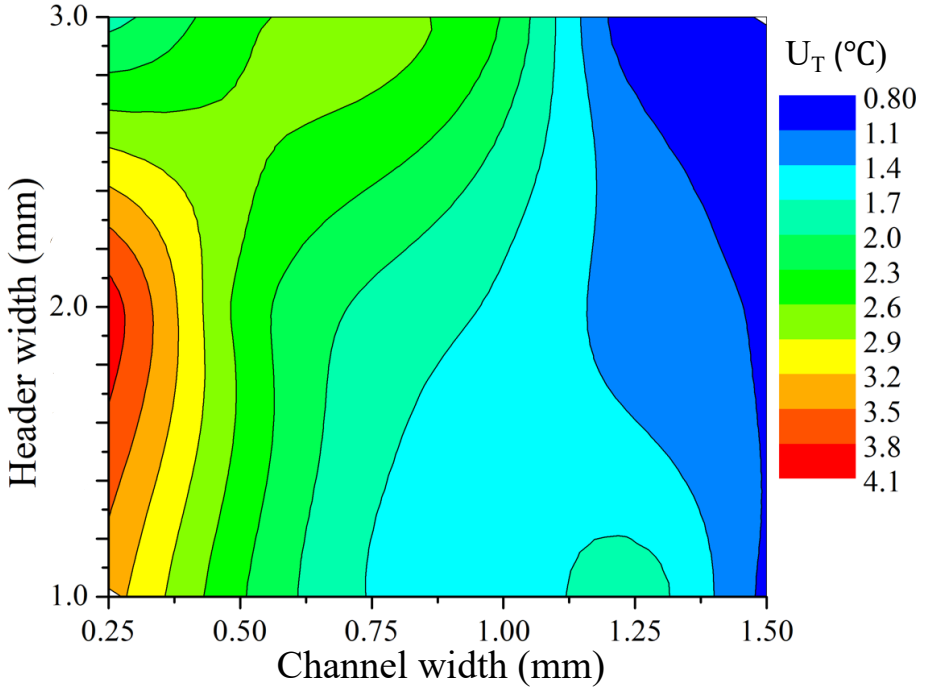



**Figure 42:** $U_T$ against channel width and header width

It was determined that the temperature difference decreased by approximately 33.3% compared to the base case. Further, it was reported that for case 4, 5 and 6 the temperature difference was 4.393 ℃, 4.286 ℃ and 4.254 ℃ respectively. While the effect of header width isn't significant, it

is noted that a wider header leads to a decrease in temperature difference. These results indicate a clear trend of the effectiveness of thermal distribution with the change in geometrical parameters. To further quantitively evaluate the thermal regulation, the uniformity indices were also calculated. Figure 42 shows $U_T$ in relation to the channel width and header width, highlighting a trend that parallels the temperature difference. The $U_T$ for the base case with CR ratio of 1 was found to be 1.44 ℃. The data indicates that the minimum $U_T$ value (0.98 ℃) is found at a CR ratio of 3.125, supporting the notion that designs featuring an optimized channel width improves heat dissipation. A numerical study by S.M. Baek et al. [63] supports the argument that design with minimum $U_T$ helps in providing better heat dissipation. However, the highest value of $U_T$ was observed to be 4.00 ℃ for the CR ratio of 0.14. It is to be noted that the $U_T$ decreased by 31.72% compared to the base case.

For cases 4,5 and 6 $U_T$ values were observed to be 1.0604 ℃, 1.0436 ℃ and 0.9854 ℃, following the similar trend as of the temperature difference. Widening the header reduced the $U_T$ value, though not drastically. This may be due to the header's smaller size compared to the overall cooling plate area. To more effectively illustrate the results, Figure 43 (a), (b), and (c) demonstrate how the value of $U_T$ varies with channel width and header width. For cases 1,4,7,10 and 13, Figure 43(a) clearly shows that with increase in the channel width, $U_T$ tends to decrease. For the Cr ratio of 0.14, value of $U_T$ is 3.372 ℃ which converges to 0.9854 ℃ for the Cr ratio of 3.125. A consistent behaviour is observed for cases with header width of 2 mm and 3 mm, suggesting that increasing channel width contribute to more efficient temperature distribution.

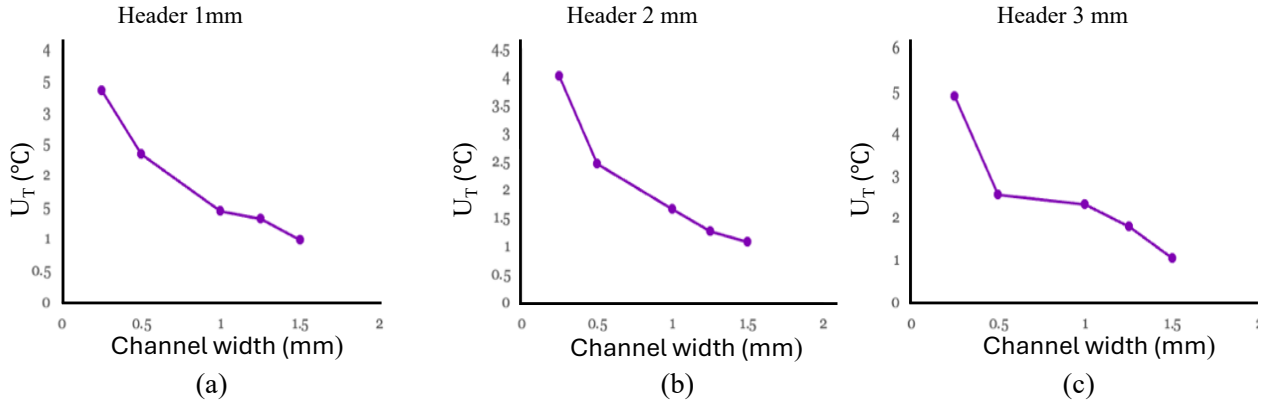
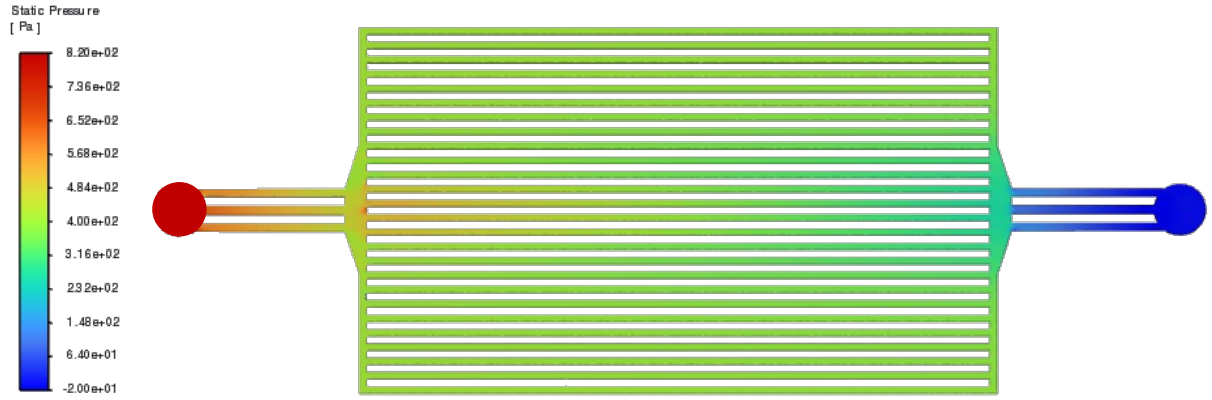
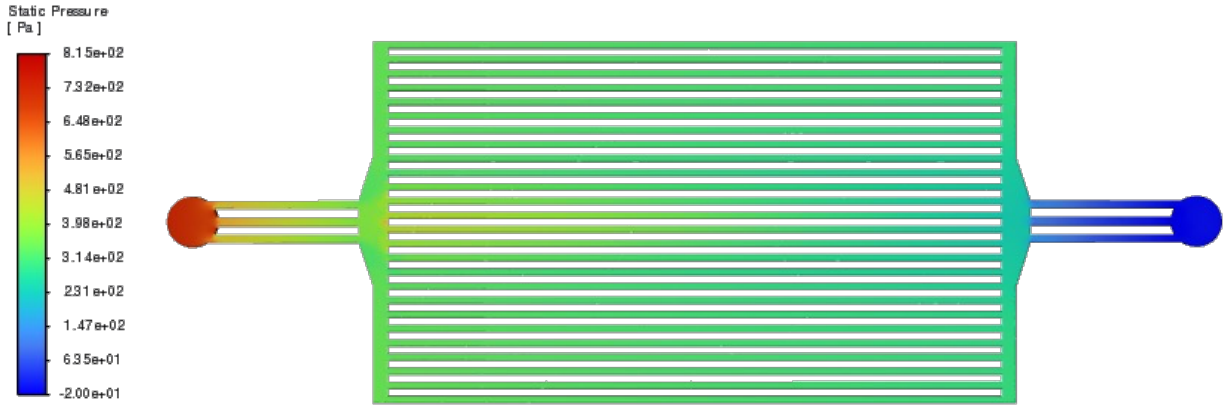



**Figure 43:** (a) $U_T$ Vs channel width for header 1 mm, (b) $U_T$ Vs channel width for header 2 mm, (c) $U_T$ Vs channel width for header 3 mm

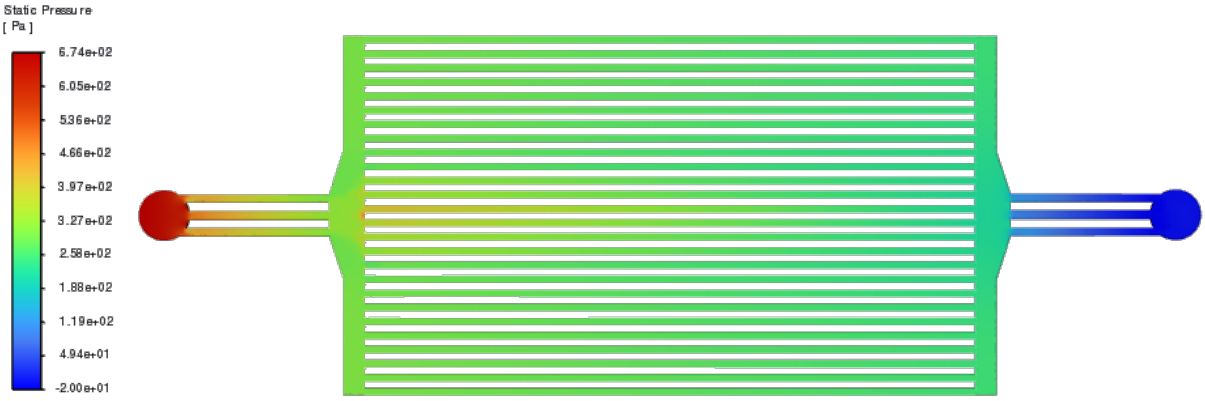
Effective temperature control is essential for ensuring the performance and lifespan of the PEMFC; however, it must be carefully balanced with pressure drop considerations. High pressure losses can result in greater parasitic power consumption and lower system efficiency. This section will discuss the pressure drop findings, emphasizing the impact of variations in CR ratio and header width on the system. The results of the pressure drop are depicted in Figure 44, demonstrating the reduction along the channels. The study indicates that the design with higher CR ratio tend to have lower pressure drop compared to their narrower counterparts, a finding that is corroborated by the research conducted by M. Sauermoser et al. [86]. Specifically, Cases 4, 5, and 6 demonstrate a reduced pressure drop in comparison to the baseline Cases 1, 2, and 3. Furthermore, a similar trend is observed in other cases.



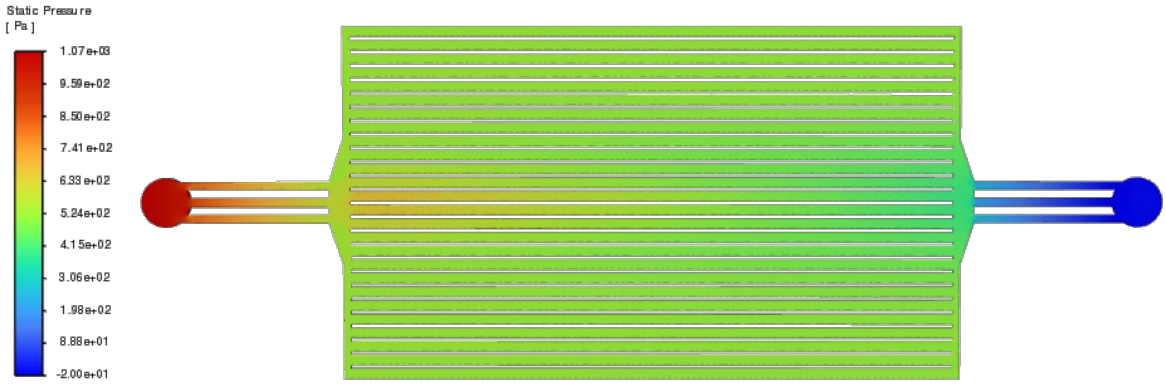

Case 1



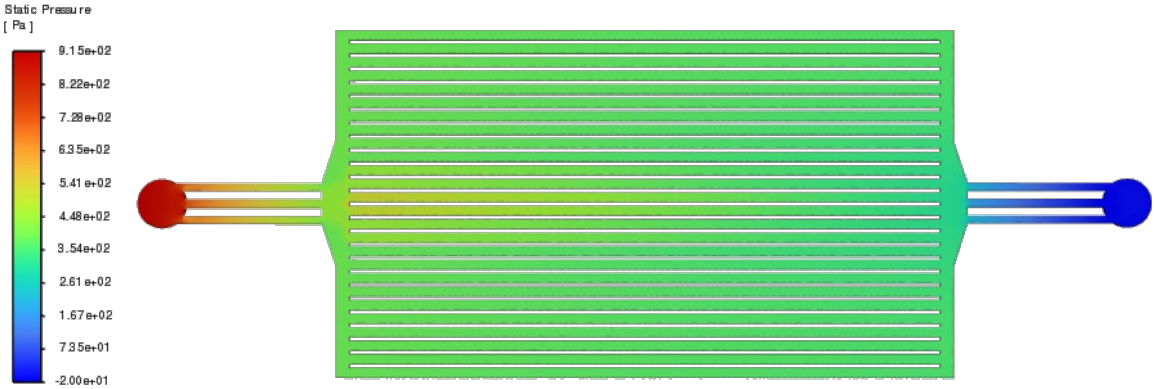

Case 2



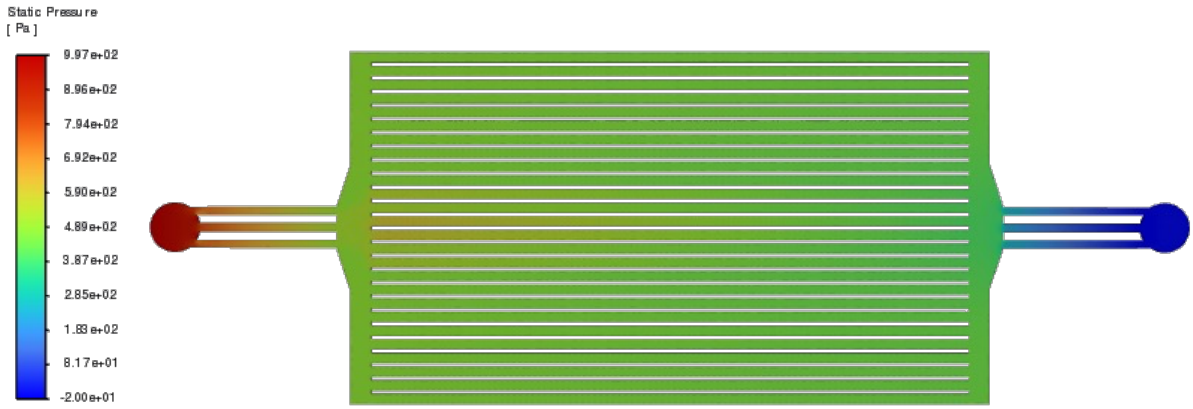

Case 3



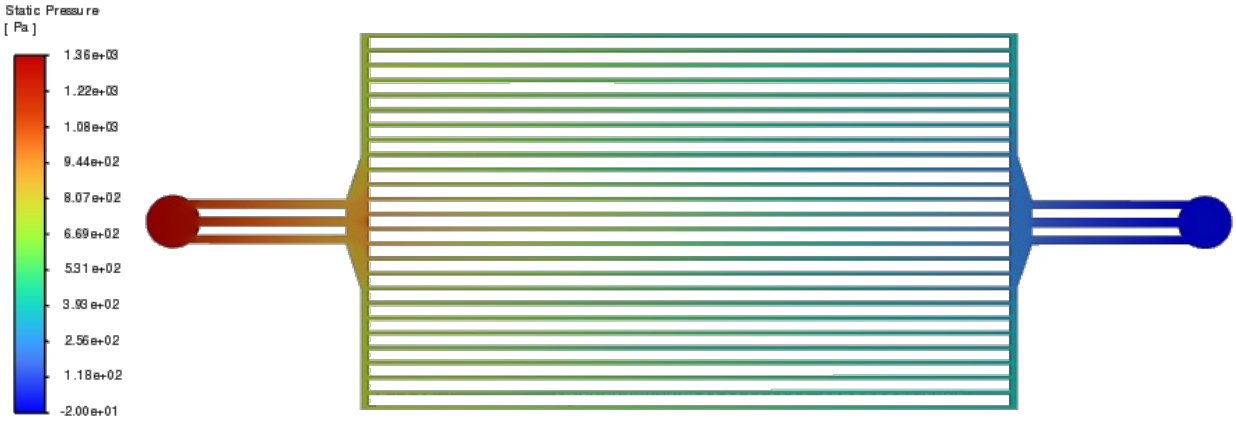

Case 4



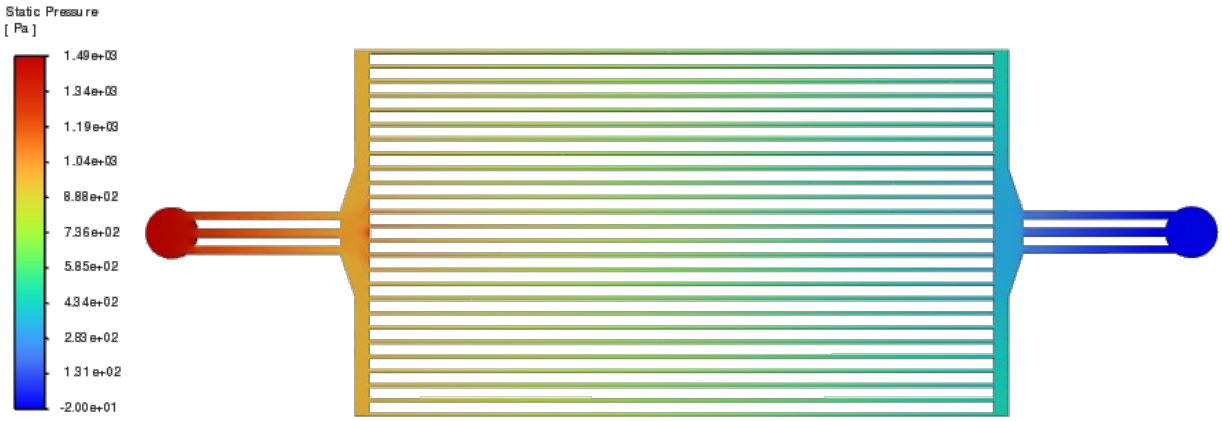

Case 5



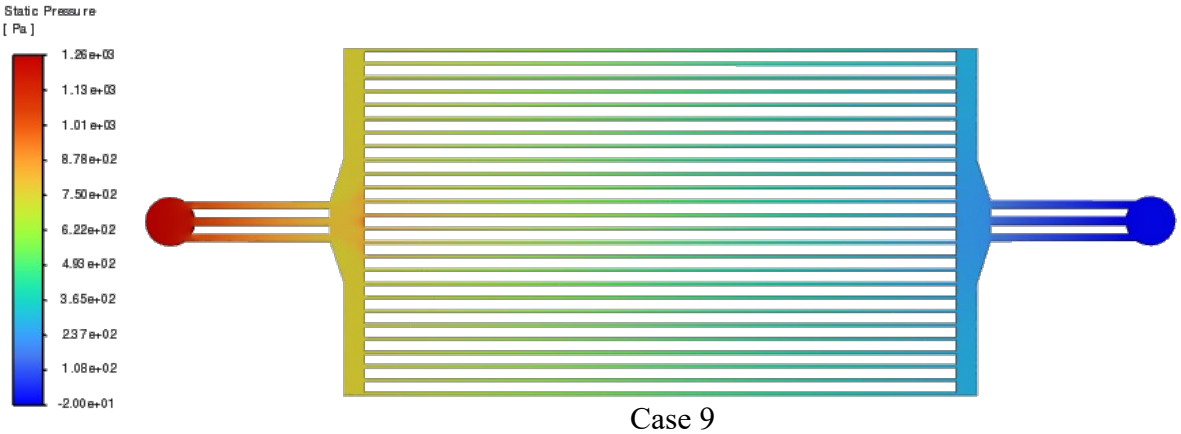

Case 6



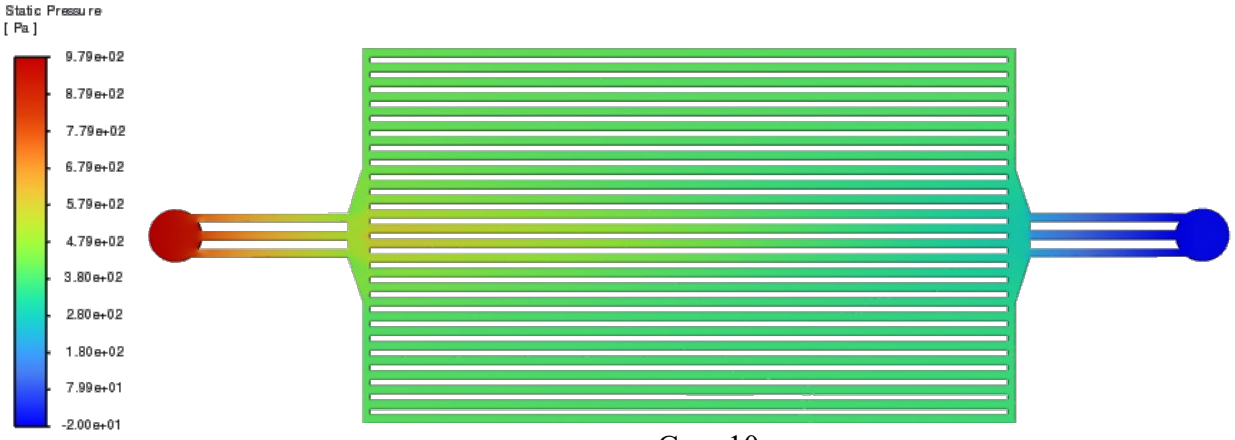

Case 7



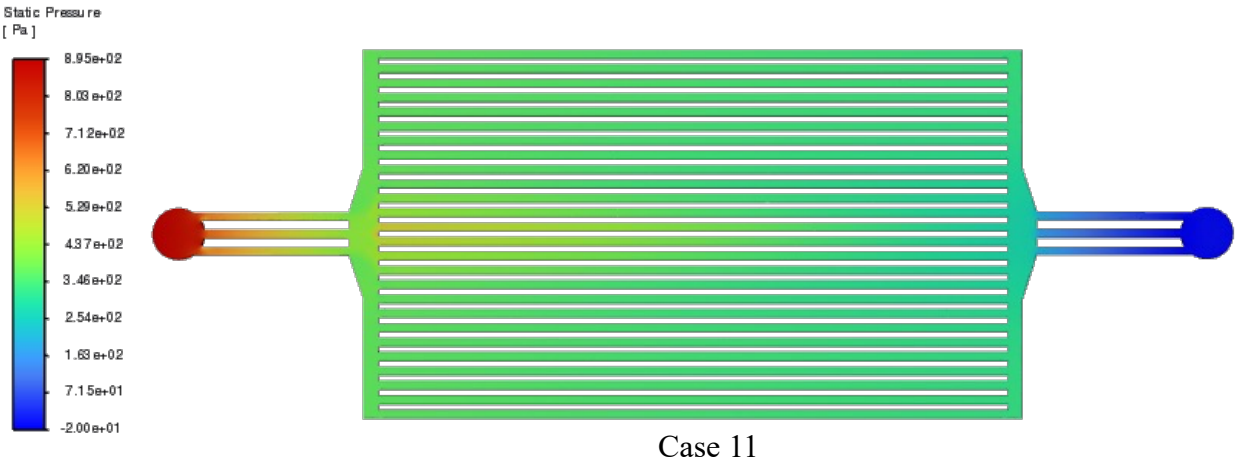

Case 8



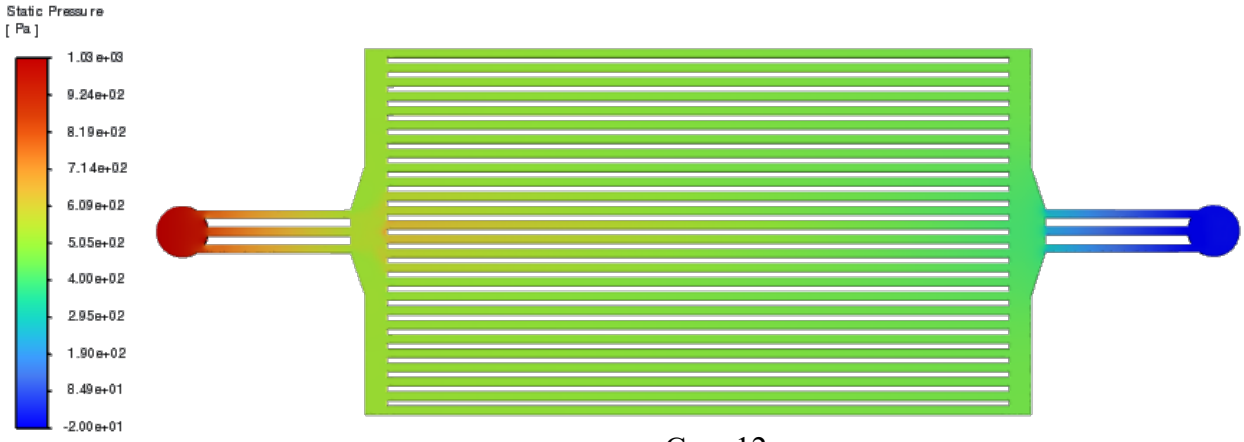

Case 9



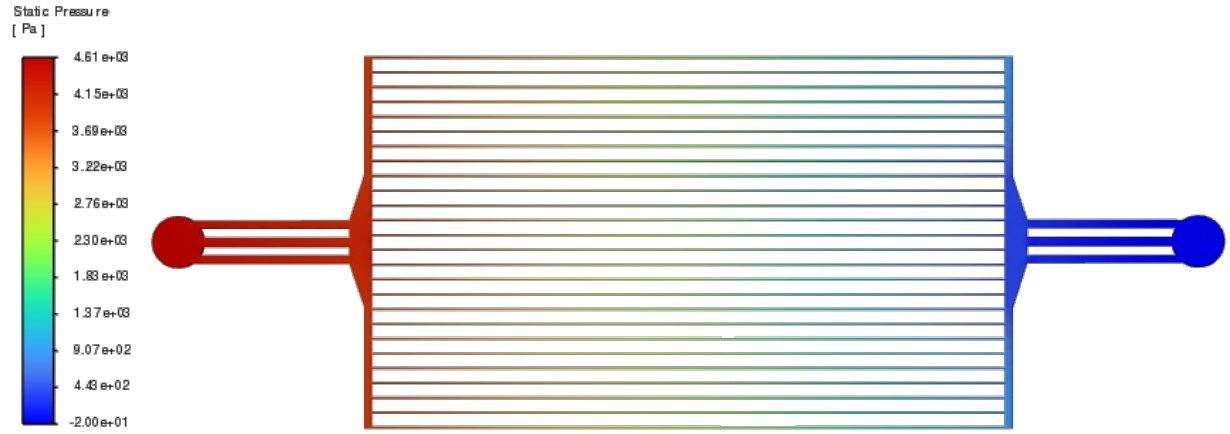

Case 10



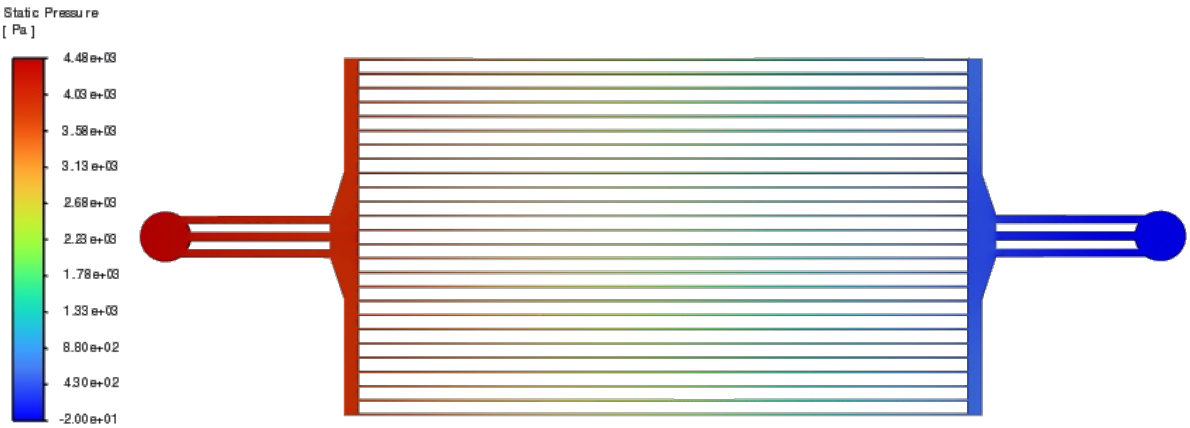

Case 11




Case 12




Case 13




Case 14

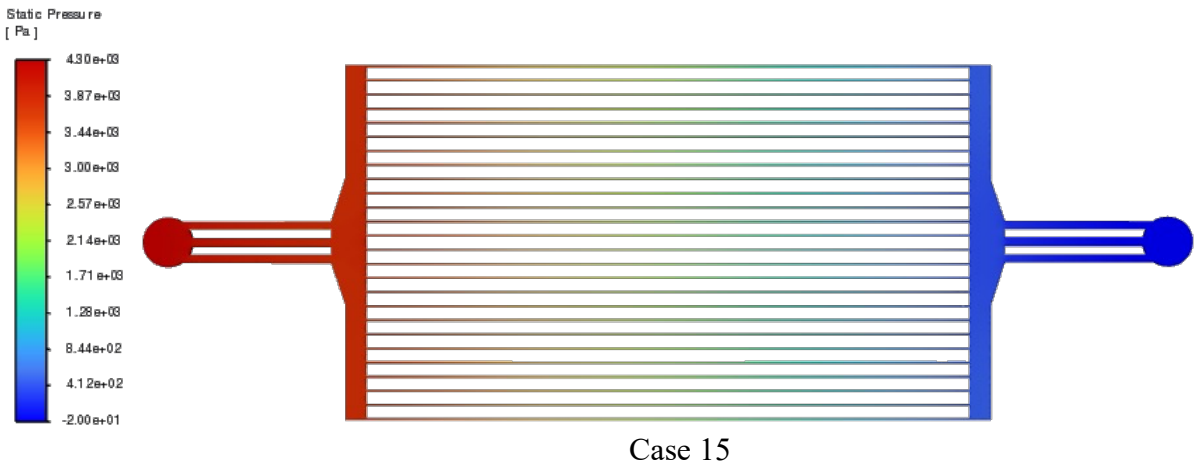



**Figure 44:** Pressure drop along the channel for case 1 to case 15

Additionally, the pressure drop results across different coolant channel geometries indicates a clear correlation between channel dimensions and flow resistance. Figure 45 illustrates the pressure drop relative to both the channel and header widths. The graph clearly indicates that a wider channel with CR ratio of 3.125 results in a lower pressure drop (1067.6 Pa), which suggests a reduction in flow resistance and thus enhances fluid flow in the cooling channels. While pressure drop with channel width of 0.25 mm comes out to be 4613.2 Pa, suggesting that careful consideration of the channel size is essential for minimizing energy losses while maintaining adequate cooling performance. Results underscores that channel with higher CR ratio would help minimizing the pumping power because of lower pressure drop.

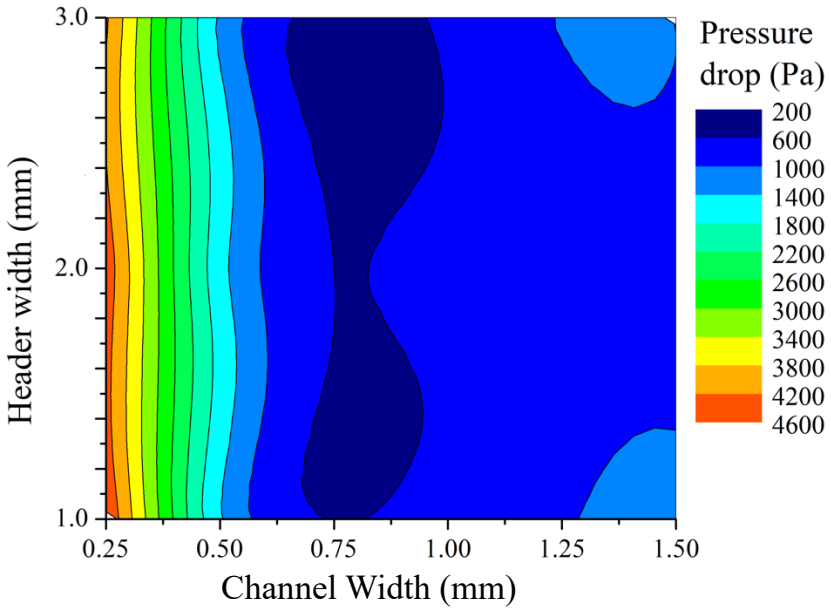



**Figure 45:** Pressure drop against channel width and header width

## 4.2 Design Modification

Given that the optimal channel width among all fifteen cases is determined to be 1.5 mm (CR = 3.125), additional investigations are conducted to assess the effects of the pins' placements at the inlet and outlet headers of the cooling plate. The idea is to use pins to serve as flow disruptors and help breaking up the coolant flow in the header to ensure more uniform distribution across the channels. Once again, the indicators utilized to assess the impact of pin placement on the heat dissipation of the cooling plate include the temperature difference, temperature uniformity index, and pressure drop.

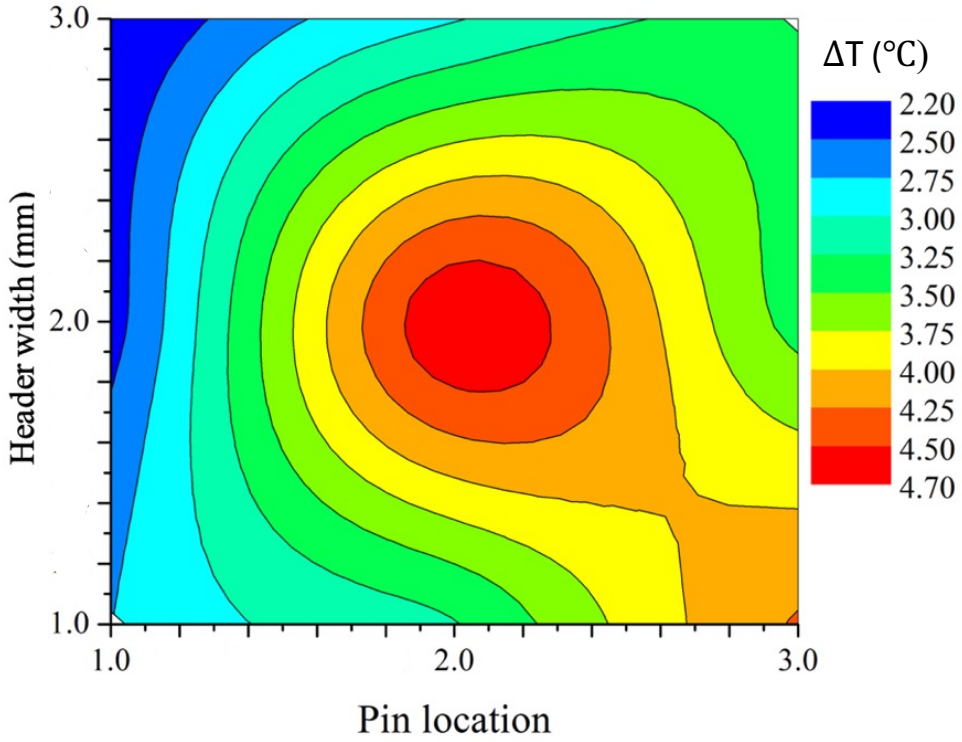



**Figure 46:** Temperature difference against pin location and header width

Figure 46 illustrates the temperature difference in relation to the pin locations and the header width and it is observed that placing the pins exhibits lower value of minimum temperature difference that that of cases without pins. It is observed that pin location 1 exhibits the lowest temperature difference of 2.75 ℃, 2.37 ℃ and 2.19 ℃ for header width of 1 mm, 2 mm and 3 m respectively and is lower than that of cases without pins (4.25 ℃). A similar trend of lower temperature difference values is seen for pin location 2 and pin location 3. Therefore, incorporating pins at strategic locations in the header is a viable design modification, and this observation is further corroborated by the plot of $U_T$ against pin locations and header width, as presented in Figure 47.

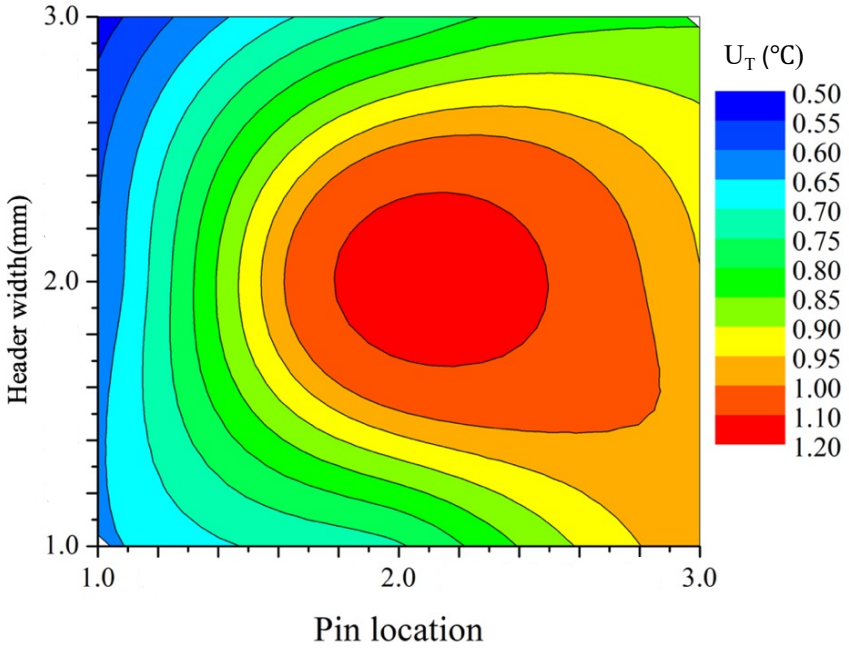



**Figure 47:** $U_T$ against pin location and header width

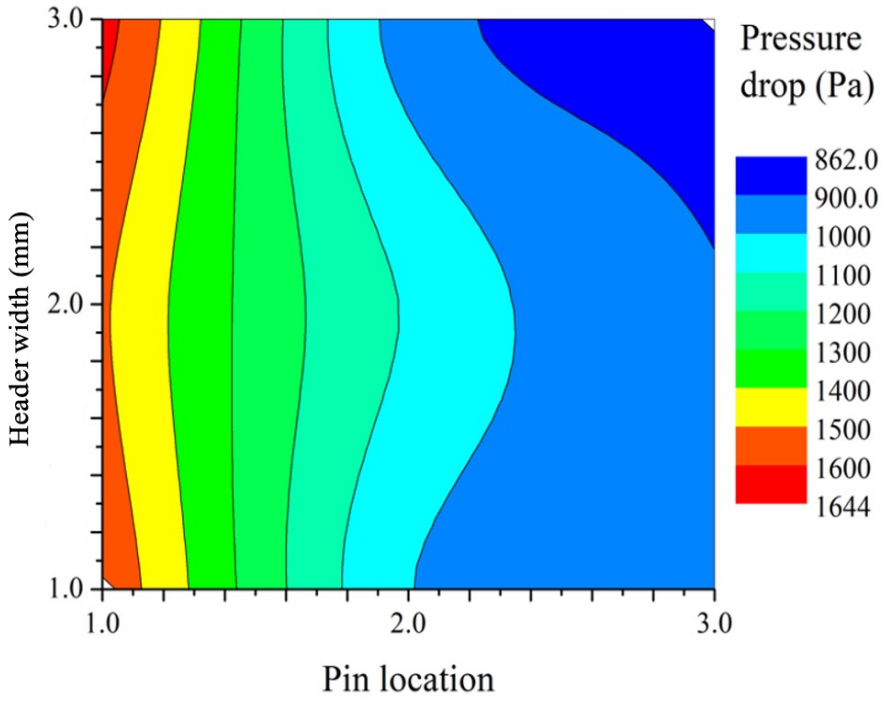



**Figure 48:** Pressure drop against pin location and header width

$U_T$ for pin location 1 turns out to be 0.64 ℃, 0.59 ℃ and 0.52 ℃ for header width of 1 mm, 2mm and 3 mm respectively, demonstrates a clear improvement to the case without the pins ($U_T$ = 0.98 ℃). This significant reductions in the $U_T$ values leads to better temperature control

within the cooling channels. A comparable pattern of reduced uniformity indices is observed for pin locations 2 and 3, possibly due to the consistent flow dynamics.

In addition, when considering the pressure drop values, a similar consistency is observed indicating the importance of thermal and fluid properties to optimize the performance of the system. The pressure drop is observed to decrease from 1067 Pa to 915 Pa at pin location 1 and further to 909 Pa and 862 Pa at pin location 2 and 3. There is a clear gradient in pressure drop values from left to right, as can be seen in Figure 48, suggesting that as the pin location changes, the pressure drop is bound to change. Identifying areas with lower pressure drop (blue regions) could be important for optimizing flow characteristics and reducing energy consumption. This indicates that the system exhibits regions of uneven temperature distribution, and that the uniformity of temperature could be enhanced through the optimization of the placement of pins or the header arrangement.

# 5. Conclusion and Recommendations for Future Work

## 5.1 Conclusions

The primary role of PEMFC is to mitigate the worldwide energy crisis through the electrochemical reaction process in fuel cells to create renewable electricity. Researchers and scientific community focus its efforts on the development of high efficiency fuel cells [87]. One of the important aspects of achieving high performance of PEMFCs is its efficient thermal management, which can be achieved by effectively managing the heat generated during the fuel cell's operation. A key method for ensuring uniform temperature distribution in PEMFCs is through the use of liquid cooling strategies by varying the geometry of cooling channels [88]. By optimizing the design of these channels and integrating specific design elements can greatly contribute to enhance the heat dissipation and thermal stability.

The analysis conducted on fifteen distinct cases has demonstrated favorable outcomes regarding the influence of geometrical modifications on critical performance indicators, including temperature distribution and pressure drop. Design of parallel channels is optimized by varying the channel to rib ratio and header width of the cooling plate to maintain a more consistent temperature across the fuel cell. The scenario characterized by the maximum CR ratio displayed the lowest maximum temperature across the cooling plates. Moreover, this case had the minimum pressure drop, indicative of diminished flow resistance and enhanced coolant distribution. This emphasizes the critical role of optimization of the channel geometry in enhancing the temperature distribution within PEMFCs, underscoring its significance for improving overall system performance.

Additionally, pins have been strategically incorporated at various locations within the inlet and outlet headers to optimize flow distribution. Although the influence was minimal due to the small dimensions of the headers, this modification facilitated a reduction in the maximum temperature compared to the baseline cases. This suggests that even minor changes to the cooling channel design can significantly affect the thermal management of the system.

In this study, aluminum has been investigated due to its properties such as lightweight composition, high thermal conductivity, and good electrical conductivity. These characteristics of aluminium enables efficient heat dissipation while maintaining the structural integrity of PEMFCs. However, future research can explore the development of different variations in channel designs and alternative materials to fully harness the capabilities of PEMFC system.

## 5.2 Recommendations for Future Work

It is evident that the contact area between the coolant plate and the coolant plays a significant role in reducing the maximum temperature. The change in geometry of cooling channels with varying widths can assist in achieving this objective. The coolant can be evenly distributed across the plate by using a wider inlet and a narrower outlet for the channel. Such a design can facilitate the optimization of the balance between pressure drop and cooling efficiency. In the study, there exists significant potential to further refine the design to achieve greater uniformity of temperature of the PEMFC.

Further, to improve the impact of pin placement, enlarging the size of the headers could yield additional space for more efficient flow. Larger headers would allow for the strategic placement of more pins with different pin size and shape. Moreover, varying the location of the pins play an important role in influencing the flow dynamics of the system, enabling better control over localized temperature hotspots. Investigating various pin geometries (such as cylindrical or conical) may further offer insights into how different designs affect pressure drop and enhance the performance effectiveness of the system.

In addition to optimizing the geometry of channels and headers, the selection of materials is crucial in the thermal management of PEMFC. The thermophysical properties of both the coolant and the bipolar plate material significantly influence temperature distribution; for instance, materials with high thermal conductivity might improve heat dissipation. Furthermore, materials that demonstrate low thermal expansion coefficients should be evaluated to minimize deformation caused by temperature changes, thereby enhancing the structural integrity and longevity of the fuel cell. Further advancements may be achieved by considering alternative materials such as graphite composites, which combine high thermal conductivity with mechanical stability.

# REFERENCES


[1] S. Chu, Y. Cui and N. Liu, "The path towards sustainable energy", *Nature materials*, vol. 16, pp. 16-22, 2017.

[2] L. Yang et al., "A review on thermal management in proton exchange membrane fuel cells: Temperature distribution and control", *Renewable and Sustainable Energy Reviews*, vol. 187, pp. 113737, 2023

[3] Y. Duan et al., "Materials, components, assembly and performance of flexible polymer electrolyte membrane fuel cell: A review", *Journal of Power Sources*, vol. 555, pp. 232369, 2023

[4] T. Sutharssan et al., "A review on prognostics and health monitoring of proton exchange membrane fuel cells", *Renewable and Sustainable Energy Reviews,* 2016

[5] S. Mo et al., "Recent Advances on PEM Fuel Cells: From Key Materials to Membrane Electrode Assembly", *Electrochemical Energy Reviews,* 2023

[6] S. Rogg et al., "Cooling Modules for Vehicles with a Fuel Cell Drive", *Fuel Cells*, vol. 3, no. 3, pp. 200311, 2003

[7] P. Rodatz, F. Buchi, C. Onder and L. Guzzella, "Operational aspects of a large PEFC stack under practical conditions", *Journal of Power Sources*, vol. 128, pp. 208-217, 2004

[8] G. Zhang and S.G. Kandlikar, "A critical review of cooling techniques in proton exchange membrane fuel cell stacks", *International Journal of Hydrogen Energy*, vol. 37, pp. 2412-2429, 2012

[9] M.H.S. Bargal et al., "Liquid cooling techniques in proton exchange membrane fuel cell stacks: A detailed survey", *Alexandria Engineering Journal*, vol. 59, pp. 635-655, 2020

[10] A. Faghri and Z. Guo, "Challenges and opportunities of thermal management issues related to fuel cell technology and modeling", *International Journal of Heat and Mass Transfer*, vol. 48, pp. 3891-3920, 2005

[11] Y. Li, G. Chang and W. Zhao, “Experimental Investigation on the Operating Characteristics of Flat-Plate CLPHP for PEMFC Cooling”, *World Electric Vehicle Journal*, vol. 12, pp. 116, 2021

[12] T.L. Bergman, *Fundamentals of heat and mass transfer*.

[13] M.R. Islam, B. Shabani, G. Rosengarten and J. Andrews, “The potential of using Nanofluids in PEM fuel cell cooling systems: A review”, *Renewable and Sustainable Energy Reviews*, vol. 48, pp. 523-539, 2015

[14] M.N.I. Johari, I.A. Zakaria and N.S.M. Affendy, “Thermal Behaviour of Hybrid Nanofluids in Water: Bio Glycol Mixture in Cooling Plates of PEMFC”, *CFD Letters*, vol. 14, no. 6, pp. 43-55, 2022

[15] A. Fly and R.H. Thring, “A comparison of evaporative and liquid cooling methods for fuel cell vehicles”, *International Journal of Hydrogen Energy*, vol. 41, no. 32, pp. 14217-14229, 2016

[16] Y. Yu et al., “Thermal management system for liquid-cooling PEMFC stack: From primary configuration to system control strategy”, *eTransportation*, vol. 12, pp. 100165, 2022

[17] S. Maharudrayya, S. Jayanti and A.P. Deshpande, “Flow distribution and pressure drop in parallel-channel configurations of planar fuel cells”, *Journal of Power Sources*, vol. 144, pp. 94-106, 2005

[18] Y. Wang, “Modeling of two-phase transport in the diffusion media of polymer electrolyte fuel cells”, *Journal of Power Sources,* vol. 185, pp. 261-271, 2008

[19] G.Y. Choe et al., “Proton Exchange Membrane Fuel Cell (PEMFC) Modeling for High Efficiency Fuel Cell Balance of Plant (BOP)”, *Proceeding of International Conference on Electrical Machines and Systems*, 2007

[20] A. Jayakumar et al., “A technical review on gas diffusion, mechanism and medium of Pem fuel cell”, *Springer-Verlag Berlin Heidelberg*, 2014

[21] G.P.D. Costa et al., “Advancements in printed components for proton exchange membrane fuel cells: A comprehensive review”, *International Journal of Hydrogen Energy*, vol. 69, pp. 710-728, 2024

[22] X. Li, *Principles of fuel cells*. CRC press, 2005.

[23] T. Ozgur and A.C. Yakaryilmaz, “Thermodynamic analysis of a Proton Exchange Membrane fuel cell”, *International Journal of Hydrogen Energy*, vol. 43, pp. 18007-18013, 2018

[24] S. Rashidi et al., “Progress and challenges on the thermal management of electrochemical energy conversion and storage technologies: Fuel cells, electrolysers, and supercapacitors”, *Progress in Energy and Combustion Science*, vol. 88, pp. 100966, 2022

[25] J. Xu et al., “Modelling and control of vehicle integrated thermal management system of PEM fuel cell vehicle”, *Energy*, vol. 199, pp. 117495, 2020

[26] S.G. Kandlikar and Z. Lu, “Thermal management issues in a PEMFC stack – A brief review of current status”, *Applied Thermal Engineering*, vol. 29, pp. 1276-1280, 2009

[27] B. Frano. *PEM fuel cells: theory and practice.* 2005

[28] Z. Shao and M. Ni, “Fuel cells: Material needs and advances”, *MRS Bulletin*, vol. 49, pp. 451-463, 2024

[29] Q. Li et al., “A Review on Temperature Control of Proton Exchange Membrane Fuel Cells”, *Processes*, vol. 9, pp. 235, 2021

[30] F. Barbir. *PEM fuel cells: theory and practice.* 2012

[31] D.K. Madheswaran, A. Jayakumar and E.G. Varuvel, “Recent advancement on thermal management strategies in PEM fuel cell stack: a technical assessment from the context of fuel cell electric vehicle application”, *Energy Sources, Part A: Recovery, Utilization, and Environmental Effects,* vol. 44, no. 2, pp. 3100-3125, 2022

[32] F. Valle, *Electrocatalyst degradation in high temperature PEM fuel cells*. 2015

[33] S.G. Kandlikar and Z. Lu, “Fundamental Research Needs in Combined Water and Thermal Management Within a Proton Exchange Membrane Fuel Cell Stack Under Normal and Cold-Start Conditions”, *Journal of Fuel Cell Science and Technology*, vol. 6, pp. 044001, 2009

[34] P.Rodatz, F. Buchi, C. Onder and L. Guzzella, “Operational aspects of a large PEFC stack under practical conditions”, *Journal of Power Sources*, vol. 128, pp. 208-217, 2004

[35] J. Kim, S.M. Lee and S. Srinivasan, “Modeling of Proton Exchange Membrane Fuel Cell Performance with an Empirical Equation”, *Electrochemical Society*, vol. 142, no. 8, pp. 2670-2674, 1995

[36] J. Xu et al., “Progress and perspectives of integrated thermal management systems in PEM fuel cell vehicles: A review”, *Renewable and Sustainable Energy Reviews*, vol. 155, pp. 111908, 2022

[37] A. Baroutaji et al., “Advancements and prospects of thermal management and waste heat recovery of PEMFC”, *International Journal of Thermofluids*, vol. 9, pp. 100064, 2021

[38] Y.X. Hui et al., “The use of phase-change cooling strategy in proton exchange membrane fuel cells: A numerical study”, *Science China Technological Sciences*, vol. 64, no. 12, pp. 2762-2770, 2021

[39] X. Yu, Z. Tu and S.H. Chan, “Thermal management on an air-cooled PEMFC stack with concave-convex dual flow channel bipolar plates”, *International Journal of Hydrogen Energy*, vol. 52, pp. 1018-1032, 2024

[40] A.U. Yakubu et al., “A comprehensive review of primary cooling techniques and thermal management strategies for polymer electrolyte membrane fuel cells PEMFC”, *Heliyon*, vol. 10, pp. e38556, 2024

[41] A. Razniak et al., “Determination of Electrical and Efficiency Parameters of Air Cooling of Low-Temperature PEM Fuel Cell Stack with Power of 5kW”, *Przeglad Elektrotechniczny*, vol. 95, no. 4, pp. 140-147, 2018

[42] I. Tolj, Z. Penga, D. Vukicevic and F. Barbir, “Thermal management of edge-cooled I kW portable proton exchange membrane fuel cell stack”, *Applied Energy*, vol. 25, pp. 114038, 2020

[43] A.P. Tetuko et al., “Study of a thermal bridging approach using heat pipes for simultaneous fuel cell cooling and metal hydride hydrogen discharge rate enhancement”, *Jounal of Power Sources*, vol. 397, pp. 177-188, 2018

[44] J. Liu et al., “Carbon Nanotube-Based Materials For Fuel Cell Applications”, *Australian Journal of Chemistry*, vol. 65, no. 9, pp. 1213-1222, 2012

[45] N. Liao et al., “Effects of catalysts state on the synthesis of MWCNTs modified expanded graphite through microwave-assisted pyrolysis of ethanol”, *Journal of Materials Science*, vol. 52, pp. 11442-11452, 2017

[46] N. Rajalakshmi and R. Gopalan, “Recent trends in Science and Technology of Hydrogen and Polymer Electrolyyte Membrane Fuel Cells”, *Indian National Academy of Engineering*, vol. 6, pp. 189-218, 2021

[47] S. Hasanpour et al., “Woven gas diffusion layers for polymer electrolyte membrane fuel cells: Liquid water transport and conductivity trade-offs”, *Journal of Power Sources*, vol. 403, pp. 192-198, 2018

[48] J. Liu et al., “Design and development of coating for metallic bipolar plates in proton exchange membrane fuel cell (PEMFC): A review”, *Materials & Design*, vol. 246, pp. 113338, 2024

[49] H. Jouhara, V. Anastasov and I. Khamis, “Potential of heat pipe technology in nuclear seawater desalination”, *Desalination,* vol. 249, pp. 1055-1061, 2009

[50] Z. Huang et al., “Rapid thermal response and sensitivity analysis pf proton exchange membrane fuel cell stack with ultra-thin vapor chambers”, *Applied Thermal Engineering*, vol. 199, pp. 117526, 2021

[51] S.H. Hwang and M.S. Kim, “An experimental study on the cathode humidification and evaporative cooling of polymer electrolyte membrane fuel cells using direct water injection method at high current densities”, *Applied Thermal Engineering,* vol. 99, pp. 635-644, 2016

[52] W. Wang et al., “Thermal Management Analysis of Proton exchange Membrane Fuel Cell Filled with Phase Change Material in Cooling Channel”, *International Journal of Energy Research,* vol. 2023

[53] X. Chen et al., “Temperature and humidity management of PEM fuel cell power system using multi-input and multi-output fuzzy method”, *Applied Thermal Engineering,* vol. 203, pp. 117865, 2022

[54] E. Afshari, N. Jahantigh and M.Z. Rad, “Parametric study of the influence of cooling channel dimensions on PEM fuel cell thermal performance”, *Iranian Journal of Hydrogen & Fuel Cell,* vol. 4, pp. 265-274, 2017

[55] I. Zakaria et al., “Experimental Investigation of Al2O3 – Water Ethylene Glycol Mixture Nanofluid Thermal Behaviour in a Single Cooling Plate for PEM Fuel Cell Application”, *Energy Procedia*, vol. 79, pp. 252-258, 2015

[56] A. Raguman and P. Vedagiri, “Investigating the properties of nanoparticles from heveabrasiliensis shell for coolant application in PEMFCs”, *Process Safety and Environmental Protection*, vol. 189, pp. 628-635, 2024

[57] Y. Liu, L. Zeng, Y. Chen and X. Zhang, “Improving the cooling effect of proton exchange membrane fuel cells by using biomimetic capillary cooling channels based on topology optimization method”,*Applied Thermal Engineering*, vol. 251, pp.123633, 2024

[58] T. Locher et al., “Temperature Effects in Polymer Electrolyte Membrane Fuel Cells”, *ChemElectroChem*, vol. 7, pp. 3545-3568, 2020

[59] X. Zhang, O.J. Kwon and B.S. Oh, “A Design of the Cooling Channel in the Bipolar Plate of PEMFC Using Experimental Design Method”, *Transactions of Korean Society of Automotive Engineers,* vol. 23, no. 5, pp. 545-552, 2015

[60] F.C. Chen, Z. Gao and R. Loutfy, “Analysis of Optimal Heat Transfer in a PEM Fuel Cell Cooling Plate”, *Fuel Cells*, vol. 3, no. 4, pp. 181-188, 2003

[61] E. Afshari, M.Z. Rad and M.M. Dehkordi, “Numerical Investigation on a novel zigzag-shaped flow channel design for cooling plates of PEM fuel cells”, *Journal of the Energy Institute,* vol. 90, pp. 752-763, 2017

[62] M. Ahmed, X. Shusheng, “Comprehensive review of serpentine flow fields for effective thermal management pf proton exchange membrane fuel cell”, *Heliyon*, vol. 10, pp. e39793, 2024

[63] S.M. Baek, S.H. Yu, J.H. Nam and C.J. Kim, “A numerical study on uniform cooling of large-scale PEMFCs with different coolant flow field designs”, *Applied Thermal Engineering*, vol. 31, pp. 1427-1434, 2011

[64] Z. Wang et al., “Application progress of small-scale proton exchange membrane fuel cell”, *Energy Reviews*, vol. 2, pp. 100017, 2023

[65] J. Jhang, “High temperature PEM fuel cells”, *Journal of Power Sources*, vol.160, pp. 872-891, 2006

[66] N. Atasay, A. Atmanli and N. Yilmaz, “Liquid Cooling Flow Field Design and Thermal Analysis of Proton Exchange Membrane Fuel Cells for Space Applications”, *International Journal of Energy Research*, vol. 2023

[67] E. Hosseinzadeh, M. Rokni, A. Rabbani and H.H. Mortensen, “Thermal and water management of low temperature Proton Exchange Membrane Fuel Cell in fork-lift truck power system”, *Applied Energy*, vol. 104, pp. 434-444, 2013

[68] S.A. Atyabi, E. Afshari and N. Shakarami, “Three-dimensional multiphase modeling of the performance of an open-cathode PEM fuel cell with additional cooling channels”, *Energy*, vol. 263, pp. 125507, 2023

[69] K. Mogorosi and T. Oladiran, “The Impact of Cooling Channels and Heat Spreaders on the Performance of Proton Exchange Membrane Fuel Cells (PEMFC)”, *International Energy Journal*, vol. 22, pp. 375-388, 2022

[70] S. Asghari, H. Akkhgar and B.F. Imani, “Design of thermal management subsystem for a 5 kW polymer electrolyte membrane fuel cell system”, *Journal of Power Sources*, vol. 196, pp. 3141-3148, 2011

[71] S.M. Rahgoshay, A.A. Ranjbar, A. Ramiar and E. Alizadeh, “Thermal Investigation of a PEM fuel cel with cooling flow field”, *Energy*, vol. 134, pp. 61-73, 2017

[72] M. Ghasemi, A. Ramiar, A.A. Ranjbar and S.M. Rahgoshay, “A numerical study on thermal analysis and cooling flow fields on PEMFC performance”, *International Journal of Hydrogen Energy*, vol. 42, pp. 24319-24337, 2017

[73] S. Li and B. Sunden, “Numerical analysis on thermal performance of cooling plates with wavy channels in PEM fuel cells”, *International Journal of Numerical methods for Heat&amp Fluid Flow*, vol. 28, no. 7, 2018

[74] J. Choi et al., “Numerical analysis on the performance of cooling plates in a PEFC”, *Journal of Mechanical Science and Technology*, vol. 22, pp. 1417-1425, 2008

[75] S.H. Yu, S. Sohn, J.H. Nam and C.J. Kim, “Numerical study to examine the performance of multi-pass serpentine flow-fields for cooling plates in polymer electrolyte membrane fuel cells”, *Journal of Power Sources*, vol. 194, pp. 697-703, 2009

[76] S.M.M. Joibary, S.M. Rahgoshay, M.R. Esbo and K.D. Firouzjaee, “Numerical investigation of the influence of different cooling flow channels on the thermal and water saturation distribution in a real dimensional polymer electrolyte membrane fuel cell”, *International Journal of Hydrogen Energy*, vol. 48, pp. 2762-2787, 2023

[77] S. Li and B. Sunden, “Numerical study on thermal performance of non-uniform flow channel designs for cooling plates of PEM fuel cells”, *Numerical Heat Transfer, Part A: Applications*, vol. 74, no. 1, pp. 917-930, 2018

[78] W. Wang et al., “Optimization of Cooling Channel Structure of Bipolar Plate for Proton Exchange Membrane Fuel Cells Based on CFD Analysis”, *Energies*, vol. 16, pp. 5858, 2023

[79] A.P. Sasmito, J.C. Kurnia and A.S. Mujumdar, “Numerical evaluation of various gas and coolant channel designs for high performance liquid-cooled proton exchange membrane fuel cell stacks”, *Energy*, vol. 44, pp. 278-291, 2012

[80] X. Liu et al., “Three- dimensional multi-phase numerical study for the effect of coolant flow field designs on water and thermal management for the large-scale PEMFCs”, *International Journal of Hydrogen Energy*, vol. 48, pp. 23681-23705, 2023

[81] E. Kharouf, A. Chandan, M. Hattenberger and B.G. Pollet, “Proton exchange membrane fuel cell degradation and testing: review”, *Journal of the Energy Institute*, vol. 85, no. 4, pp. 188-200, 2012

[82] X. Xu et al., “Numerical and experimental analyses of a novel type PEMFC coolant channel”, *International Journal of Hydrogen Energy*, vol. 49, pp. 652-673, 2024

[83] E. Afshari, M.Z. Rad and N. Jahantigh, “Analytical and numerical study on cooling flow field designs performance of PEM fuel cell with variable heat flux”, *Modern Physics Letters B*, vol. 30, no. 16, pp. 1650155, 2016

[84] D. Ting. *Thermofluids*, pp. 373-395, 2022

[85] F. Moukalled and M. Darwish, “A Coupled Finite Volume Solver for Incompressible Flows”, *AIP Conference Proceedings*, 2008

[86] M. Sauermoser, B.G. Pollet, N. Kizilova, S. Kjelstrup, “Scaling factors for channel width variations in tree-like flow field patterns for polymer electrolyte membrane fuel cells – an experimental study”, *International Journal of Hydrogen Energy,* vol. 46, pp. 19554-19568, 2021

[87] M.M.T. Cruz, J. Escorihuela, O.S. Feria and V. Compan, “Proton Exchange Membrane Fuel Cells (PEMFCs): Advances and Challenges”, *Polymers*, vol. 13, pp. 3064, 2021

[88] Y. Huang et al., “Thermal management of polymer electrolyte membrane fuel cells: A critical review of heat transfer mechanisms, cooling approaches, and advanced cooling techniques analysis”, *Energy Conversion and Management*, vol. 254, pp. 115221, 2022